# THE MECHANICAL AND THERMAL PROPERTIES OF THERMOPLASTICS COMPOSITES FOR AEROSPACE APPLICATIONS

MUHAMMAD ZAID HARITH BIN RAMLAN



UNIVERSITI TEKNIKAL MALAYSIA MELAKA

# THE MECHANICAL AND THERMAL PROPERTIES OF THERMOPLASTICS COMPOSITES FOR AEROSPACE APPLICATIONS

MUHAMMAD ZAID HARITH BIN RAMLAN


A project report submitted in partial fulfillment of the requirement for the award of the degree of Bachelor of Mechanical Engineering

Faculty of Mechanical Engineering
Universiti Teknikal Malaysia Melaka

JUNE 2021

## DECLARATION

I declare that this project report entitled "The Mechanical and Thermal Properties of Thermoplastics Composites for Aerospace Applications" is the result of my own work except as cited in the references.

Signature : .....

Name : .....

Date : .....

## APPROVAL

I hereby declare that I have read this project report and in my opinion this report is sufficient in terms of scope and quality for the award of the degree of Bachelor of Mechanical Engineering.

Signature : .....

Name of supervisor : .....

Date : .....

## APPROVAL

I hereby declare that I have read this project report and in my opinion this report is sufficient in terms of scope and quality for the award of the degree of Bachelor of Mechanical Engineering.

Signature : .....

Name of supervisor : .....

Date : .....

## DEDICATION

To my beloved mother, Madam Sarifah Binti Ja'far and
my supportive father, Mr Ramlan Bin Ibrahim.
Thanks to the non-stop encouragement and guide given by my honourable supervisor, Dr. Nadlene Binti Razali, I am able to complete the task successfully.

## ABSTRACT

Thermoplastic has been a bread and butter for aerospace application. Their mechanical and thermal properties offer a lot of flexibility for engineer and scientist compared to thermoset. Besides that, the production of thermoplastic is much simpler where it simply needs to heat up past its melting temperature, consolidated and cooled and unlike thermosets which highly dependable on curing time for polymer crosslinks to form in molecular structure. This research investigates the thermal distribution of PPS laminate in thermoforming process. Three heater temperatures with three heater distances are tested. The distance between two heated surface is 200, 300 and 500 mm for 320°C, 360°C and 400°C heated surface. The desired PPS temperature (320°C) and maximum heater temperature (400°C) is taken as parameter. The test result shows that to achieve 320°C thermoplastic temperature, we can use 385°C IR heater temperature with heater distance of 200 mm. However, this 200 mm distance might be too close for the operation, and larger distance might be needed. Using 300mm or 500mm can achieve close to 320°C if heater temperature is set to 400°C. This study can provide some a preliminary knowledge to engineers and scientists to develop a new structural application for aerospace industry.

## ABSTRAK

Termoplastick sudah sebati di dalam industri aeroangkasa.Sifat mekanikal dan termalnya yang fleksibel berbanding thermoset menjadikannya kegemaran buat para jurutera dan ahli saintis. Selain itu, penghasilan termoplastik lebih mudah di mana ia perlu melepasi suhu lebur, disatukan dan disejukkan sahaja walhal untuk termoset terlalu bergantung kepada tindak balas kimia untuk membentuk struktur molekul. Objektif kajian ini untuk mengkaji pengagihan haba untuk PPS lamina di dalam proses pembentukan terma. Tiga pemanas suhu dengan tiga pemanas dengan jarak yang berbeza dikaji. Jarak untuk dua pemanas adalah 200, 300 and 500 mm untuk 320°C, 360°C dan 400°C adalah suhu untuk pemanas. Suhu yang ideal untuk PPS lamina adalah 320°C dan suhu maksimum untuk pemanas adalah 400°C. Hasil kajian mendapati untuk mencecah suhu 320°C, kita boleh menggunakan suhu pemanas pada 385°C di jarak 200 mm. Walau bagaimanapun, jarak 200 mm mungkin terlalu hampir dengan PPS lamina dan jarak yang ideal perlu diperoleh. Dengan menggunakan jarak 300 mm atau 500 mm, ia mampu untuk memperoleh suhu hampir dengan 320°C jika suhu pemanas ditetapkan pada suhu 400°C. Kajian ini membolehkan sedikit pencerahan kepada jurutera dan ahli saintis untuk mencipta struktur baharu di dalam industri aeroangkasa.

## ACKNOWLEDGEMENT

My highest gratitude towards our Faculty of Mechanical Engineering for giving me the opportunity to undergo and experience Project Sarjana Muda during my final year which entitled "The Mechanical and Thermal Properties of Thermoplastics Composites for Aerospace Applications". I was able to complete the concept design and model analysis within the time limit given by the faculty. Throughout the completion of this Project Sarjana Muda, I gained a lot of new experiences, and this acted as a suitable platform for me to apply my engineering knowledge learnt during the whole of Bachelor of Mechanical Engineering course.

I would like to thank Dr. Nadlene Binti Razali that act as my Project Sarjana Muda supervisor. Without her guidance and assistance, I would not have a clear path on how to engage this project successfully.

Lastly, I would also like to thank all lecturers, staffs and course mates that were involve in accomplishing this Project Sarjana Muda. Last but not least, warm appreciation to our parents with their moral supports and encouragement throughout the Project Sarjana Muda timeline.

## TABLE OF CONTENT

## LIST OF TABLES

## LIST OF FIGURES

## LIST OF ABBEREVATIONS

| | |
|---|---|
| PAEK | Poly Aryl Ether Ketone |
| PEI | Poly Ether Imide |
| PPS | Poly Phenylene Sulphide |
| PEEK | Poly Ether Ether Ketone |
| PP | Polypropylne |
| PE | Polyethylene |
| PU | Polyurathane |
| PA | Polyamide |
| PBT | Polybutylene terephthalate |
| PES | Poly Ether Sulphone |
| PET | Poly Ether Terephthalate |
| $T_g$ | Glass transition temperature |
| $T_m$ | Melting temperature |
| CFRP | Carbon Fibre Reinforced Polymer |
| UV | Ultraviolet |
| MMC | Metal Matrix Composite |
| CMC | Ceramic Matrix Composite |
| PMC | Polymer Matrix Composite |
| HPT | High Pressure Turbine |
| EBC | Environmental Barrier Coating |
| ARPA | Advanced Research Projects Agency |
| MACSS | Manufacture of Advanced Composite Submarine Structures |
| FSW | Friction Stir Welding |
| ASTM | American Society for Testing and Material |
| HPTP | High Performance Thermoplastic |
| TGA | Thermalgravimetric Analysis |
| DIN | Deutsches Institut für Normung e.V. (German Institute for Standardization) |
| DSC | Differential Scanning Calorimetry |

## LIST OF SYMBOLS

| | | |
|---|---|---|
| °C | = | Celsius |
| °F | = | Fahrenheit |
| σ | = | Stress |
| ε | = | Strain |
| E | = | Young's Modulus |
| *P* | = | Applied force, N |
| *L* | = | Support span, mm |
| *b* | = | width, mm |
| *h* | = | thickness, mm |

# CHAPTER 1

# INTRODUCTION

## 1.0 OVERVIEW

The global aerospace industry has enjoyed a period of significant growth over the decade, with a significant rise in passenger traffic. Airlines placed orders for large numbers of aircraft to replace ageing aircraft and thus meet the demand for air travel. This has resulted in a growing backlog of aircraft on order as aircraft manufacturers struggle to keep pace with demand (J.K. Oestergaard, 2019). To meet demand, manufacturers are searching to improve production rates so that the future and current aircraft models are not hampered by manufacturing bottlenecks. One promising avenue improves cycle times for composite part production.

Thermoplastic is another way to thermoset polymers in composites and promise for higher production rates. Contrary to composites that include thermoset polymers, after the consolidation thermoplastic composites require no cure step, in which a composite forms a solid laminate through application of thermal and pressure to multiple prepreg layers. (E. Olson, 2019).

In the aerospace applications most, advanced composite consists of glass fibre or carbon, which reinforces a polymetric matrix. Carbon fibre is one of the most used reinforcement systems in high-end applications for the preparation of composites. The enhancement in mechanical and thermal properties through the orientation, form, and content modification high strength to weight ratio and is the primary advantages of carbon fibre reinforced composites. The other important attributes of carbon fibre are low thermal expansion, corrosion resistance, high strength, modulus, and good creep resistance. The metallic components are currently used for corrosive resistance and high temperature applications to replace thermoplastic enhancing carbon fibre (Sudhin *et al.*, 2020).

The aim of this research is to evaluate the thermal distribution in thermoforming process. The novelty in the manufacturing technique is one of the main highlights of this research.

## 1.1 PROBLEM STATEMENT

Polymer composite are being the top main research nowadays. As researchers and scientist trying to overcome the disadvantages of thermoplastics composites to let it characterize as thermoset which are stable and lack of disadvantages.

Thermoplastic composites with continuous fibres are comparable to thermoplastics in the sense that they have the same enhanced fibre as carbohydrates, glass fibre, aramid, and unidirectional tapes. The distinction is the fiber-containing matrix material. Thermoplastic matrices such as polyether ether ketone (PEEK), polyether imide (PEI), and polyphenylene sulphide (PPS) can be formed repeatedly and melted thus offering new insight in the field of design and manufacture (Offringa, 1996).

PEEK, PPS, and PEI show many advantageous features for aerospace applications. Although aerospace thermoplastics raw materials may sometimes cost more than competitive thermosets, the costs of the finished product can save around 20-40% lower due to lower processing, handling, and installation costs. In addition, thermoplastics provide the option of fusing or welding moulded substrates which reduce assembly stress and weight by removing adhesives and attachments (C. Red, 2014).

## 1.2 OBJECTIVE

This research objectives are:

i. To evaluate the thermal distribution in thermoforming process.

ii. To do comparative study of PPS composites for aerospace application in terms of mechanical and thermal properties.

## 1.3 SCOPES OF STUDY

The scope for this research is:

i. Heating PPS sheet to 320°C within 8 minutes using two infrared (IR) heated surface.

ii. To determine the heater surface distance and its temperature to achieve the requirement.

iii. Reviewing 10 papers to study the mechanical and thermal properties of PPS composites.

# CHAPTER 2

# LITERATURE REVIEW

## 2.1 Introduction

Engineering material plays a massive role in improving aerospace industry. In the early part of the century, aircraft were made from wood frames with textile surfaces. The early designs were subsequently replaced by metal planes. Nowadays, modern aircraft and spacecraft, including many plastics, are made of a broad range of materials. Engineers can now produce higher-performance aircraft than would be possible with all-metal designs by utilising engineering plastics. Engineers in charge of developing the next generation of commercial aircraft will undoubtedly need to use a broader range of innovative polymers to push the envelope of aircraft performance.

The thermoplastic and thermosetting plastics are the two main types of plastics. A thermoplastic is a material that hardens when heated and softens when cooled. Because it can be heated and cooled several times, it can be recycled. When heated, thermoplastics melt and then freeze to a glassy state when cooled. Thermoplastics are not the same as thermosetting plastics. A thermosetting material is one that, during the curing process, forms an irreversible chemical bond (Ching *et al.*, 2017).



Carbon fibre reinforced epoxies are preferred among composites used in aerospace and structural applications due to properties such as failure strength, low creep, high modulus, and low cost. The primary disadvantages of epoxy-based composites are their brittleness, poor resistance to crack initiation and growth, high moisture absorption, and short shelf life. Thermosetting composites have storage, hydrothermal ageing, and insufficient toughness limitations, as well as processing constraints due to long and strict multi-step processing. As a result of these factors, intense research into the replacement of thermoset composites with high temperature thermoplastic composites is increasing. The alternate materials in this study are strong and stiff reinforcements like carbon fibre included in high performance resins like Poly Aryl Ether Ketone (PAEK), Poly Ether Ether Ketone (PEEK), and Poly Phenylene Sulphide (PPS). PAEK, for example, is a high-performance thermoplastic polymer that, due to its unique combination of properties, can be used as a matrix material. They are a more suitable material

for high performance composites due to their high glass transition temperature (Tg) of approximately 150°C, stiffness, melting point (370°C), strength, toughness, solvent and chemical resistance, low dielectric constant, thermo-oxidative stability, recyclability, flame retardancy, and shelf life (Sudhin *et al.*, 2020).

## 2.2 Aerospace Structural Material

Aluminum dominated the aerospace industry fifty years ago. It was inexpensive, lightweight, and many other benefits. In fact, aluminium was once used to make 70% of an aircraft. Other new materials, such as composites and alloys, such as titanium, graphite, and fibreglass, were also used, but in very small amounts when compared to aluminium. Aluminum, which was readily available, was used throughout the aircraft, from the fuselage to the main engine components.

As time passes, a typical jet built today may contain as little as 20% pure aluminium. Most non-critical structural materials, such as aesthetic interiors and panelling are now made of honeycomb materials and lighter-weight carbon fibre reinforced polymers (CFRPs). At the same time for critical components and engine parts, there is a higher demand for higher temperature resistance and lighter weight for improved fuel efficiency (M. Standridge, 2014).

Any aerospace engineer's dream has always been to create aircraft that fly farther and faster. Any aerospace engineer's dream has always been to create aircraft that fly farther and faster. High-speed aircraft, for example, necessitate higher temperature resistance capability materials due to frictional heating. As a result, skin materials have evolved from the early aircraft's use of wood and fabric to advanced alloys of polymer matrix composites, titanium and aluminium, which containing high strength carbon fibres. (Williams and Starke, 2003).

## 2.3 Composite Engineering

A composite material is one that is made up of two or more constituent materials. These constituent materials have markedly different chemical or physical properties and are combined to form a material with properties that differ from the individual elements. Individual elements within the finished structure remain separate and distinct, distinguishing composites from mixtures and solid solutions. Materials that are less expensive, stronger, or lighter than well-known materials are a few examples. There are 3 types of composites material that are used currently in aerospace engineering which are discussed in the subtopic below.

### 2.3.1 Polymer Matrix Composites (PMC)

Composites made of fibre reinforced polymer (FRP) are the most promising materials of the twenty-first century. The response of its constituents, as well as the existing interface and interphase between the fibre and polymer matrix in that environment, can alter their integrity and durability in multiple service environments. Their susceptibility to degradation is determined by the nature of the environment as well as the distinct and individual responses of each constituent. During their service life, all components and structures are exposed to some environment. Environmental conditions can include high and low temperatures, an alkaline environment, UV light exposure high humidity and they can be more severe if there is a hydrothermal environment, low earth orbit space environment, and cyclic temperature variation (Ray and Rathore, 2014).

It is critical to understand the fibre characteristics to expand the use of natural fibres for composites and improve their performance. The physical properties of each natural fibre are unpredictable, and these include the defects, strength, dimensions, and structure of the fibre. There are several physical properties of each natural fibre that must be understood before it can be used to its full potential. Fibre dimension, strength, crystallinity, strength, structure, and defects must be considered. A strong interface that is very brittle with easy crack propagation through the fibre and matrix could achieve an exemplary strength and stiffness (Balakrishnan *et al.*, 2016).

Table 2.1: Some man-made fibre and natural properties (Balakrishnan *et al.*, 2016)

| Fibre | Density ($g/cm^3$) | Elongation (%) | Tensile Strength (MPa) | Young's modulus (GPa) |
|---|---|---|---|---|
| Cotton | 1.5 – 1.6 | 3.0 – 10.0 | 287 – 597 | 5.5 – 12.6 |
| Jute | 1.3 – 1.46 | 1.5 – 1.8 | 393 – 800 | 10 – 30 |
| Flax | 1.4 – 1.5 | 1.2 – 3.2 | 345 – 1500 | 27.6 – 80 |
| Hemp | 1.48 | 1.6 | 550 – 900 | 70 |
| Ramie | 1.5 | 2.0 – 3.8 | 220 – 938 | 44 – 128 |
| Sisal | 1.33 – 1.5 | 2.0 – 14 | 400 – 700 | 9.0 – 38.0 |
| Coir | 1.2 | 15.0 – 30.0 | 175 – 220 | 4.0 – 6.0 |
| Softwood Craft | 1.5 | - | 1000 | 40.0 |
| E-glass | 2.5 | 2.5 – 3.0 | 2000 – 3500 | 70.0 |
| S-glass | 2.5 | 2.8 | 4570 | 86.0 |
| Aramid (normal) | 1.4 | 3.3 – 3.7 | 3000 – 3150 | 63.0 – 67.0 |
| Carbon (standard) | 1.4 | 1.4 – 1.8 | 4000 | 230.0 – 240.0 |



The most common polymer that we know are thermoplastic, thermoset, and elastomer. Polymer has a broad application spectrum that includes almost in every department of advanced engineering structure. Their usage includes various components in helicopters, boats, spacecraft, ships, offshore platforms, and aircraft (Shrive, 2006). However, like other material they have their own advantages and disadvantages especially in structural application in aerospace.

Table 2.2: Polymer advantages for aircraft structural applications are compared (Steyer, 2013).

| Thermoplastic | Thermoset | Elastomer |
|---|---|---|
| No cure required | Low processing temperature | Low processing temperature |
| Rapid processing | Low viscosity | High ductility and flexibility |
| High ductility | Good compression properties | High fracture toughness |
| High fracture toughness | Good creep resistance | High impact resistance |
| High impact resistance | Highly resistance to solvents | |
| Absorbs little moisture | Good fiber wetting for composites | |
| Can be recycled | | |

Table 2.3: Polymer disadvantages for aircraft structural applications are compared (Steyer, 2013).

| Thermoplastic | Thermoset | Elastomer |
|---|---|---|
| Very high viscosity | Long processing time | Long processing time |
| High processing temperature (300 – 400°C) | Low ductility | Poor creep resistance |
| High processing pressure | Low fracture toughness | Low Young's Modulus |
| Poor creep resistance | Low impact resistance | Low tensile strength |
| | Absorb moisture | |
| | Limited shelf life | |
| | Cannot be recycled | |

Carbon fibre's high strength-to-weight ratio has made it a more appealing energy-saving material than traditional strength-bearing materials such as steel. With the trend in mind, the high-weight steel in many strength applications is being gradually substituted by the low-weight and corrosion-proof carbon fibre composites. The carbon fibre-reinforced polymer matrix composite (PMC) has thereby become forefront material in automobile, aerospace, and other applications which demand high modulus and high strength. Moreover, the gradual cut in the costs of carboxylic fibre technology has opened up its market in various construction applications in recent years, with extensive research (Das, Ghosh and Das, 2019).

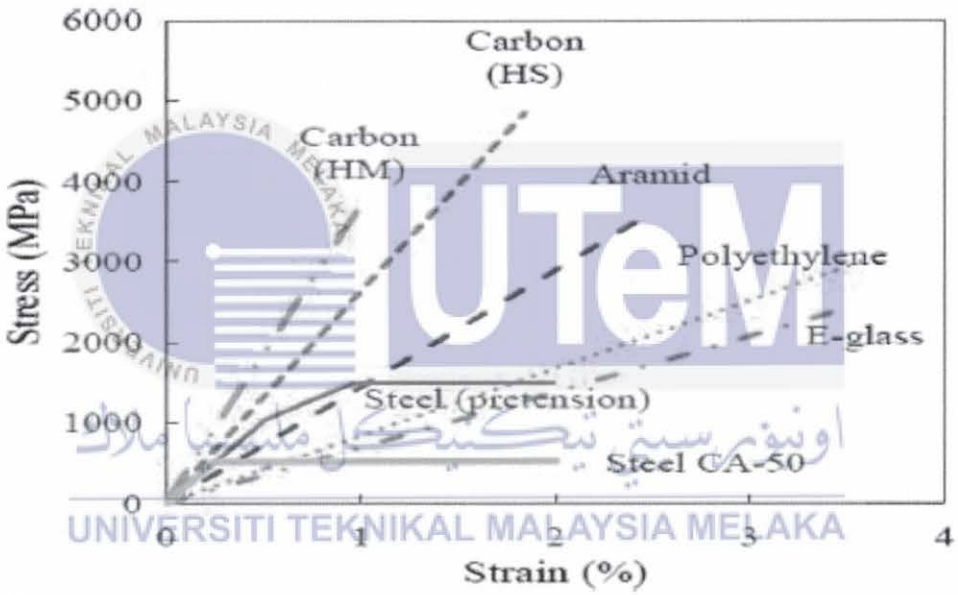




Figure 2.1: Comparison of the carbon fibre stress-strain plot with other materials (Pinheiro *et al*, 2017).

A fibre enhanced composite includes a fibre reinforced network embedded in resin matrix, which can also be supplemented by other materials such as fillers and pigments. The resin is generally a liquid or powder that can be crossed into a hard, infusible solid when combined with a catalyst or hardener. By impregnating the fibrous material with catalysed resin in the form of a process that allows the resin to heal, the so-called reinforcing plastics are produced. E – glass, for example, is used in composite

fibre enhancement. Due to its light weight and improved mechanical properties, it has been commonly used in aerospace and automotive applications as a substitute material. E – glass fibre is stronger and less alkali content (<1%). The tensile strength is better, the electrical conductive and rigidity qualities are good (S, K and Govindaraju, 2018).

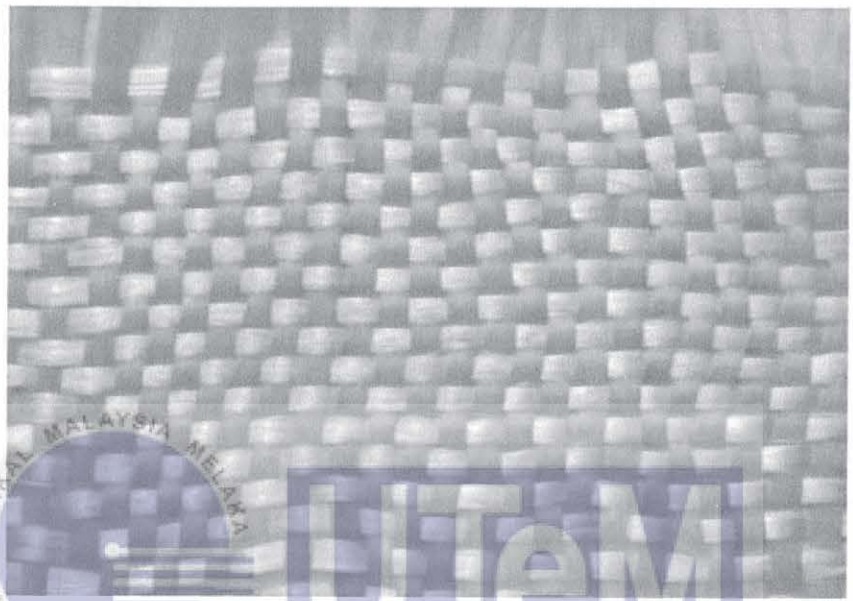

Figure 2.2: E – glass fabric (S, K and Govindaraju, 2018).

### 2.3.2 Metal Matrix Composites (MMC)

Most of today's metal matrix composites are based on its alloy and aluminium, both in research and development as well as for different industrial application. Aluminum is light, which in most applications of today's metal matrix composites is the first requirement. Furthermore, compared to other light metals like titanium and magnesium, it is cheap. Due to the large quantities used in many applications, such as aircraft and automotive, the conventional aluminium alloys are very ductile, robust, and corrosive and they can be modified to fulfil the requirements of many different applications. The hardened alloys, such as al-Zn-Mg-Cu and al-Cu-Mg, are of particular attention among all the excellent aluminium alloys. Li has the effect of simultaneously lowering the density and increasing the elastic modulus of the alloy when it is alloyed to alloy. Therefore, it is not unusual for the aerospace industry to be interested in the possible composites in Al-Li (Lindroos and Talvitie, 1995).

Table 2.4: Elastic module of the composite light metal matrix and ultimate tensile resistance (Lindroos and Talvitie, 1995)

| Matrix | Reinforcement | Vol. fraction (%) | Longitudinal tensile strength (MPa) | Longitudinal elastic modulus (GPa) |
|---|---|---|---|---|
| Al – 72n | Graphite fiber | 40 | 90 | 190 |
| Al 2024 | Boron fibre | 60 | 1500 | 270 |
| Al 6061 | SiC fiber | 50 | 1500 | 205 |
| Al 2024 | $Al_2O_3$ | 50 | 450 | 175 |
| Al 6061 | SiC whisker | 15 | 480 | 100 |
| Al 6061 | SiC particulate | 15 | 370 | 100 |
| Ti-6Al-4V | BORSIC | 40 | 900 | 205 |
| Ti-6Al-4V | SCS-6 | 35 | 1600 | 240 |
| Ti-6Al-4V | Sigma SM1240 | 35 | 1550 | 230 |
| Mg | Graphite fiber | 40 | 560 | 230 |
| Mg | SiC fiber | 50 | 1300 | 230 |

Aluminum is still light, technologically advanced, and still cost relatively little, in relation to titanium and composites in terms of forming and alloying. For example, in 2013, Alcoa forecasts a 6 percent increase in aluminium in aircraft over 2011. The Airbus A380, one of the world's largest airliners for passengers, contains 10 times the aluminium used by the Airbus A320 and Boeing's Dreamliner 787, often referred to as a composite plane, contains a relatively novel aluminium alloy of 20 per cent by weight, which includes 7085 aluminium (S. Mraz, 2014).

A study has been carried out that improvement in construction materials is necessary in order to improve the demands for increased performance of current aerospace systems. This is true for airframes as well as motors. For example, fighter planes must be operated with supersonic persistence in wider combat envelopes, higher turning rates, maximum Mach numbers, and high load factor. The main part in reducing structural weight is shown in Figure 2.3 which is new and improved materials. It can be clearly seen that the material factor exceeds significantly the contribution of other advanced technologies such as flood control, structural concepts, active load control, and automated design (Bandyopadhyay, 2014).

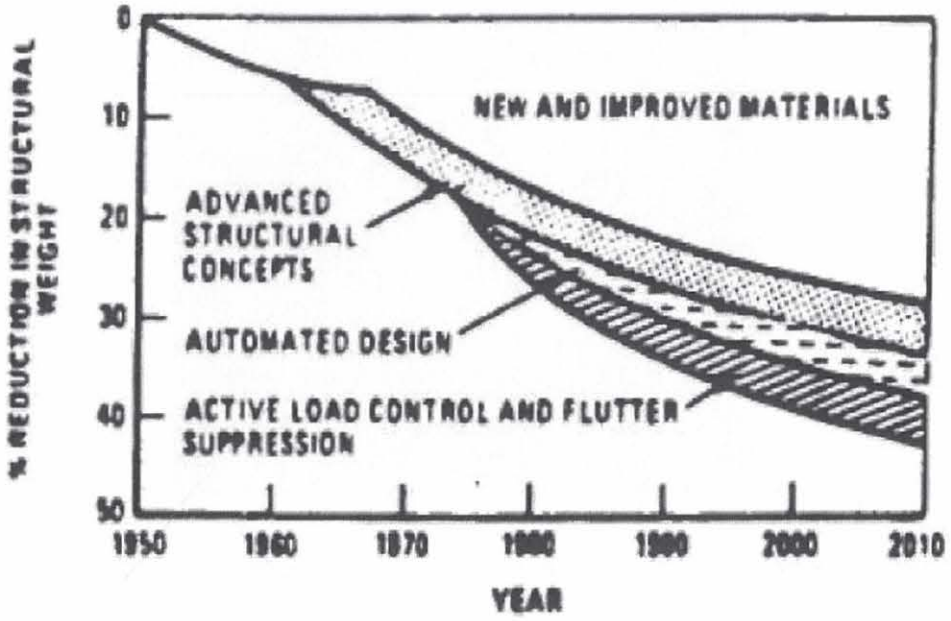


Figure 2.3: Structural weight reduction trends for combat aircraft show the importance of new and improved materials (Bandyopadhyay, 2014).

As high cost, high-performance materials and processes are "allowable" to the aerospace industry, many new materials/proceedings for aeronautical applications have been assessed. The casting approach produced large, fast solidification, conventional titanium motor parts and mechanical alloy approaches were used to manufacture several aerospace components such as the parts shown in Figures 2.4 and 2.5.(Kumar, Agnihotri and Purohit, 2015).

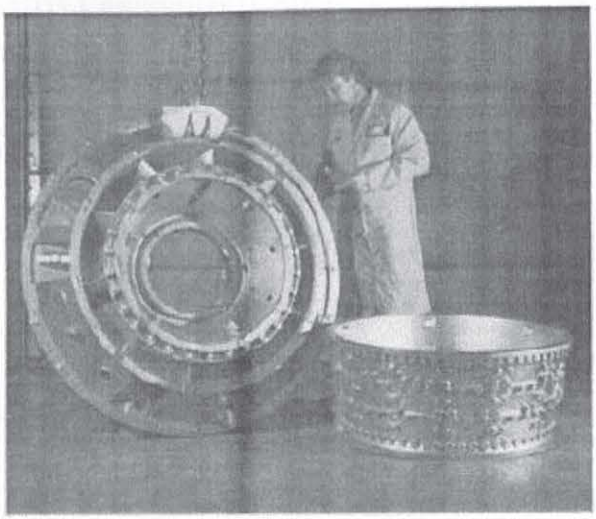

Figure 2.4: Large engine part casting (Kumar, Agnihotri and Purohit, 2015)

Figure 2.5: Forged landing wheel using RS Aluminum Alloy (Kumar, Agnihotri and Purohit, 2015)

### 2.3.3 Ceramic Matrix Composites (CMC)

Ceramic Matrix composites (CMC) can withstand high oxidation resistance, high temperatures, and can have the potential for high strength, catastrophic failure resistance, low thermal expansion, and high fracture toughening. These types of materials have far greater resistance than metals or other conventional engineering materials to high temperatures and aggressive environments. The ceramics are non-metallic inorganic materials, composed of the ion and/or covalent bonded. The two types of SiC (silicon carbide) and NaCl (sodium chloride) bonds are present in Figure 2.1. (Alves, Baptista and Marques, 2016).

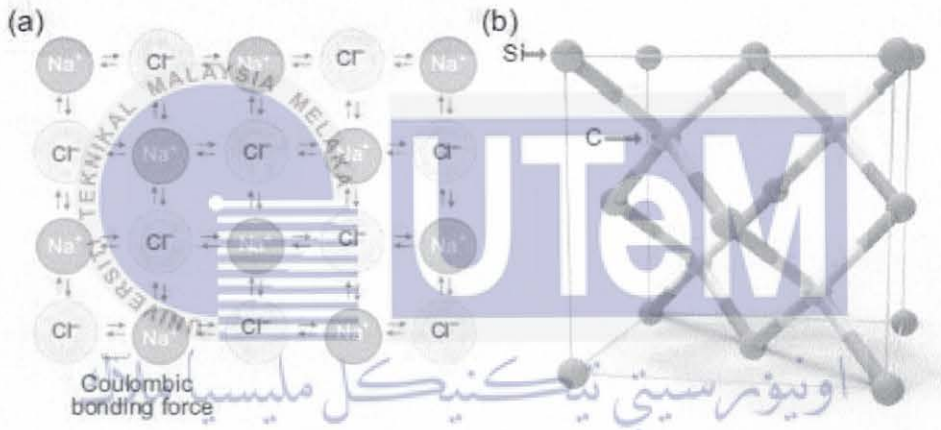




Figure 2.6: Ceramic bond types: (a) Ionic bonding (NaCl) and (b) Covalent bond (SiC) (Alves, Baptista and Marques, 2016)

The increased demand for structural materials that have superior long-term mechanical properties, and retain these properties at high pressure, high temperatures, and several environmental factors including humidity, has been increased in the generation of electricity for rockets, ground-based turbines, aircraft engines, and hypersonic missiles and vehicles. At the interface there are two main types of binding: chemical binding or mechanical. Mechanical bonding from residual stresses, which lead to a matrix seizure of the fibre. When the interface is rough, radial griping can be enhanced. Interface properties depend on the matrix and fibre because during cooling,

binding is a result of thermal shrinkage or chemical reactions (Bansal and Lamon, 2015).

Motor producers have recently gained voice over the prospects of using ceramic matrix composites in the hot motor section. The higher SiC based systems' temperature capable at 1200°C makes them more attractive than traditional systems, by offering weight reduction that requires less cooling air (Mechum, 2012).

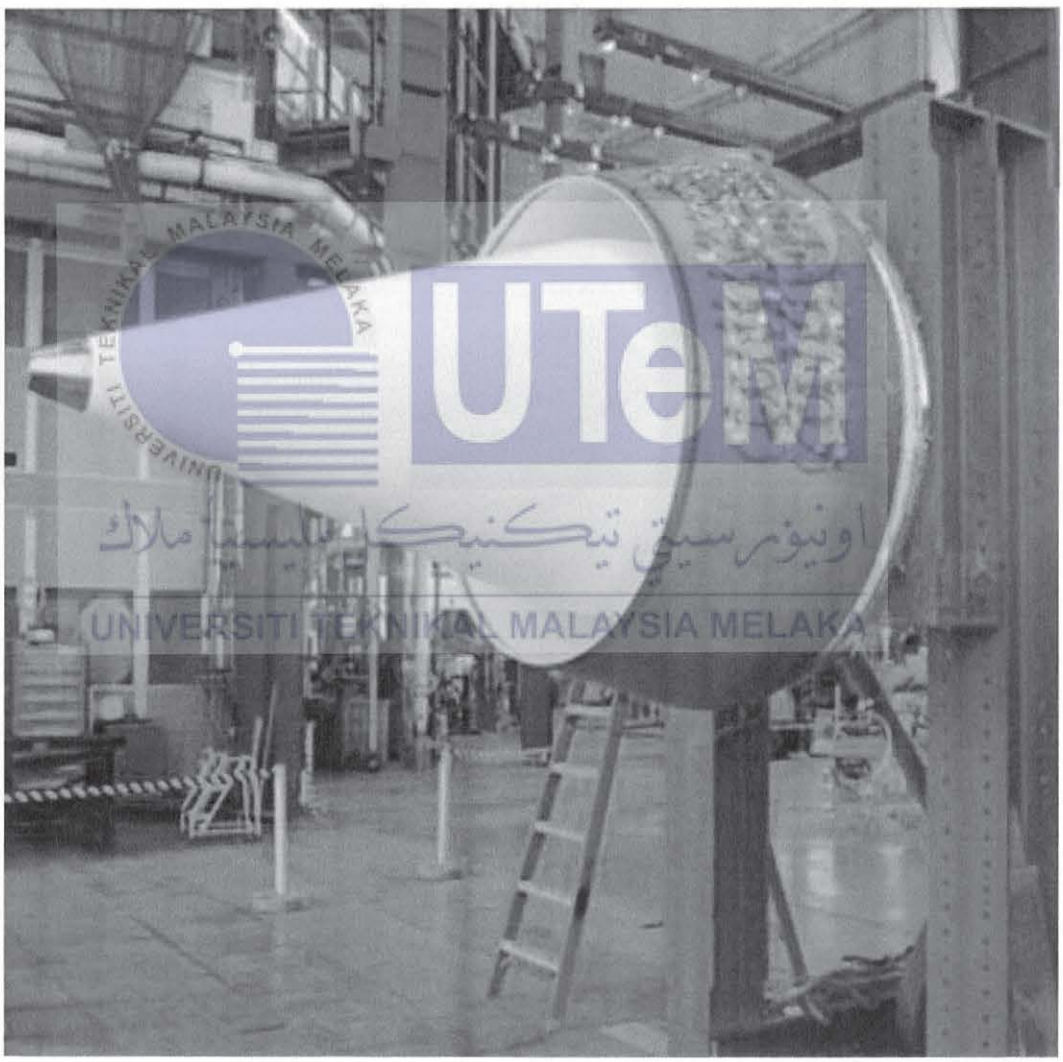


Figure 2.7: Oxide ceramic matrix composite tube exhaust tube with 1.60 m diameter and a diameter of 2.34 m conical to the titanium end cap inspection panel with a diameter of 1.60 m (Steyer, 2013)

The operating temperature is directly linked to the performance and efficiency of aero propulsion turbine motors. Ceramic thermal-barrier coatings (TBCs), due to their ability to reduce cooling needs and increase turbine operational temperatures are technologically important, thus contributing to emission objectives and engine performance. Ceramic TBCs have been applied to air-cooled, critical turbine engine hot section components such as combustors, high-pressure turbine vanes and blades as shown in Figure 2.8 as advances in ceramic material and processing technologies particularly in the zirconia-based ceramic field (Padture, 2016).

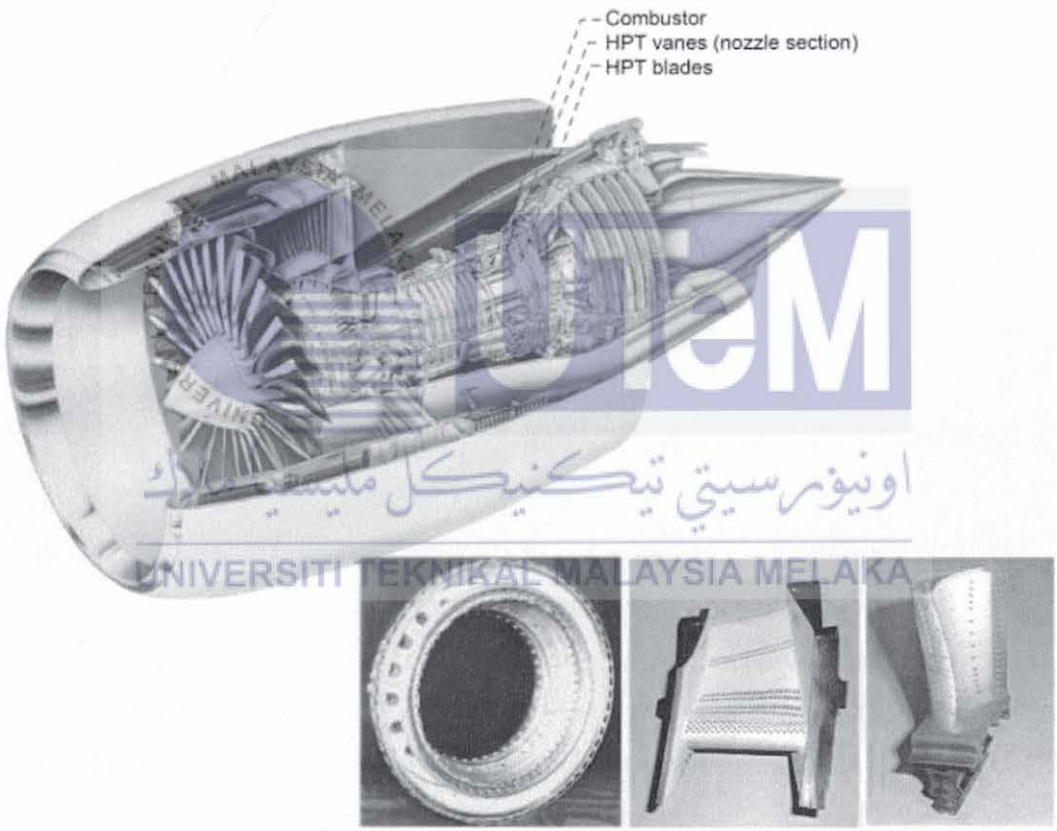




Figure 2.8: A high bypass turbofan engine schematic diagram. In the heat section of the turbine components, including combustors, HP blades and turbine (HPT) vanes at thermal barrier coatings are widely used. (Zhu, 2019)

Silicon-based composites and ceramics are desirable for the high temperature, oxidation resistance, low density, high temperature, and cranking strength such as SiC/SiC ceramic matrix composites. Environmental barrier coatings (EBC), due to a Volatilize Silica Protective ($SiO_2$) scales in SiC when reacting with water vapour, are necessary to prevent a SiC/SiC vapour attack in motor combustion environment. The loss of SiO2 from the ceramic surfaces causes accelerated strength degradation in engine operating environments with combined mechanical loading conditions and thermal. As a result, EBC are regarded as critical in enabling CMC component technologies for aerospace propulsion engine systems (Opila and Hann, 1997).

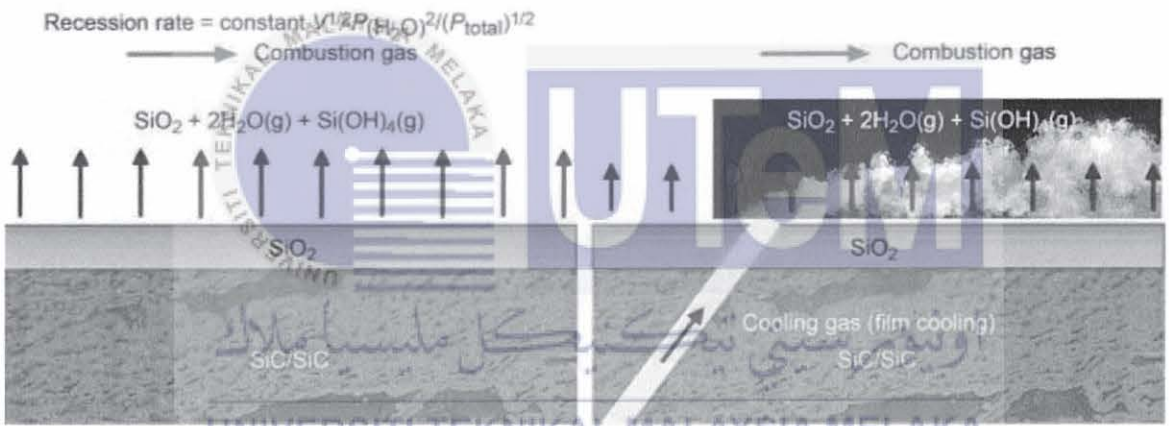




Figure 2.9: Surface recession of $SiO_2$ scales on a SiC/SiC ceramic matrix composite specimen is depicted schematically. (Left) In a convective combustion gas flow, recession occurs. (Right) Recession of a convective combustion gas and flow of film-cooling air. (Zhu, Sakowski and Fisher, 2019).

## 2.4 Thermoplastic Material

Major structures of modern aircraft, such as the Airbus A350XWB and long-range Boeing 787 are mostly made of carbon-fibre-reinforced polymers (CFRP). Hundreds of complex metallic load introduction elements, such as hinges, brackets, or fittings, are attached to these CFRP primary structures, which are made up of reinforcing profiles and skins. Those numerous components are still metallic, but complex metallic load introduction elements have several disadvantages in aerospace applications. As shown in Figure 2.10, aluminium parts integrated into rotorcraft CFRP airframes must be protected against galvanic corrosion with a number of costly measures. (Eguemann *et al.*, 2014).

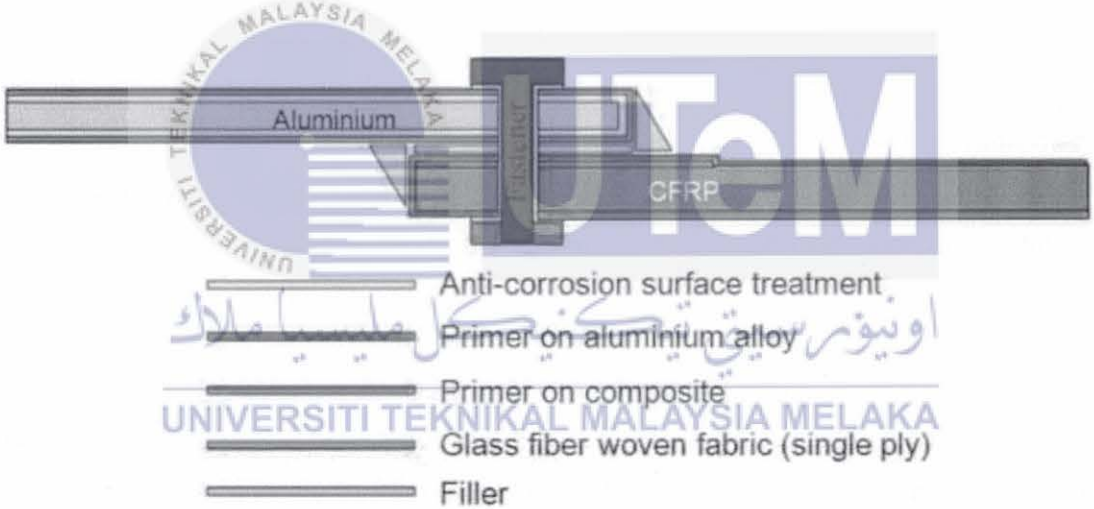




Figure 2.10: EASA recommended protection against galvanic corrosion (Eguemann *et al.*, 2014)

Toray Industries, Inc. conducted early research that resulted in a patent in 1990 clearly describing how strip pieces (chips) made of chopped thermoplastic pre-impregnated unidirectional fibres (UD tapes) are distributed in a plane parallel to the surface cavity. The ideal length of the chips is sufficient to gather mechanical properties like those of a quasi-isotropic laminate while remaining short enough to maintain the benefit of well fitting. (Kimoto *et al*, 1992).

Figure 2.11: UD tape, 10mm chopped tapes, 20mm chopped tapes, recycled fragments, injection moulding granules, from left to right. (Eguemann *et al.*, 2014)

Thermoplastic polymers and composites can also be used for processes such as autoclave processing, fibre placement technique, tape, and rapid thermoforming. In addition, many thermoplastics tolerate greater deflections without deformation and have better fatigue characteristics than metals. PEEK is a thermoplastic that is fast becoming a popular metal replacement in aerospace. PEEK's mechanical strength, fatigue resistance, sluggishness, lightweight nature, and ease of processing make it extremely versatile. The range of applications of PEEK includes aerodynamic components, fuel system, interior aircraft, and flight control (J. Macdonald, 2018).



Plastics and polymers are easy to obtain and plentiful. Therefore, they have many unusual features in several new applications which drive new innovations and breakthrough products and solutions as we shift our way of life. In infrastructure, plastic plays a vital role, and it is the second largest consumer. Structures that are made of plastic material and are not yet identified as plastic material are rarely seen as structures (Ching *et al.*, 2017).

## 2.5 Thermoplastic Research

For about 25 years, automatic fibre has become popular. A large part of the early development of MASS (Manufacturing of Advanced Composite Submarine structures) was undertaken in the US under ARPA (Advanced Research Projects Agency) (Richard Sharp, Scott Holmes, 1995).

The composites industry in the aerospace industry is undergoing substantial growth, mainly because lightweight composite structures have more fuel efficiency than metal structures. The industry's current focus is on thermosets, but there is also the usage of thermoplastic in the industry. PEEK composites for commercial aerospace and military are available in a comprehensive database. Substantial investments in the qualification and production of thermo-plastic composites were made by Airbus contractors and suppliers, such as TenCate and Fokker. Up to now this investment has led to both Airbus A340 and A380 production. (Favaloro, 2018).

It is best described by their distinct chemical characteristics that the principal difference between thermosets and thermoplastic matrix systems. Thermoplastics can be characterized as linear polymers, which normally do not need a cure when consolidated in a composite. While thermosets are cross linkable polymers. The thermoplastic consolidated composites can be reformed and molded. In all ambient environments with endless shelf life, thermoplastic preforms or prepregs are available, unless solvent is included which may reduce their shelf life. The thermoset prepregs with a cross-linked matrix need to be stored coolly, consolidated by cure (chemical reaction) and cannot be reformed after cure. In recent years, a number of high-performance thermo-plastic matrix system with linear characteristics, Polymers such as PEEK, PEKK, PPS, J-polymer and K-polymer, have demonstrated the reform capacity and processability of fiber-reinforced thermoplastic composites (Chang and Lees, 1988).



Proper composite parts assembly is a main thing to the well-being of secondary and primary structural assemblies in industry. Mechanical fixing methods often lead to damage both to the matrix and the fibres in the composite material. Fastening and drilling are slow, expensive and failure sensitive (Weber, 2013).

Instead of fastening and drilling, fusion connections of thermoplastic composites can be used. Currently available techniques are autoclave-based integral consolidation, induction welding, resistance welding, ultrasonic welding, and rotational welding. Technique for fusion bonding involve reconsolidation and melting of the material (Ageorges, Ye and Hou, 2006).

The diagram of the FSW process is illustrated in Figure 2.12. The objective of this process is to heat the material in the temperature range of operation by producing thermal energy by friction. It starts from the $T_g$ and ends below $T_m$ of the thermoplastics (Ahmed *et al.*, 2018).

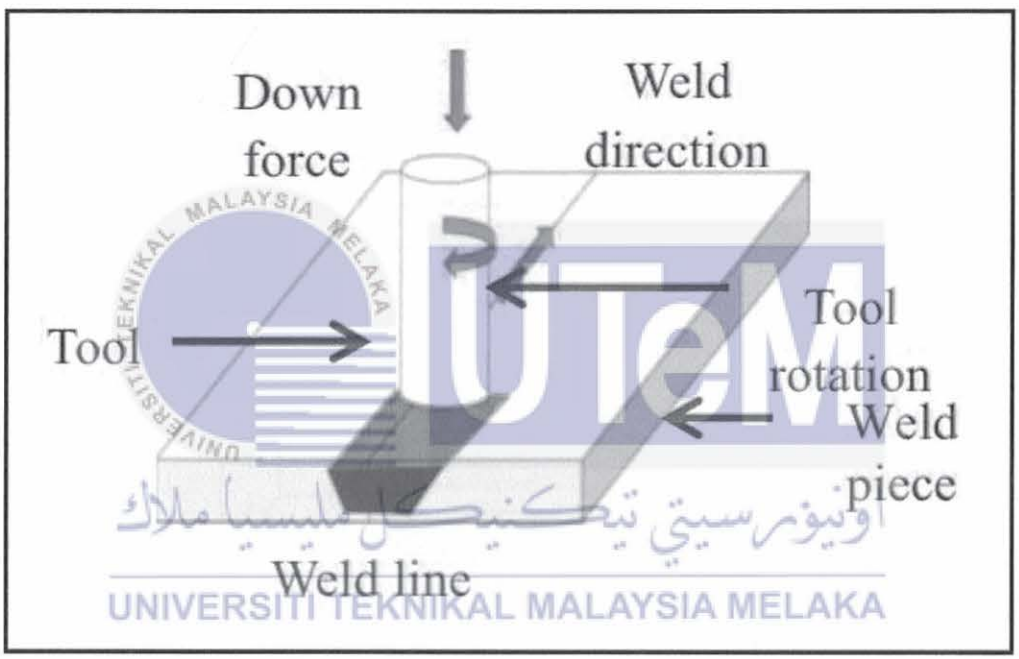




Figure 2.12: Fundamental FSW process. (Ahmed *et al.*, 2018)

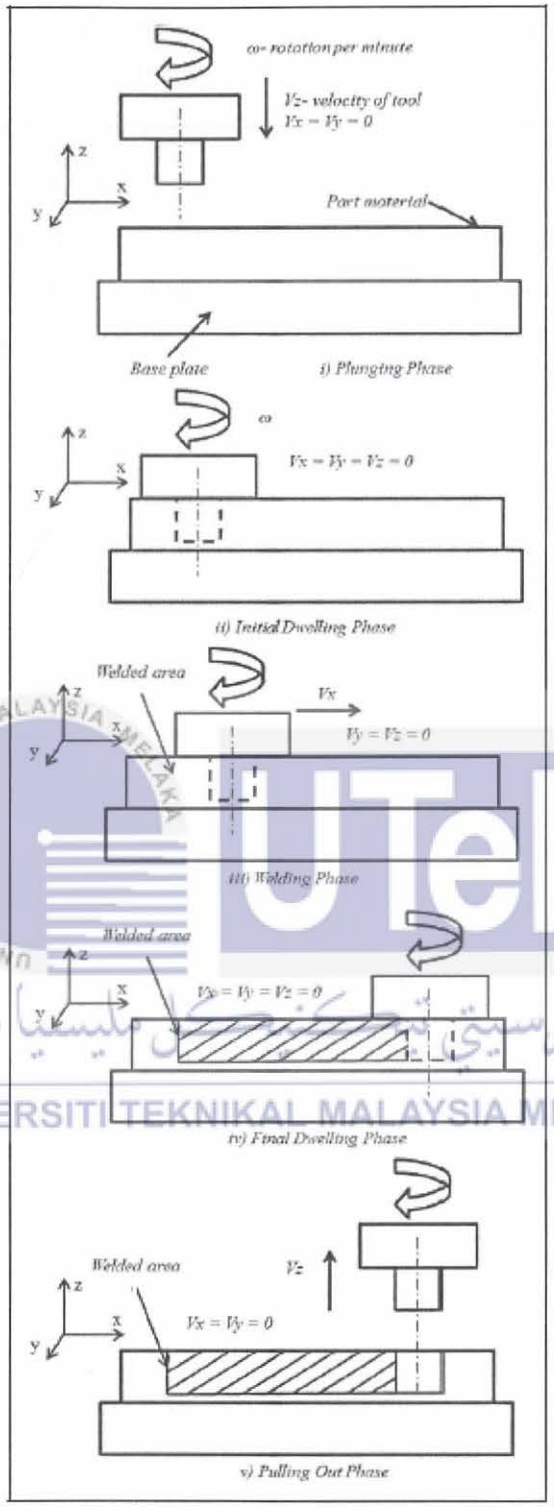


Figure 2.13: Various FSW phases. (Ahmed *et al.*, 2018)

In FSW, this transformation is a multiplex process, as illustrated in Figure 2.13, involving friction, material recrystallisation, use, deformation, and adhesion. Depending on the heat production process, FSW of thermoplastic can be class into five steps: (i) plunge, (ii) initial dwelling, (iii) weld, (iv) final dwelling, and (v) pulling. The friction between the tool's contact surfaces with the specimen generates heat in all these phases. However, in the pulling-out stage the heat production does not contribute to connection; it is necessary to finish the welding process. (Arbegast, 2006).

## 2.6 Thermal and Structural Analysis of Thermoplastic

### 2.6.1 Experiment 1 (ASTM D790M Flexural Test)

ASTM D790M was used to conduct flexural testing. From a flat portion of the frame, as shown in figure 2.15, five carbon/PPS measured in rectangular shape of 50 x 25 x 2 mm3 were prepared. The test was conducted with a 0.85mm/min crosshead-motional screw-operated universal testing machine. Table 2.5 represent the actual result. The average ultimate tensile strength and flexural modulus of the processed carbon/PPS composites was found 322.63 MPa and 28.50 GPa, respectively. No visible fibre fracture was observed on the tensile face while the fibre fracture was apparent around the compression face load line. Figure 2.16(a) shows a load vs displacement plot of a carbon/PPS specimen for the flexural test. The failure mode was debonding between the plies and wrinkling on the compression, was shown in the Figure 2.16(c) and (d), respectively. Multiple peaks in the load vs displacement curve of Figure 2.16(a) indicate debonding between the plies. The first peak was because of the creased on the compression face, and the other peaks are caused from delamination of the plies (Ning *et al.*, 2007).

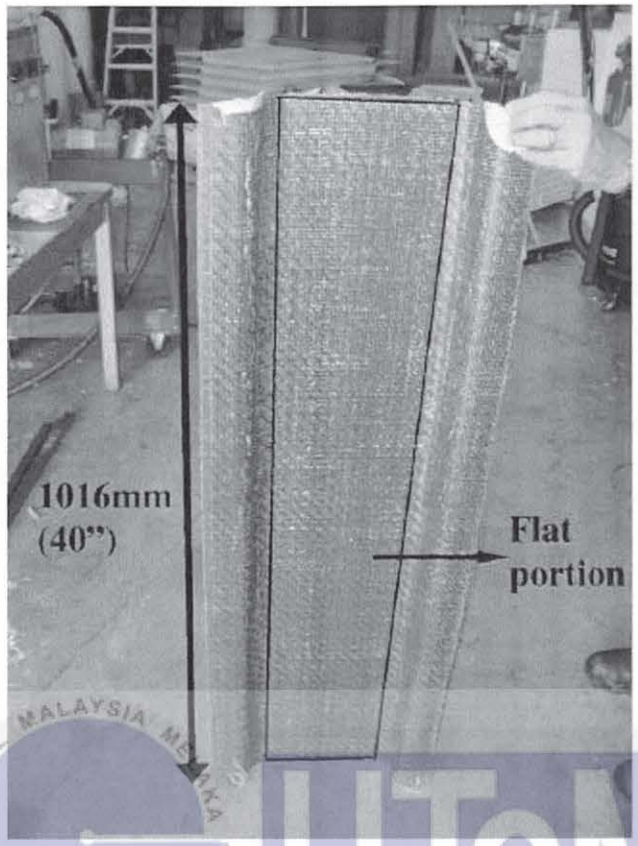


Figure 2.14: Carbon/PPS frame specimens (Ning *et al.*, 2007).



Table 2.5: Summary of the Carbon/PPS Flexural Test (Ning *et al.*, 2007)



| Specimen | Modulus (GPa) | UTS (MPa) | Statistical data | Modulus (GPa) | UTS (MPa) |
|---|---|---|---|---|---|
| 1 | 22.54 | 255.94 | Mean | 28.50 | 322.63 |
| 2 | 26.85 | 295.30 | Standard error | 1.86 | 22.30 |
| 3 | 33.60 | 374.55 | Standard deviation | 4.15 | 49.86 |
| 4 | 30.63 | 367.86 | Minimum | 22.54 | 255.94 |
| 5 | 28.88 | 319.49 | Maximum | 33.60 | 374.55 |

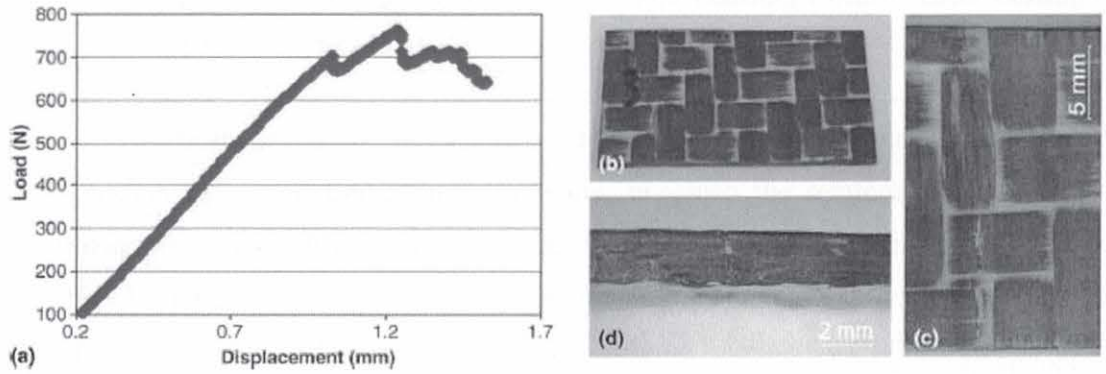


Figure 2.15: (a) Flexural Test Load vs Displacement plot; (b) Specimen with a rectangular shape with dimension 25 x 50 $mm^2$; (c) Loading failure delamination failure (d) Lateral view of the specimen detachment (Ning *et al.*, 2007)

### 2.6.2 Experiment 2 (ASTM D6641 Combined Loading Compression Testing for CFRP

The thermoplastic composite laminates 5-harness weave were manufactured by TenCate Advanced Composites Company, in which the reinforcement and matrix materials were T300JB carbon fabric and Fortron 0214 PPS, respectively, as shown in Fig. 1 where the locations marked as a, b and c denote respectively crossover point, resin-rich region and warp fibre. The fibre volume fraction for CF/PPS was 50%. The composite laminates with Q-I lay-up sequence: [(±45)/ (0,90)] were made by using hot pressing technique and the thickness was 3.72 mm (Wang *et al.*, 2018)


Figure 2.16: Surface and lateral observations tissue structure (Wang *et al.*, 2018)

Compressive testing was conducted on a universal mechanical inspection engine Instron 3382, which had environmental chamber and 100kN loading cell. The loads crosshead speed of 0.5 mm/min were registered as a displacement controls. For the strain measurements, strain gauge and laser extensometer were used in unnotched and notched compressive tests, respectively. A DSC accomplished by Pyris Diamond DSC was ran on the CF/PPS composite. Both the cooling and heating rate used were 10°C /min. Three-point bending dynamic mechanical analysis was carried out by Perklin Elmer Pyris Diamond DMA. Temperature examined from room temperature to 250°C with a heating rate of 5°C and a frequency of 1Hz were accomplished in nitrogen atmosphere. (Wang *et al.*, 2018).

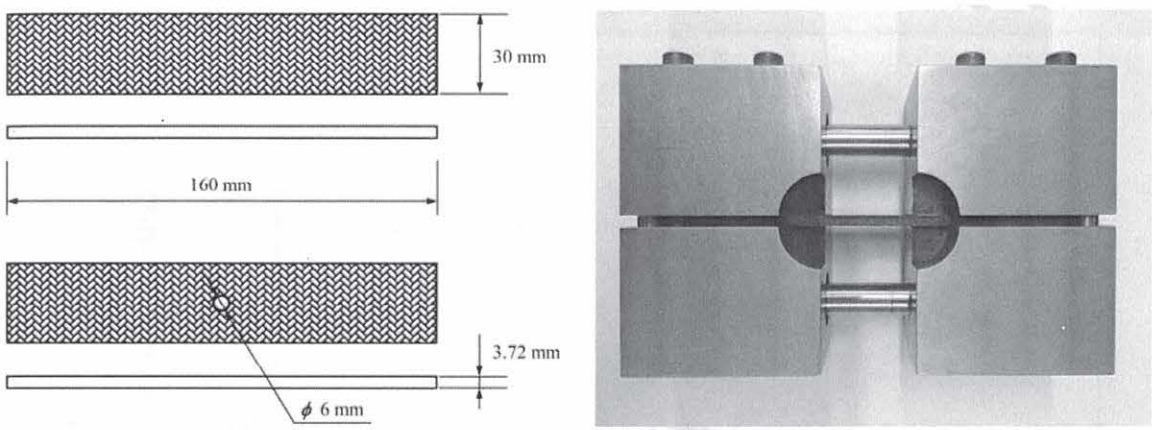


Figure 2.17: Compressive and experimental specimen geometries (Wang *et al.*, 2018)

In a composite, the matrix state holds a commanding role in mechanical properties, especially for the semi-crystal polymer, which may experience melting, recrystallization, and decomposition with the escalated of temperature. The CF/PPS thermal properties obtained by DSC and DMA analysis were indicated respectively in Figure 2.19 and Figure 2.20, where $T_c$, $T^c_g$, and $T_m$ indicated respectively as crystallization temperature glass transition temperature of composite and melting temperature and $T_2$ and $T_1$ signalled as the end of the peak and temperature of the initiation. In Figure 2.19, $T^r_g$ means the glass transition temperature of CF/PPS composites equivalent to 105°C, which represent as loss modulus peak temperature, which was higher than the glass transition temperature of neat resin ($T^r_g$ = 90 °C). It is because of the growth of PPS crystallinity after the addition fibers and the negligible deviation which resulted from the different stacking sequence. The locations of melting peaks and crystallization in DSC curve were presented in Figure 2.20 (a), (b) and (c). (Wang *et al.*, 2018).

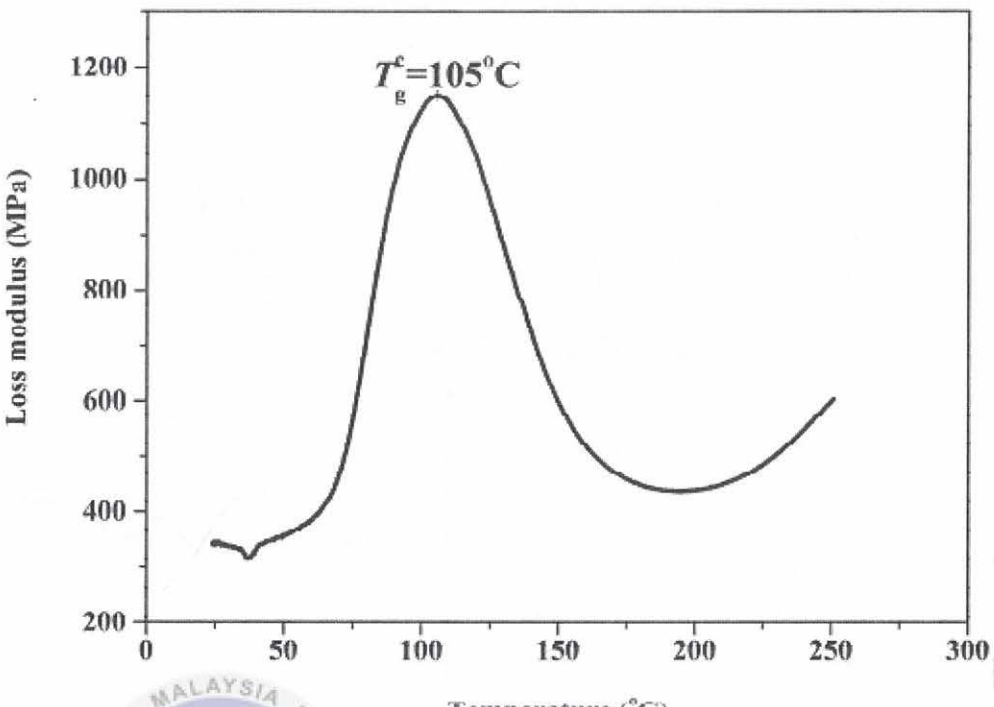


Figure 2.18: DMA curve for CF/PPS composite (Wang *et al.*, 2018)

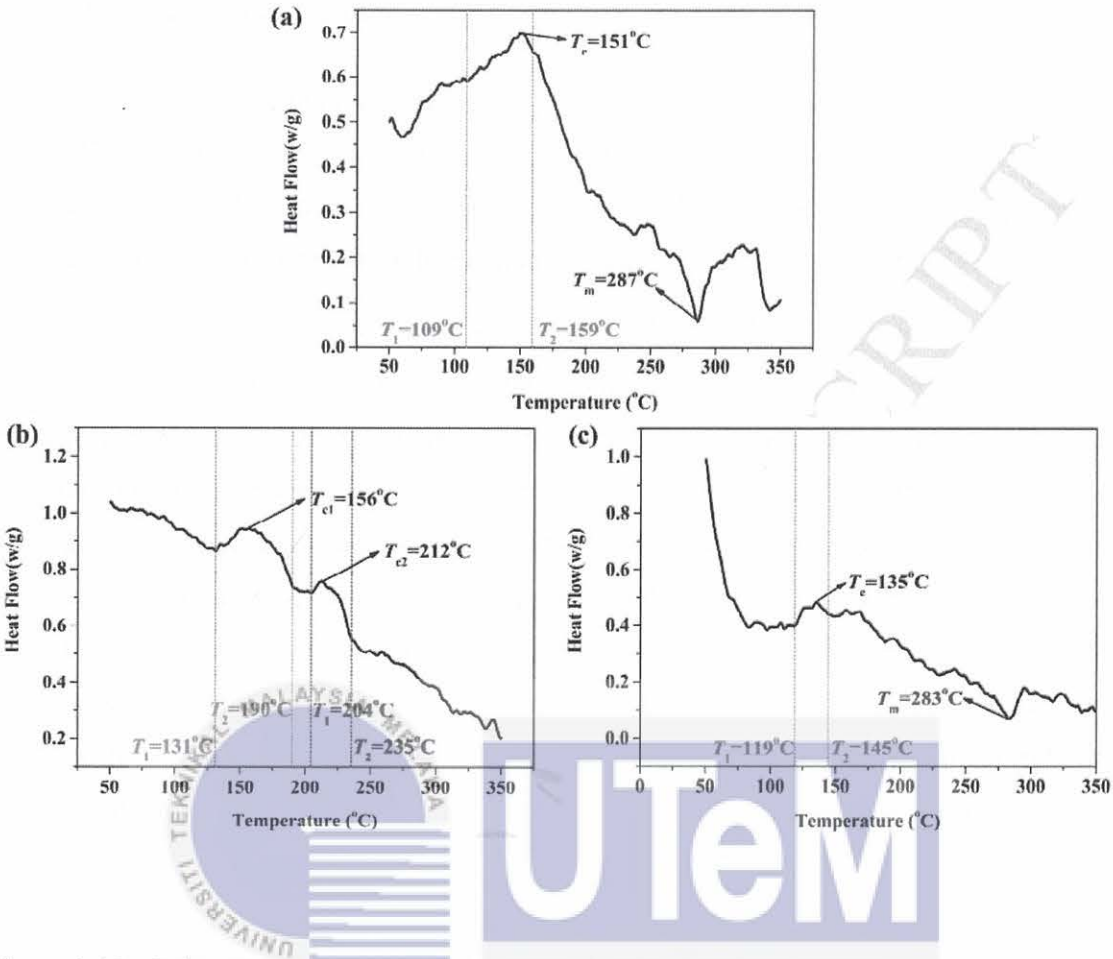


Figure 2.19: CF/PPS DSC curves: (a) Sequence for first heating, (b) Sequence for cooling and (c) Sequence for second heating (Wang *et al.*, 2018)

### 2.6.3 Experiment 3 (ASTM D3039 Tensile Strength Test)

The equipment and materials mainly used for this experiment are shown as: CF/PPS: TC1100PPS laminate, TenCate, Netherlands. 2 mm was the thickness per laminate which embodies of 10 prepreg plies stacked at a direction of [0/90]. Last but not least, 50% was the mass fraction for CF/PPS (Liu, Zhou and Wang, 2020).

ASTM D3039 standard was used on the tensile strength test for composite material. Instron 5982 universal testing machine was utilized to measure the tensile properties of CF/PPS specimens under various isothermal heat treatment. When the tensile test is carried out on the specimen, the specimen must be clamped in a wedge-shaped made of aluminium and the length of the lower and upper clamping is consistent. The equipment used was Instron 2580-301, and 2 mm/min of strain rate was set. Throughout the measurement, resistance meter present on the dynamic strain measuring system must be firm. The tensile strength test will be executed on until the specimens reach its breaking point. Finally, the load-displacement and stress-strain curve to five specimen will be tested in exact condition in order to remove potential errors and collect precise result (Liu, Zhou and Wang, 2020).

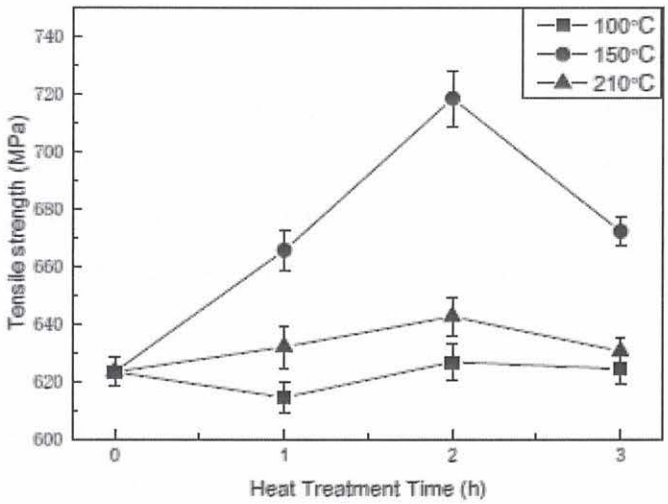


Figure 2.20: CF/PPS tensile strength result under various isothermal heat treatment (Liu, Zhou and Wang, 2020).

Table 2.6: CF/PPS mechanical properties result under various isothermal heat treatment (Liu, Zhou and Wang, 2020).

| Specimen number | Tensile strength/MPa |
|---|---|
| T-as-received | 623.1 ± 5.0 |
| T-100°C-1 h | 614.3 ± 5.2 |
| T-100 °C-2 h | 626.6 ± 6.3 |
| T-100 °C-3 h | 624.2 ± 5.3 |
| T-150 °C-1 h | 665.4 ± 7.1 |
| T-150 °C-2 h | 718.2 ± 9.8 |
| T-150 °C-3 h | 671.9 ± 5.1 |
| T-210 °C-1 h | 631.8 ± 7.2 |
| T-210 °C-2 h | 642.4 ± 6.5 |
| T-210 °C-3 h | 630.3 ± 4.6 |

Figure 2.21 displayed the CF/PPS tensile strength curve after isothermal heat treatment at 100°C, 150°C and 210°C. Table 2.6 indicate the test result. CF/PPS tensile strength experienced significant improvement to different stage compared with the as-received specimen (laminate with zero heat treatment). As a result, when CF/PPS laminate is under the condition of isothermal heat treatment temperature of 150°C and heat treatment time of 2 hours, the specimen obtained the best tensile strength at the level of 718.2 MPa, increased by 15.3% comparing with that of the as-received specimen. Therefore, it was clear that after CF/PPS received isothermal heat treatment at a suitable time and temperature, it can gave a better improvement for CF/PPS tensile strength (Liu, Zhou and Wang, 2020).

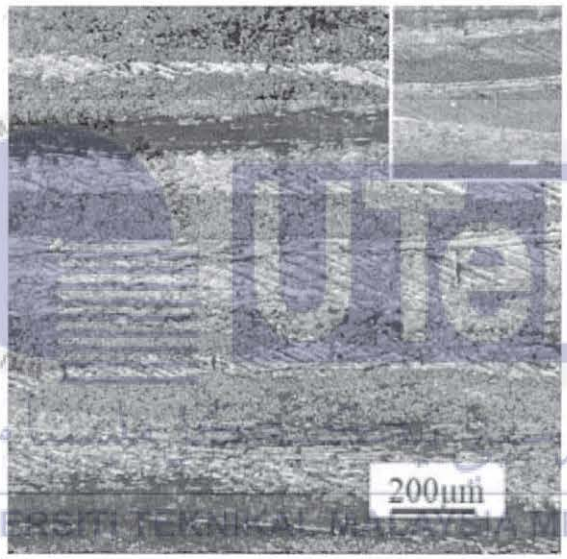


Figure 2.21: Transversal morphology of CF/PPS laminate as-received (Liu, Zhou and Wang, 2020)

### 2.6.4 Experiment 4 (Thermal Gravimetric Analysis)

TGA was conducted to measure weight changes as a function of time and temperature. The weight transpose of polymer can be caused by oxidation and decomposition reactions which lead to physical processes such as vaporization, sublimation, and desorption.

PPS/GF composite materials with 30% (weight content) short glass fibre are kindly supplied by Valeo Company France in the form of injected plate. The material presents a water absorption of about 0.02% and density of 1.58 g/cm$^3$ (Zuo *et al.*, 2018).

Thermal mass change of PPS/ GF samples using TGA Q500, the temperature program is 10°C/min in the nitrogen atmosphere (40 ml/min) from room temperature to 800°C. The original which is put in the $Al_2O_3$ crucible has a sample mass of 12.32 mg. This study may give an idea about the thermal distribution of GF/PPS (Zuo *et al.*, 2018).

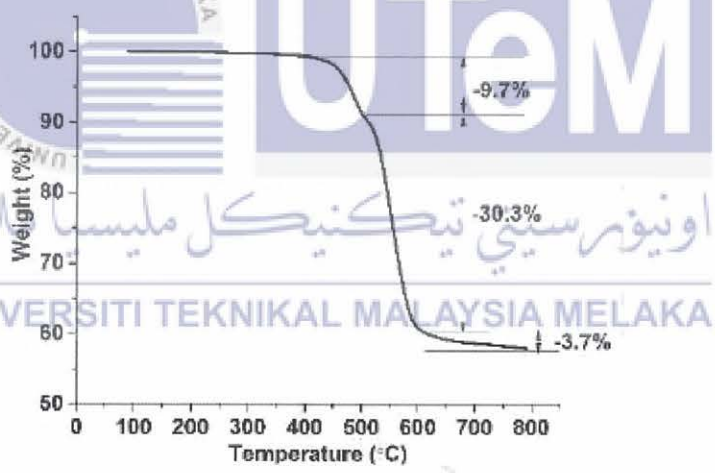




Figure 2.22: TGA curve for PPS/GF (Zuo *et al.*, 2018)

Figure 2.22 recorded TGA curve for PPS/GF. The results show that the PPS/GF has no obvious weight loss before 370°C. Until it reaches to 500°C, the sample losses almost 10% of its initial weight. Then, the movement of weight loss changes recorded another process. At the end of TGA test, all matrices will be transformed and only the glass fibres remain intact inside the the system (almost 60%). In view of the TGA

results, it was safe to say that PPS/GF possessed a good thermal stability (Zuo *et al.*, 2018).

## 2.7 Properties of Thermoplastic

Some types of thermoplastics are strong, expensive, and used in place of metal, while the rest are used in typical daily products. They are easy to shape and mold when they reach $T_g$, at high temperatures they turn into liquid, when it is are cooled, they turn into solid and hard plastic. The most popular methods of processing thermoplastics are extrusion, injection moulding, and thermoforming. Thermoplastics can be as strong as aluminium or like rubber depending on their chemical bonding. (H. Soffar, 2017).

Thermoplastic polymers such as PA, PP, PU, PEKK, PEI, PES, PET, PE, PEEK and PPS exhibit minimal cross linking; they have reversible mechanical, thermal, and rheological properties and can also be reinforced with fibres such as carbon, glass, or aramid. Unlike thermosets, the key advantage of thermoplastic include better mechanical properties notably in terms of abrasion, impact, unlimited shelf life of raw materials, improved assembly can be recycle, and joining method, low tooling cost and rapid cycle time etc (Vaidya and Chawla, 2008).

Table 2.7: Thermal and mechanical properties of reinforced thermoplastic polymers applied in aerospace application (Vaidya and Chawla, 2008)

| Materials | Tensile modulus (GPa) | Tensile strength (MPa) | Melt flow (g/10 min) | Melting point (°C) | Density (g $cm^{-3}$) |
|---|---|---|---|---|---|
| Polypropylene (PP) | 1.50 – 1.75 | 28 – 39 | 0.47 – 350 | 134 – 165 | 0.89 – 0.91 |
| Polyethylene (PE) | 0.15 | 10 – 18 | 0.25 – 2.6 | 104 – 113 | 0.918 – 0.919 |
| Polyurathane (PU) | 0.028 – 0.72 | 5 – 28 | 4 – 49 | 220 – 230 | 1.15 – 1.25 |
| Polyamide (PA) | 0.7 – 3.3 | 40 – 86 | 15 – 75 | 211 – 265 | 1.03 – 1.16 |
| Poly phenylene sulphide (PPS) | 3.4 – 4.3 | 28 – 93 | 75 | 280 – 282 | 1.35 – 1.43 |
| Polybutylene terephthalate (PBT) | 1.75 – 2.5 | 40 – 55 | 10 | 230 | 1.24 – 1.31 |
| Poly ether ketone ketone (PEKK) | 4.4 | 110 | 30 | 360 | 1.31 |
| Poly ether ether ketone (PEEK) | 3.1 – 8.3 | 90 | 4 – 49.5 | 340 – 344 | 1.3 – 1.44 |
| Poly ether imide (PEI) | 2.7 – 6.4 | 100 – 105 | 2.4 – 16.5 | 220 | 1.26 – 1.7 |
| Poly ether sulphone (PES) | 2.4 – 8.62 | 83 – 126 | 1.36 – 1.58 | 220 | 1.36 – 1.58 |
| Poly ether terephthalate (PET) | 2.47 – 3 | 50 – 57 | 30 – 35 | 243 - 250 | 1.3 – 1.33 |

## 2.8 High Performance Thermoplastic in Aerospace Engineering

High-performance thermoplastics (HPTPs) are low volume polymers and high-priced which require extreme mechanical and thermal properties. Moreover, these HPTP are considered lightweight materials in industry and can replace metal parts. These types of polymers represent a very small subset in thermoplastics industry, which consists primarily of medium-volume engineering thermoplastics and high-volume commodity thermoplastics (ihsmarkit.com, 2018).

With the rise of high-performance thermoplastic, thermoplastic composites now dominate for structural applications. Thermoplastic matrix composites possess distinct advantages compared to thermoset matrix composites in terms of high specific strength, recyclability, and cost effectiveness, specific stiffness, enhanced impact toughness, corrosion resistance, and flexibility of design. Since 1990s, the number of combination and material forms fibre reinforced thermoplastic polymers has expanded exponentially, thereby expanding application avenues in military, transportation, automotive, aerospace, and construction sectors (Vaidya and Chawla, 2008).

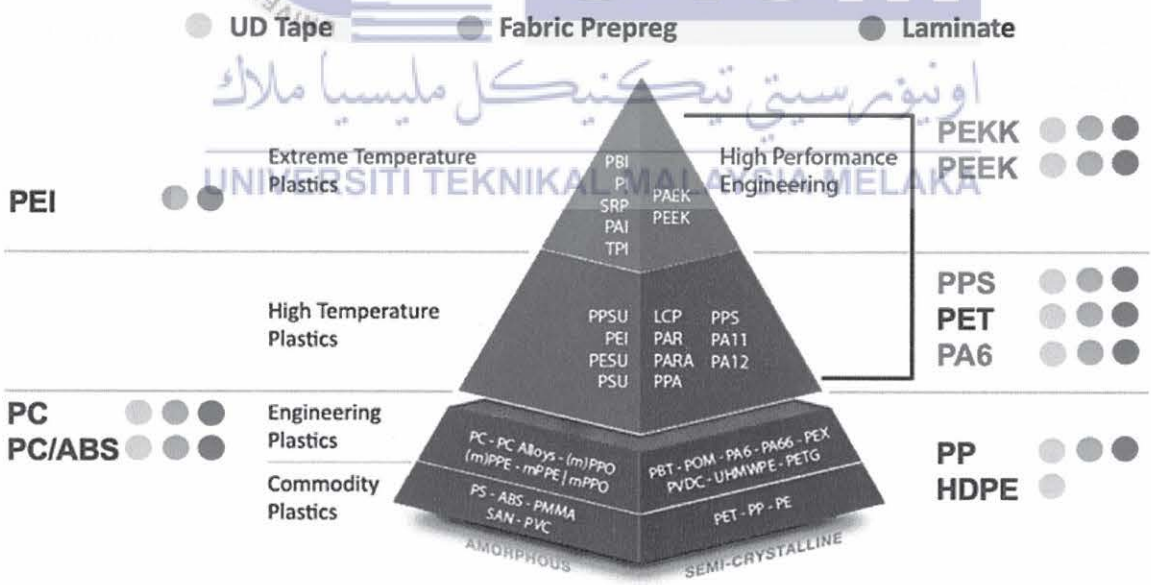


Figure 2.23: Example of range variation for thermoplastic (sekisuiaerospace.com)

## 2.9 Thermoplastic in Future

On 29th October 2020, Boeing has announced that they approved Stratasys Ltd. usage of Antero 800NA as 3D printing. Specifically designed for Stratasys FDM 3D printers in production-grade, Antero 800NA is a PEKK polymer. After a comprehensive analysis of the material performance, Boeing has issued the BMS8-444 specification and added 800NA to the Qualified Product List (QPL). It is the first Boeing qualified material from Stratasys for use in applications with high fatigue demands and chemical resistance. The promising moves means that thermoplastic for Boeing aircraft can now be installed in aircraft (aero-mag.com, 2020).

It is promising the future for aerospace high-performance thermoplastics. This is demonstrated by the recent increase in application numbers. Application to non-structural and structural assemblies will move forward (Offringa, 1996).

## 2.10 Summary

The rise in productive products has shown promising signs towards fibre reinforced thermoplastics in aerospace. Analytical studies confirmed the economic suitability of these product. An increasing number of cost-effective processing techniques approved this material application. A wide application is anticipated for thermoplastic components, which has been possible through the continuous development of the availability of chemically resistant materials and manufacturing technologies.

# CHAPTER 3

# METHODOLOGY

## 3.1 Introduction

Thermoforming is an industrial process that involves a heating step before forming. In most of the thermoforming machine, this step is performed using an infrared oven constituted of long waves infrared emitters. In industry, process start up and control is still based on personal experience and trial and error methods. This leads to varying machine settings, and eventually high start-up times and costs.

This project requires PPS sheet materials to be heated for 320$^{O}$C within 8 minutes using two infrared (IR) heated surface. Therefore, the aim of the study is to determine the heater surface distance and its temperature to achieve the requirement. An unsteady numerical method of radiative transfer is developed to compute the heat distribution between the heater and a thermoplastic sheet. 3D control-volume software, called ANSYS, has been developed to compute heat transfer during the infrared-heating step. At the end of the simulation, it is hypothesized that to determine the heated surface temperature and distance between two heated surfaces.



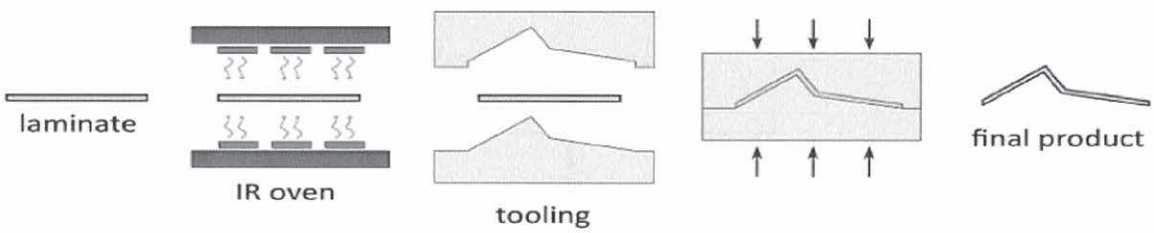


Figure 3.1: Illustration of thermoforming process.

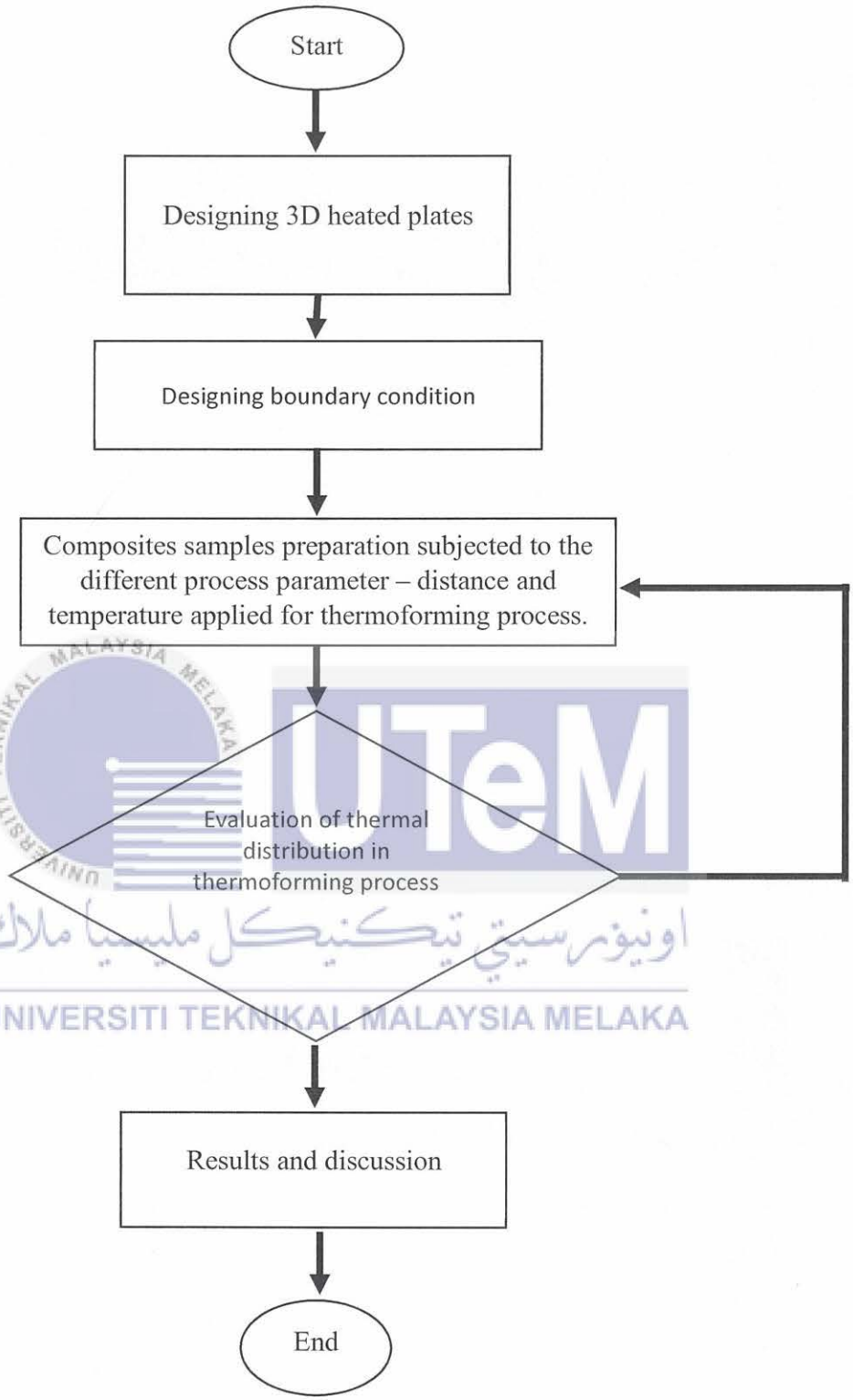




Figure 3.2: Methodology process.

| Job scope | Weeks | | | | | | | | | | | | | | |
|---|---|---|---|---|---|---|---|---|---|---|---|---|---|---|---|
| | 1 | 2 | 3 | 4 | 5 | 6 | 7 | 8 | 9 | 10 | 11 | 12 | 13 | 14 | 15 |
| Literature review | | | | | | | | | | | | | | | |
| Preparation of Sample | | | | | | | | | | | | | | | |
| Final Report of Final Year Project | | | | | | | | | | | | | | | |

Figure 3.3: Gantt chart of FYP I

| Job scope | Weeks | | | | | | | | | | | | | | |
|---|---|---|---|---|---|---|---|---|---|---|---|---|---|---|---|
| | 1 | 2 | 3 | 4 | 5 | 6 | 7 | 8 | 9 | 10 | 11 | 12 | 13 | 14 | 15 |
| Review on mechanical and thermal properties | | | | | | | | | | | | | | | |
| Simulation of Sample | | | | | | | | | | | | | | | |
| Final Report of Final Year Project | | | | | | | | | | | | | | | |

Figure 3.4: Gantt chart of FYP II.

Based on the flow chart, the Gantt chart has been produced to make the work schedule much easier and to see the time duration that had been taken in each task that was done. The Gantt chart also help to manage the time parallel with the task given.

## 3.2 Method and Materials

Table 1 shows the total 9 cases study use to investigate the relation between heater distance and heater temperature to the thermoplastic temperature. Three heater temperatures with three heater distances are tested. The distance between two heated surface is 200, 300 and 500 mm for 320°C, 360°C and 400°C heated surface. The desired PPS temperature (320°C) and maximum heater temperature (400°C) is taken as parameter. While the distance of the heater is based on the comfortable movement of the specimen during the process.

Table 3.1: Total number of case study.

| Case Number | Heater Temperature (°C) | Heater Distance (mm) |
|---|---|---|
| 1 | 320 | 200 |
| 2 | 320 | 300 |
| 3 | 320 | 500 |
| 4 | 360 | 200 |
| 5 | 360 | 300 |
| 6 | 360 | 500 |
| 7 | 400 | 200 |
| 8 | 400 | 300 |

### 3.2.1 Domain Geometry and Meshing

The geometry domain in the present task for the heating area are simple cuboid shape with 600 mm x 600 mm base area. The height of the domain which represent the heater distance are varied according to the simulated case. Figure 3.4, 3.5 and 3.6 shows the domain geometry of the simulated case for 200 mm, 300 mm, and 500 mm heater distance, respectively. The thickness of the plastic plate is constant 6 mm as per PPS sample thickness.

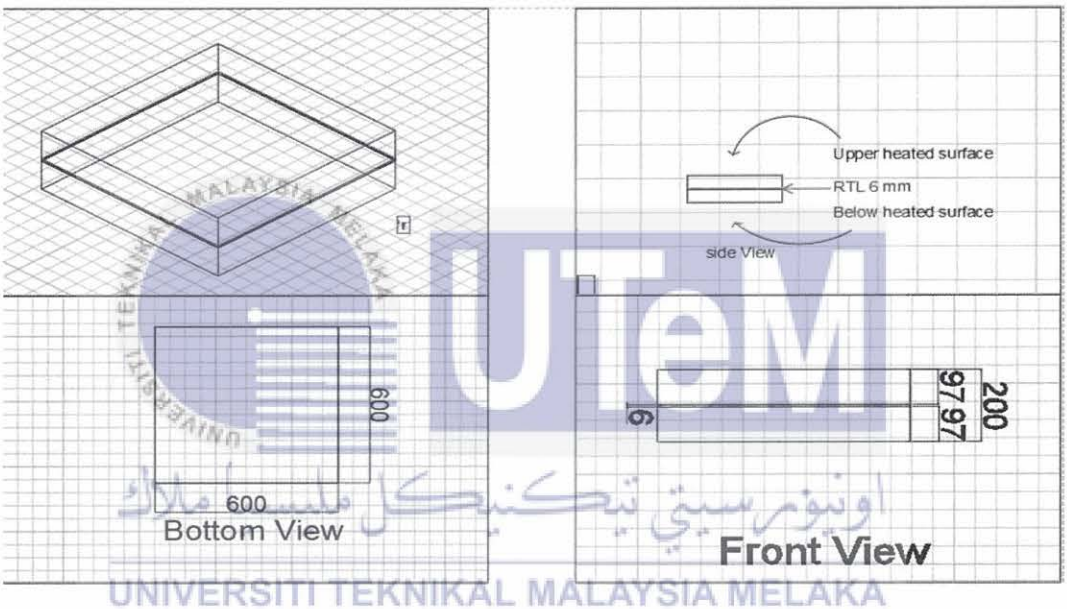




Figure 3.5: 3D modelling for PPS heating process for 200 mm distance between two heated plates. All units in mm.

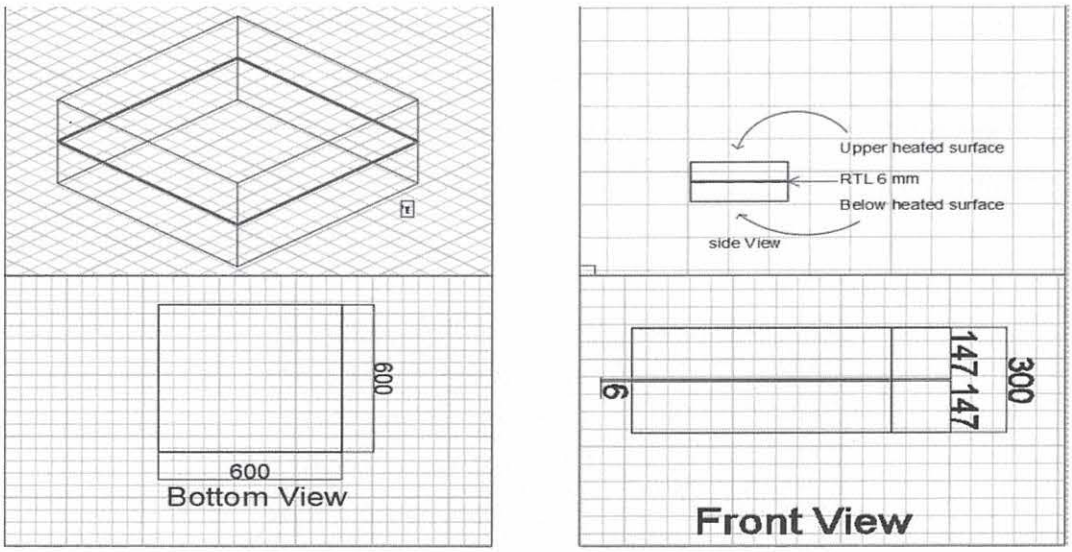


Figure 3.6: 3D modelling for PPS heating process for 300 mm distance between two heated plates. All unit in mm.

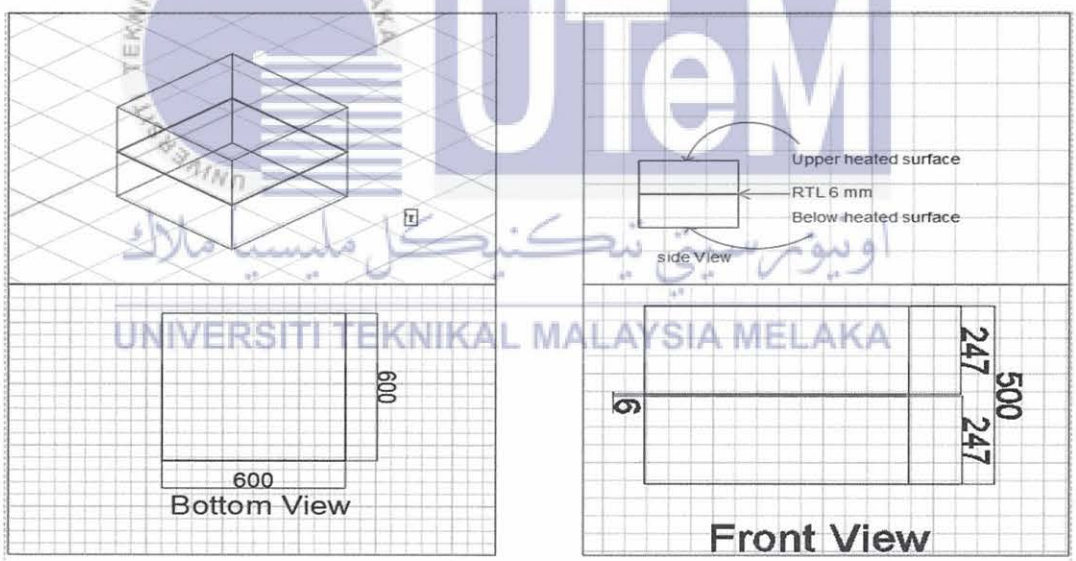




Figure 3.7: 3D modelling for PPS heating process for 500 mm distance between two heated plates. All unit in mm.

Figure 3.7 shows the example meshing for the 500 mm heater distance. The maze cell size use is 1.0 x 102 m with minimum of 4.9 x10-4 m. For this geometry, the number of elements is 183,600. All case is use similar face size but different number of elements depending on domain size. Separate study shows that this mesh number achieve the grid independent test.

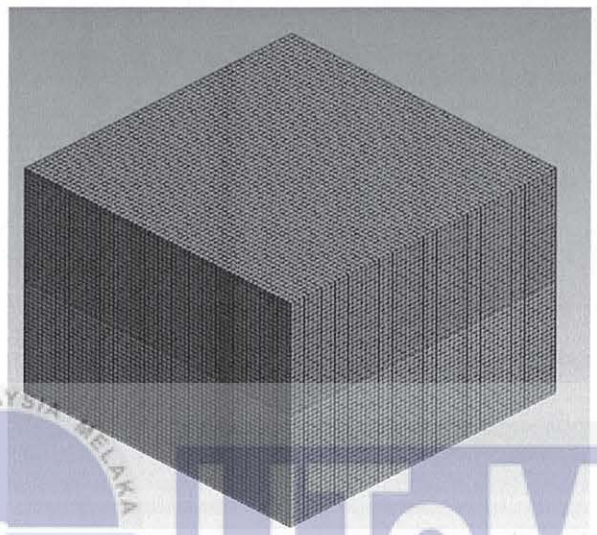

Figure 3.8: The mesh modelling with maximum size 6mm size element.

### 3.2.2 Boundary Condition

The boundary condition in the present study comprises of two main parts as shown in Figure 3.8. The first one is the heated surface located at the upper and bottom of the domain. These two heated surfaces imposed free stream and radiative temperature valued either 320°C, 360°C or 400°C depends on the case studied. The heat transfer coefficient is taken as 20 $W/m^2K$ as the general value for the contacting air undergone natural convection. Detail value of boundary condition was provided in Table 3.2.

The second part is the side wall of the domain consist of four surfaces. All surface of this domain is assumed zero heat flux means no heat loss would occur. Although this assumption is a bit impractical due to non-zero heat loss for real situation, the outcome of the study is concerning for the ideal and worst-case scenario.



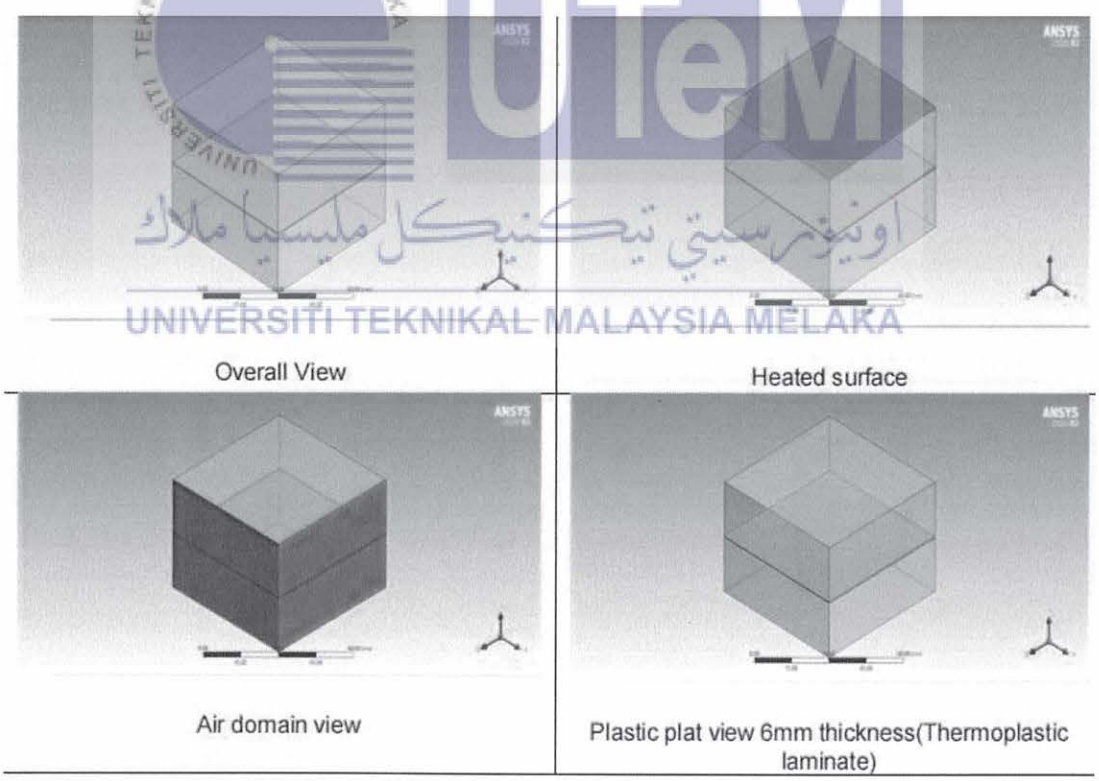


Figure 3.9: The modelling for PPS heated process for 500 mm distance between two heated surfaces in ANSYS.

Table 3.2: Boundary condition use in present task

| Properties | Heated Surface | Domain Wall |
|---|---|---|
| Mode of heat transfer | Mixed (Rosseland Radiation) | Insulation |
| Free stream temperature (°C) | 320/360/400 | N/A |
| Heat Flux | 0 | 0 |
| Heat transfer coefficient ($W/m^2K$) | 20 | N/A |
| External emissivity | 0 | N/A |
| External radiation temperature | 320/360/400 | N/A |
| Heat generation rate | 0 | N/A |

### 3.2.3 Material Properties

Table 3.3 shows the material properties of the substance use in the present simulation. The main material is used which are PPS plate, air, and infrared heater.

Table 3.3: Material properties of the domain studies.

| Properties | PPS Plate | Air | Infrared Heater |
|---|---|---|---|
| Density ($kg/m^3$) | 1600 | 1.225 | 2719 |
| Specific heat (J/kgK) | 871 | 1006 | 871 |
| Processing Temperature (°C) | 320 | N/A | N/A |
| Thermal Conductivity (W/mK) | 0.19 | 0.0242 | 202.4 |
| Viscosity (kg/m.s) | N/A | $1.79 \times 10^{-5}$ | N/A |
| Absorption coefficient (1/m) | N/A | 0 | N/A |
| Scattering coefficient (1/m) | N/A | 0 | N/A |
| Scattering phase function | N/A | 1 | N/A |
| Refractive index | N/A | 1 | N/A |

## 3.3 A Review on Mechanical and Thermal Properties of PPS Composite

In this study, 10 papers have been reviewed to study the mechanical and thermal properties of PPS composite. We want to identify PPS behavior under various parameter; therefore, it can help us to understand more about the influence of those experiments towards PPS. Their findings can provide some preliminary knowledge to engineers and scientists in the field and develop new set of structural composites.

Khairul et. al. (2016) studied the effects of UV light towards the mechanical properties of carbon fiber reinforced PPS thermoplastic composites. The objective of their studied is to evaluate the correlation between thermoplastic fabrication parameters the final properties of composites. Wabash heat press machine was used to produce the carbon fiber reinforced PPS thermoplastic composite laminates. Ten plies of carbon fiber were used with PPS composites as the first and final layer to avoid dry fibers. After the samples we cooled, they were machined to the desired dimensions. Regarding the degradation of CF/PPS laminate resulting from UV exposure, the samples were put in the QUV weathering chamber with three fluorescent lamps. UVA-340 were used to replicate the UV rays of sunlight with the wavelength region of 290-365 nm. The samples were exposed to the UV radiation for duration of 120, 240, 360, and 480 hours at room temperature (30°C). After that, they will be removed and tested. The condition of the specimen and light intensity were monitored periodically to guarantee accurate test results.



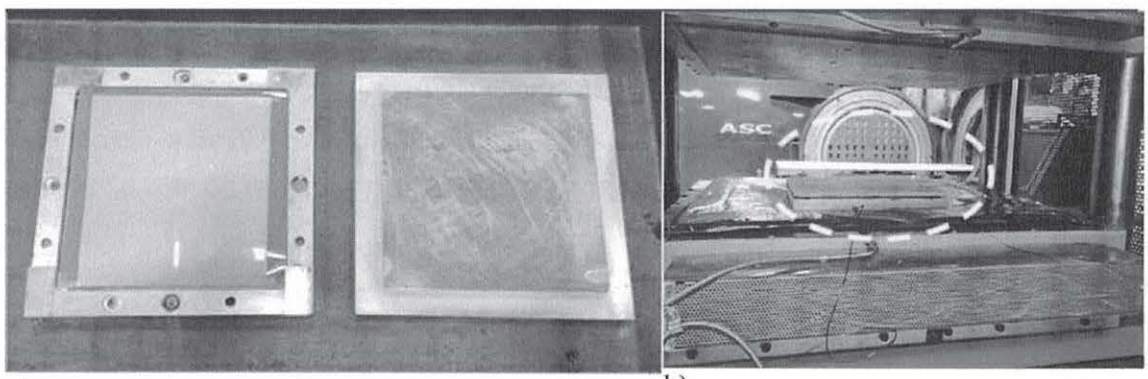


a) b)

Figure 3.10: a) Film stacking method, and b) Mold secured inside the hot pressed machine (Mahat *et al.*, 2016).

Tensile test was done by using MTS 810 servo hydraulic testing machine. It was used to observe the change in tensile properties of the specimen that were subjected to UV. The specimen size was 127 x 25.4 x 1.8 mm with a strain rate of 2 mm/min. The test was performed by following ASTM D3039 with 240-grit sandpaper was used at the end of the specimen to enhance the grip between the specimen and tensile clamp. Three sets of specimens for each UV conditions were tested to ensure repeatability.

Mustafa et. al. (2016) studied the influence of heat treatment towards mechanical properties of surface treated volcanic ash particles on PPS composites. There are two objectives for this experiment. First is ecology and economy being the second. In their study, the specimens undergo heat treatment in a vacuum oven at 200°C for 2 hours according to differential scanning calorimetry (DSC) analysis of pure PPS. Then, the samples were heated at 10°C/min from room temperature to the thermodynamic melting point of 340°C under the influence of nitrogen gas flow of 50 ml/min. After the completion of the heat treatment process, PPS samples were left to cool down to room temperature in the oven and carefully observed for homogenous and phase separation. Later, tensile test was carried out at a crosshead speed of 1 mm/min according to ISO 527-2. 5 samples were tested, and the average tensile strength and modulus were reported with standard deviations.

Avcu et. al. (2014) did a study concerned with thermal and mechanical properties of VA-filled PPS composites. The objective their studied was to improve engineering properties of polymer composites and to lower the cost of final products. In their study, TA Instruments Q50 TGA was used to collect the TGA of the samples. The samples with the size of 2 x 4 x 27 $mm^3$ were prepared. 10 mg of the samples were heated from ambient to 700°C at a heating rate of 20°C/min under a nitrogen atmosphere with the flow rate of 50 ml/min. Thermal degradation characteristic were determined from TGA curves. The temperature at 10 wt% loss ($T_{10}$) was taken as the onset of degradation and the maximum degradation temperature ($T_m$) was determined as the peak maximum obtained by the first order derivative weight curve.

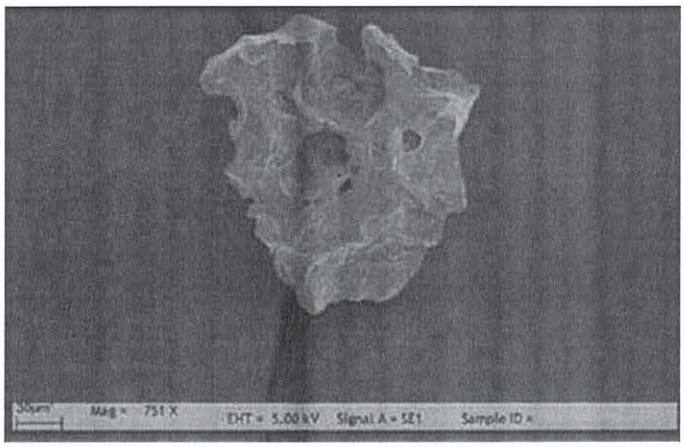


Figure 3.11: SEM images of filling VA (Avcu *et al.*, 2014)

Flexural test was conducted on uneroded and eroded samples having dimensions of 80 x 10 x 4 $mm^3$ by using Shimadzu AG-X test machine having a load cell of 10 kN. Five test samples of VA/PPS were tested according to ASTM D790 method. The crosshead velocity in flexural test is 2 mm/min. The results obtained were correlated with a function of flexural strength and flexural modulus.

Benoit et. al. (2014) did a study concerned to post fire behavior of CE/PPS and epoxy-based laminates for aeronautical applications. The general idea of this study is to find out whether it is relevant to replace epoxy composites by TP based (PPS) composites for applications in nacelles of plane's engines. Therefore, to meet the exact requirements, it was necessary to evaluate how detrimental a prior thermal stress can be on the post high-temperature tensile mechanical PPS-based laminates compared to epoxy-based laminates.

In their study the toughened PPS resin (Fortron 0214) and the epoxy resin (914) were supplied by Ticona and Hexcel Companies. Volume fraction each of the fibers is 50% in laminates. The prepreg plates are hot pressed into two lay-ups. The first lay-up [(0/90), (±45), (0/90), (±45), (0/90), (±45), (0/90)] can be considered as quasi-isotropic (Q-I) which is suitable for application in aircraft engine nacelles. Second stacking sequence [±45] which can be defined as an angle-ply (A-P) lay-up is not suitable for aircraft structural application. For each lay-up, dog-bone specimens were cut by using water jet from 600 x 600 $mm^2$.

For fire exposure test method, radiant heater of a cone calorimeter to burn laminate specimens were used. The significant advantage of this test is that the heat flux and heating conditions are repeatable and well controlled. Due to the usage of cone heater, three different heat release rates (20 kW/m$^2$ – 35 kW/m$^2$ – 50 kW/m$^2$) have been applied to the specimens for different exposure times (1 – 2 – 5 min). After fire exposure test, all the samples were cooled in the air for one night.

MTS 810 servo hydraulic testing machine were used for thermomechanical testing. The test was performed by using a 100 kN capacity load cell and the temperature control system includes an oven and a temperature controller at 120°C. The mechanical properties were gathered according to EN 6035.

Carpier et. al. (2018) did a study of CF/PPS Composites mechanical and thermal behavior when exposed to heat flux and constant compressive force. The objective of their study was to investigate the deformation mechanism along with damage evolution in 5-harness satin weave carbon fabric reinforced PPS laminates subjected simultaneously to compressive loading and fire exposure whose effect was reproduced by using radiant heater. In their study, 7 plies of carbon fiber reinforced PPS prepreg laminate plates were arranged to the following quasi-isotropic lay-up: [(0/90), (±45), (0/90), (±45), (0/90), (±45), (0/90)]. The specimen thickness is 2.2m and consist of 50% volume fraction of fibers. The glass transition temperature $T_g$ of PPS is 98°C and the melting temperature, $T_m$ is 280°C as measured by DSC. For this study, thermal decomposition was considered starts at 490°C and the specimens used for the mechanical tests were 150 x 100 mm$^2$.



Cone calorimeter was used to heat vertical laminate specimens subjected to a constant load. In this study, the imposed heat flux has been set to 50 kW/m$^2$ because it was enough to cause thermal decomposition to enable creep and prevent from quick oxidation. Aluminum tape was chosen for its low emissivity has been placed onto the front of the specimens to limit the region to be exposed to fire to a 75 x 70 mm$^2$ area. The heat flux distribution of the exposed surface was measure with a heat flux gauge.

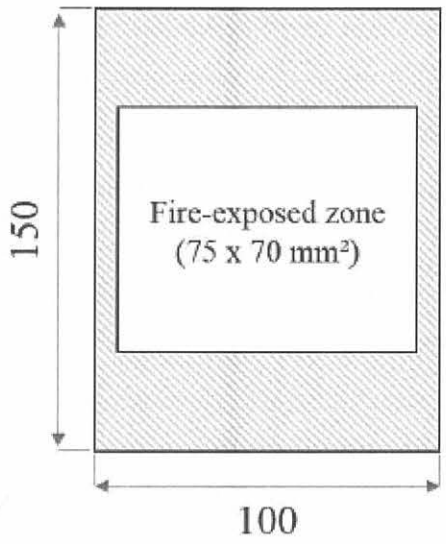


Figure 3.12: Specimen size (Carpier *et al.*, 2018)

Compression test were carried with a 100 kN MTS 810 servo hydraulic machine. The accuracy of the machine ±0.150 kN. There were two different tests were carried out where the first test aims at determining which maximum stress levels can withstand the specimens under monotonic compression. The specimens are first exposed to heat flux and the compression loading was applied after 100 seconds (approximate time needed to reach a thermal equilibrium) at a constant crosshead speed of 0.2 mm/min hence following the standard Airbus AITM 1-0010. The second experiment aims studying the response of a composite part in a service condition if a fire breaks out. The specimens were subjected to a compressive force with a value was 75%, 50% and 25% of the ultimate force $F_u$ measured during the monotonic compression under fire. The force is kept constant while the specimens were exposed to heat flux. For each test, three samples have been tested.

Liu et. al (2020) work concentrates on the crystallinity, tensile strength and failure mode of CF/PPS laminate subjected to isothermal heat treatment of different temperatures and time periods. In this study, the aimed was to investigate the change of crystallinity and the effect on their mechanical properties. Universal testing machine was used to test and calculate the change of differentiation isothermal heat treatment on the tensile property of the material. CF/PPS was cut into 200 mm x 25 mm x 2 mm by using high pressure water jet cutting technology then the sample were then dried at 60°C in the vacuum drying oven for 2 hours. The heat treatment temperatures for the CF/PPS laminate specimens in this test are selected as 100°C, 150°C, 210°C and 270°C, respectively. Three different heat treatment times have been conducted under each temperature which are 1 hour, 2 hours and 3 hours. Each specimen was cooled down to ambient temperature by itself. After that, the specimens were tested for tensile strength. At every condition, four to five specimens have been tested to get an average value.

Tensile test according to ASTM D3039 standard on the tensile strength test for composite materials was used. Instron 5982 universal testing machine was used to test the tensile properties of CF/PPS specimens under the influence of isothermal heat treatment conditions. The strain rate is set as 2 mm/min and the test will be carried on until to the fracture failure of the specimens. Four to five specimens will be tested in under the same condition to eliminate potential errors and obtain more accurate results.

Faria et. al. (2011) studied the effect of the ocean water immersion and UV ageing on the dynamic mechanical properties of the PPS/GF composites by using DMA instruments. The aimed for this study was to evaluate how the salt water and the UV light radiation conditioning affect the viscoelastic properties of the PPS/GF laminates.

The specimen's dimension was followed using ASTM D 1141-98. In their study, the saltwater solution pH was adjusted to 8.2 to replicate sea water. Three samples were immersed into a container that contain artificial ocean water solution which was heated at 60°C. The purpose was to accelerate water diffusion process and the specimens were kept immerse during 1000 h.

To reproduce damages resulted from UV light radiation influenced with water condensation, the PPS/GF specimens were placed into a weathering chamber and exposed it to different conditions as 650, 1300, and 1900 h. The degradation mechanism was determined in accordance with ASTM G 154. The UV-B radiation is generated by fluorescent UV lamps that

have 295 – 365 nm in wavelength. The light intensity was calibrated every 400 h of service with the purpose of evaluate the lamps performance.

DMA was used to determine changes $T_g$ in the PPS/GF composites. It was performed at a fixed frequency of 1 Hz. The temperature heating rate was 3°C/min from 20 to 250°C. Four specimens for each situation were used in the DMA measuring 60 x 10 x 2 mm and were performed in a DMA 2980 Thermal Analysis instrument.

Pantelakis et.al (2007) did a study about effect of a thermal treatment on the in-plane shear behavior of carbon fiber reinforced PPS composite specimens. The studied investigate the effects of the PPS resin evolution during melting in air at temperatures that are relevant for processing PPS on the mechanical properties.

The laminates were produced including eight plies in a stacking sequence of [0/90°] and the thickness each of the laminate was 2.5 mm. The consolidation was made at 325°C (±5°C) with under pressure of 20 bars. Heating speed to the dwell temperature was 3°C/min, the consolidation time was 20 min. Cooling was under pressure at a cooling rate of 5°C/min.

In-plane shear test dimension was rectangular 25 x 230 mm according to the Airbus AITM 10002 specification were used. Diamond band saw according to the ISO 2812 were used to cut the laminates in ±45°. To obtain longitudinal and transverse strain during testing, Kyowa biaxial strain with a gauge length of 5 mm were attached at the centers of both faces each to have a mean value of two measurements. The tests were carried out with a constant elongation rate of 1 mm/min. The properties evaluated were in-plane shear strength and in plane shear modulus.

Vieille et. al. (2013) conducted an experimental study to investigate changes in the mechanical behavior of carbon woven ply PPS laminate obtain from thermo-compression for aeronautics purpose. The woven ply prepreg laminate consists of 5 Harness satin weave carbon fiber fabrics in a toughened PPS resin matrix. The mass fraction is 57% and volume fraction of carbon fibers is 50%. The specimens were obtained from hot pressed prepreg plates according to two lay-ups: [(0/90), (±45), (0/90), (±45), (0/90), (±45), (0/90)] and [(0/90)]. Finally, the test specimens were sawn from 600 x 600 plates at a minimum distance of 30 mm from the plate edges with a water-cooled diamond saw.

In their study, quasi-static test was performed using a 100 kN capacity load cell of an MTS 810 servo hydraulic testing at room temperature. The temperature control system includes an oven and a temperature controller which set at 120°C. The specimens were exposed to hygrothermal aging for 1000 h in the following environment: 85% RH and 70°C. For tensile test, strains were evaluated with an extensometer and was followed accordance to EN 6035. Four specimens were tested in each configuration (consolidated or stamped) and the average values were recorded with their corresponding the standard deviation.

Zhang et. al. (2014) did a study to investigate the effect of the aminated PPS (PPS – $NH_2$) used as compatibilizer on the mechanical properties of CF reinforced PPS composites. The synthesis of aminated PPS (PPS – $NH_2$) occurred inside of 1000 ml high pressure reactor. Firstly, the mixture was stirred at 180°C for 1 hour to remove the presence of water. Next, DCB and DCA were added into the reactor, stirred at 230°C for 8 hours to yield PPS – $NH_2$ granules. Next the product was washed with water and ethanol and then dried under vacuum 100°C for 12 hours. After 12 hours, the PPS – $NH_2$ was obtained.

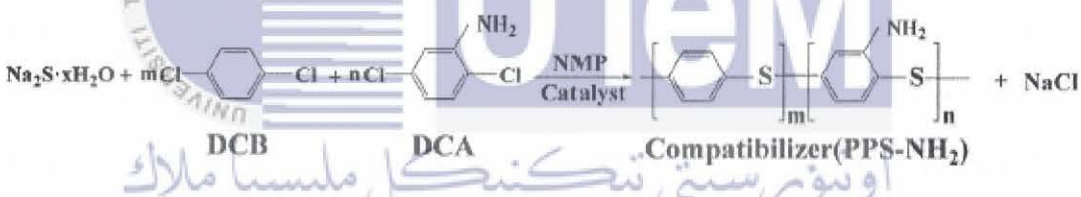


Figure 3.13: Synthesis route of compatibilizers PPS – $NH_2$ prepared by $Na_2S$, DCB and DCA (Zhang *et al.*, 2014).

In this work, tensile properties and flexural properties of PPS/CF composite and PPS/PPS – $NH_2$/CF composites were performed using Universal Testing Machine (Instron 5567, USA) at ambient temperature according to ISO 527 and ISO 178, respectively. Each value that was obtained represented the average of five samples.

# CHAPTER 4

# RESULTS & DISCUSSION

## 4.1 PPS Temperature Distribution During Preheating Process

In this study, steady-state thermal analysis was used in ANSYS Workbench software. It evaluated the thermal equilibrium of a system which in isothermal state (constant temperature over time). In general, the analysis assessed the state of equilibrium of PPS laminate under constant heat loads and environmental conditions.

Figure 4.1, 4.2 and 4.3 shows the thermoplastic temperature at 320°C, 360°C and 400$^0$C respectively for different heater distance. As expected, the shortest distance provides higher and fastest heat distribution. For a 320°C heater temperature, there are no distance can achieve 320°C temperature for thermoplastic plate within 8 minutes. Same situation goes for 360oC heater plate in Figure 7, with the highest temperature are 310°C for 200mm heater distance.

For the heater temperature of 400°C in Figure 8, 300 mm and 500 mm heater provide closed to the required thermoplastic temperature with 312°C and 308°C each. The 200 mm heater temperature achieve target temperature of 320°C as early as 6 minutes as high as 350°C after 8 minutes. Therefore, as of now, the choice of 400°C heater temperature and 20mm heater distance could fulfil the requirement criteria.

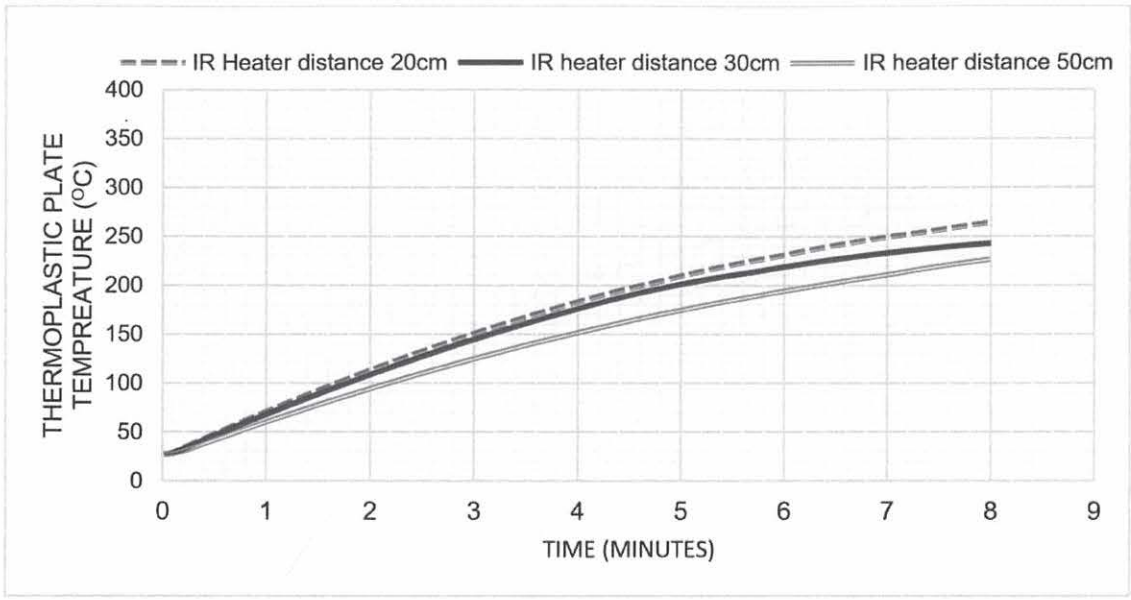


Figure 4.1: PPS plate temperature at heater temperature 320°C for various infrared (IR) heater distance.

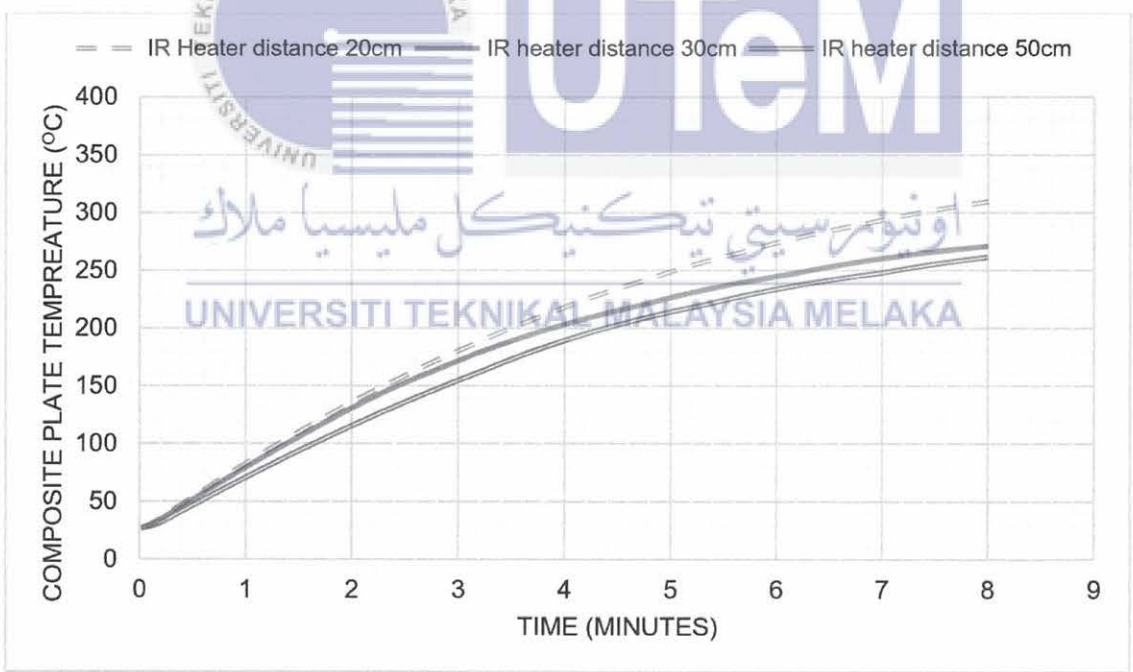




Figure 4.2: PPS plate temperature at heater temperature 360°C for various infrared (IR) heater distance.

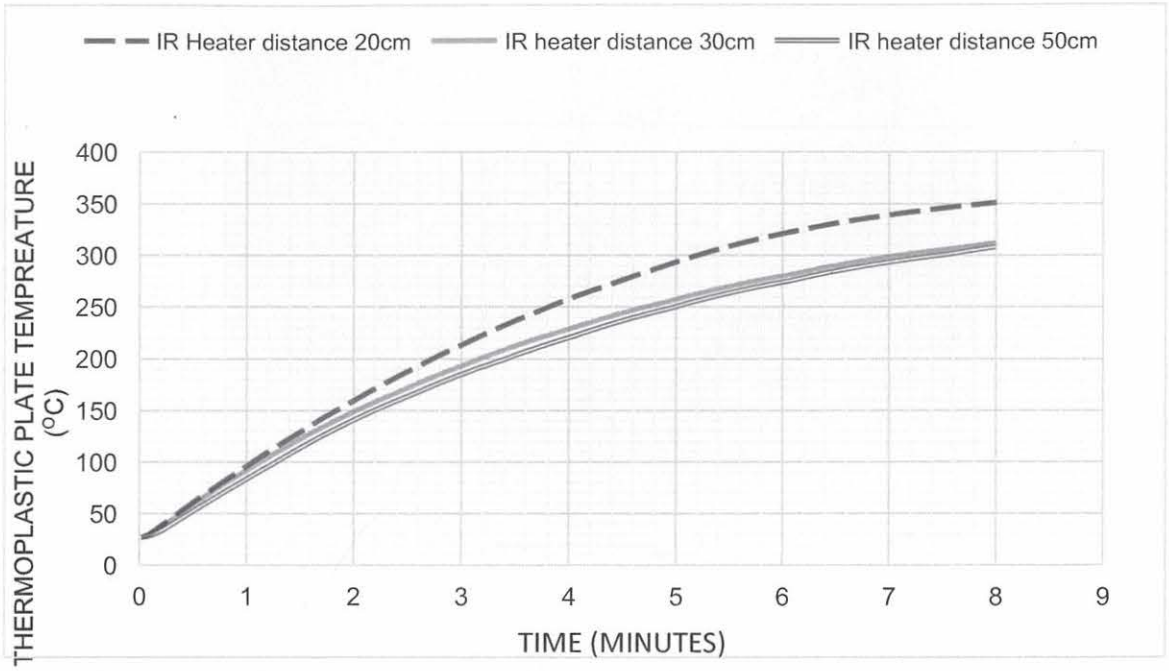


Figure 4.3: PPS plate temperature at heater temperature 400°C for various infrared (IR) heater distance.

Figure 4.4 shows the temperature distribution of the thermoplastic plate at 8 minutes for the 400°C heater temperature and 200 mm infrared heater distance. As seen, the temperature is uniform with 624 K (351°C).

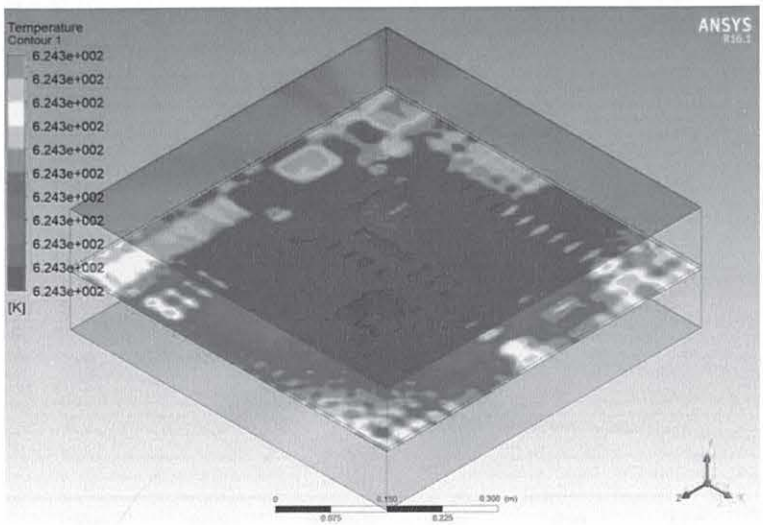


Figure 4.4: Sample contour shows uniform temperature distribution at 400°C heater and 200mm heater distance.

## 4.2 Optimum Heater Temperature and Distance After 8 Minutes

In this section, two additional results are present. There is effect of heater distance at different heater temperature and effects of heater temperature at different heater distances. These two results could provide estimated data based that is not lying on previous simulated case.



For example, in Figure 4.5 which shows the relation of thermoplastic plate temperature against IR heater distance for different heater temperature, one can predict the thermoplastic temperature at 400mm heater distance (not in previous simulated case) and 400°C heater temperature. As can be seen, the maximum thermoplastic temperature can achieve is 310°C. Furthermore, let say if required temperature of thermoplastic is 320°C, the pre-setting heater distance should be set to around 275mm with 400°C heater distance. In addition, IR heater temperature of 360°C and 400°C did not affected much the thermoplastic temperature for the heater distance in between 350 mm to 500 mm.

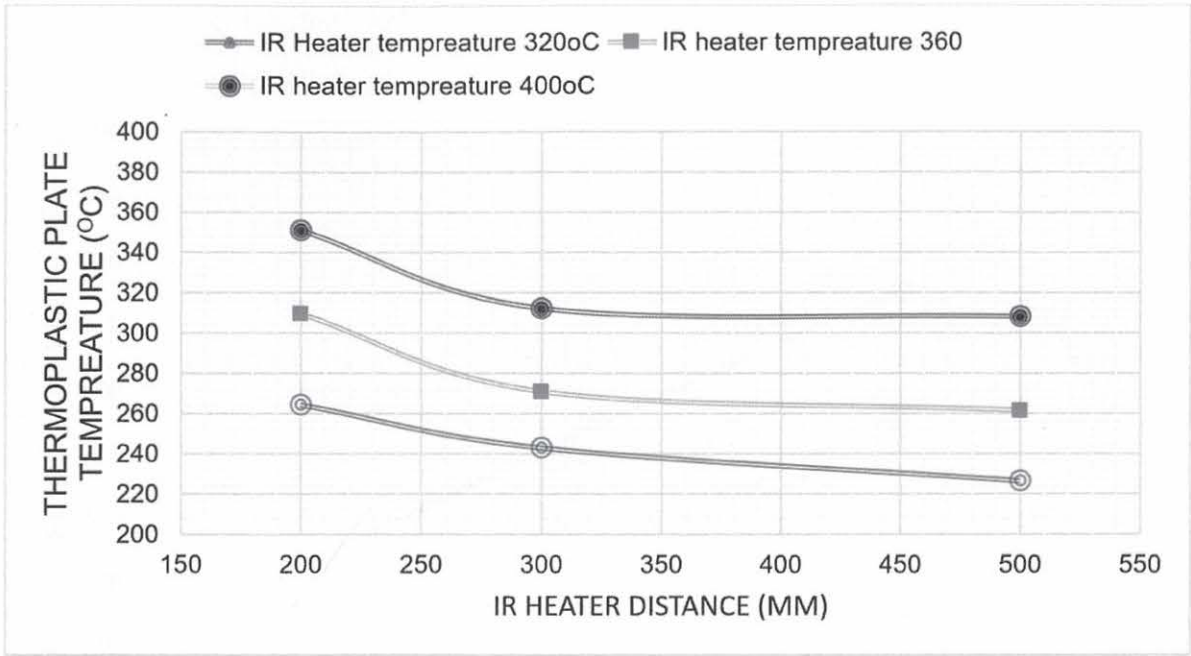


Figure 4.5: PPS plate temperature at 8 minutes for various infrared (IR) heater temperature.

Figure 4.6 shows the relation of thermoplastic temperature to the IR heater temperature with different IR heater distance. As seen, to achieve 320$^{O}$C thermoplastic temperature, we can use 385$^{O}$C IR heater temperature with heater distance of 200 mm. However, this 200 mm distance might be too close for the operation, and larger distance might be needed. Using 300mm or 500mm can achieve close to 320$^{O}$C if heater temperature is set to 400$^{O}$C.

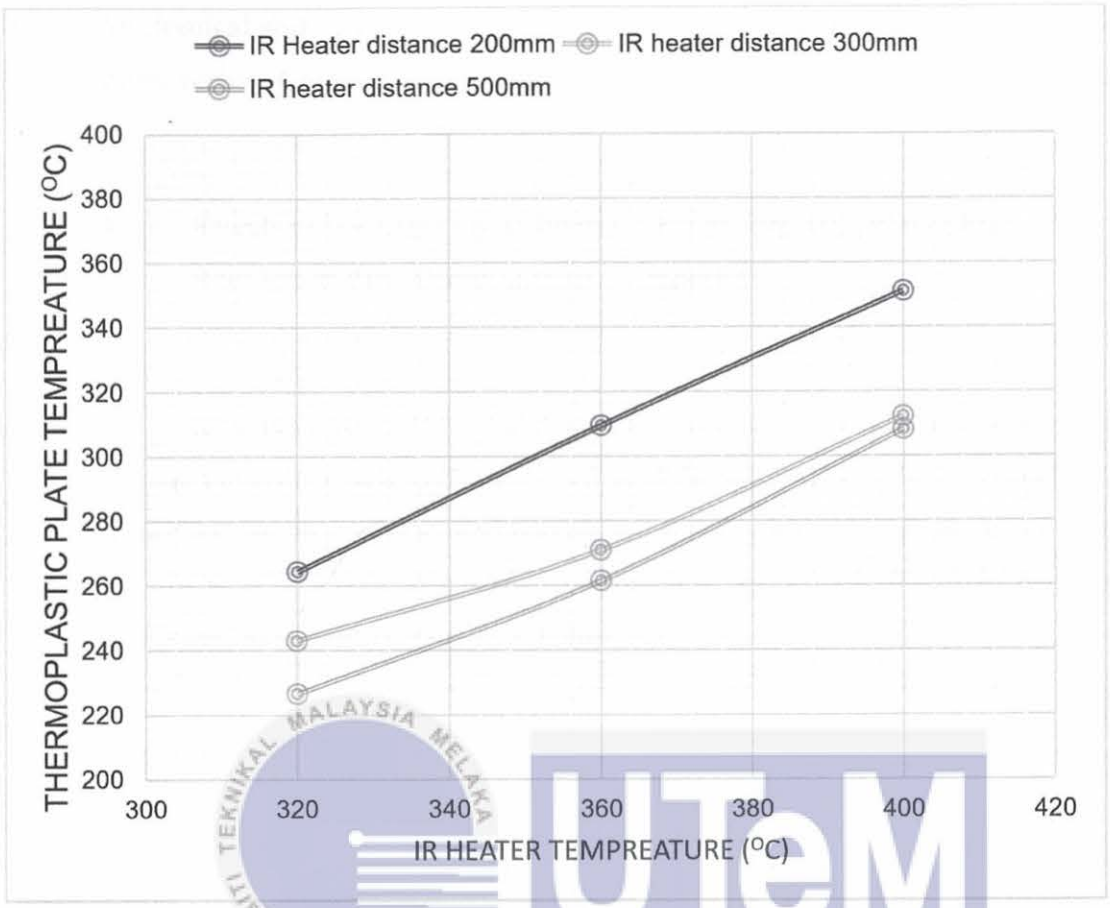


Figure 4.6: PPS plate temperature at 8 minutes for various infrared (IR) heater distance.

## 4.3 Mechanical and Thermal Properties of PPS Composite for Aerospace Engineering: Comparative Study

### 4.3.1 Effects of UV Light on Mechanical Properties of Carbon Fiber Reinforced PPS Thermoplastic Composite

Khairul et. al. (2016) stated that failure occurred at the areas that were relatively close to the grip as well as the mid-section of the specimens in the 0° tensile test. The failure was because of fiber de-bonding and splitting and subsequent delamination of the specimen. The reduction in matrix strength prevents the load transfer between the matrix and fiber which causing the failure.

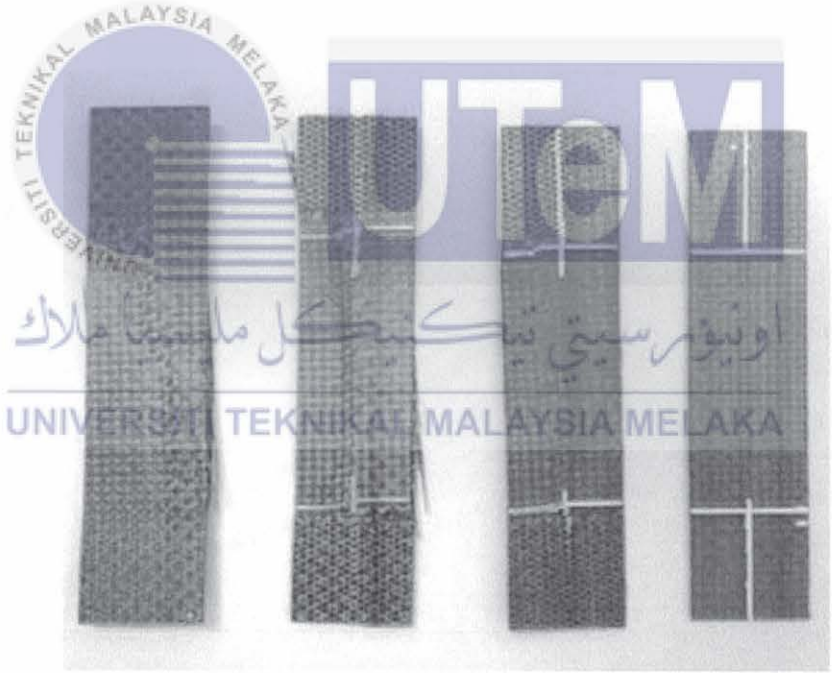



Figure 4.7: Tensile test failure of CF/PPS (Mahat *et al.*, 2016).

Figure 4.8 plots the result of tensile test that was performed on one sample (five specimens) that were exposed to various exposure intervals of UV radiation. The result from tensile strength was obtained from ultimate failure load. The expected tensile strength can be obtained using the laminate theory 'rule of mixture' with the PPS strength value ($\sigma_m$) of 30 MPa and CF fabric strength value ($\sigma_f$) of 840 MPa. According to the rule of mixture equation with fiber volume fraction ($v_f$) of 0.6, the theoretical value of laminate tensile strength is 516.5 MPa. The experimental tensile strength of the specimen of 580.05 MPa as shown in Figure 4.8 is fairly close to the theoretical value.

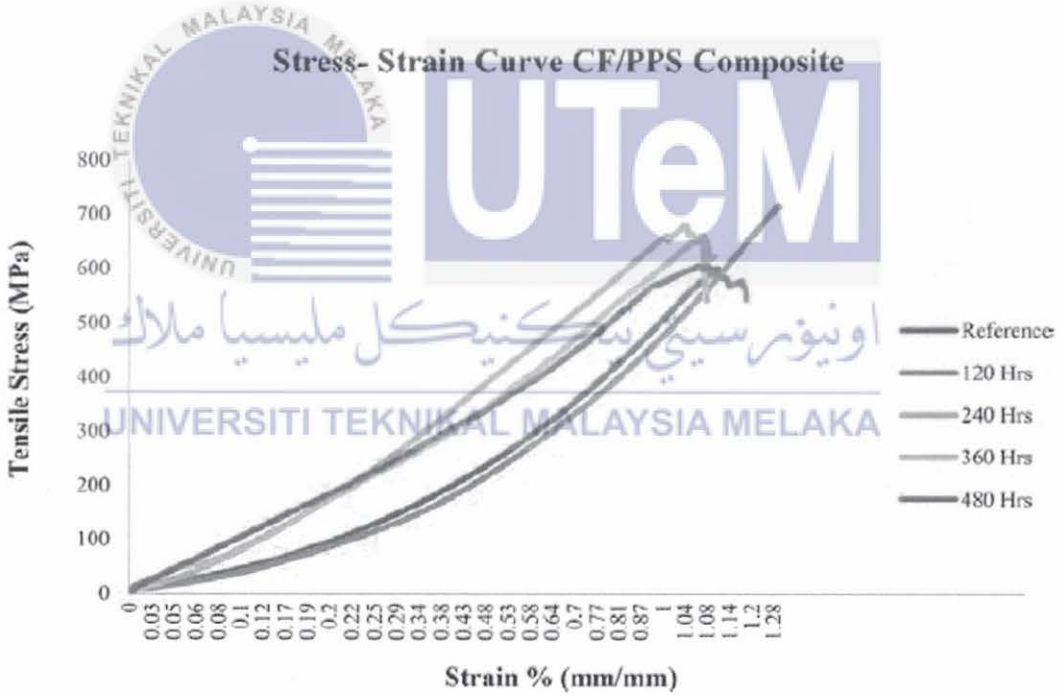


Figure 4.8: Stress-strain curve for one set of samples of the CF/PPS specimens (Mahat *et al.*, 2016).

Three tensile tests were performed for each environmental condition and the average strength is plotted in Figure 4.9. Crystallinity percentage was also included to study the relation between crystallinity and strength. According to Figure 4.9, crystallinity increase with the increase in the duration of UV exposure thus improving tensile strength of the material but at 360 hours of UV exposure the tensile properties of the material experienced sudden decreased. From the observation, it suggested that photo oxidation degradation leads to chain scission is more dominant than the effect of crystallinity thus resulting in reduction strength. The result showed that when CF/PPS was exposed to UV radiation, the crystallinity and chain scission mechanism operate in a competing manner which mean while crystallinity improved the properties while chain scission induces the degradation process. Furthermore, chain scission reduced the polymer molecular weight where leads to excessive brittleness and micro cracking in the polymer. Finally, modulus of CF/PPS composite also shows similar behavior.

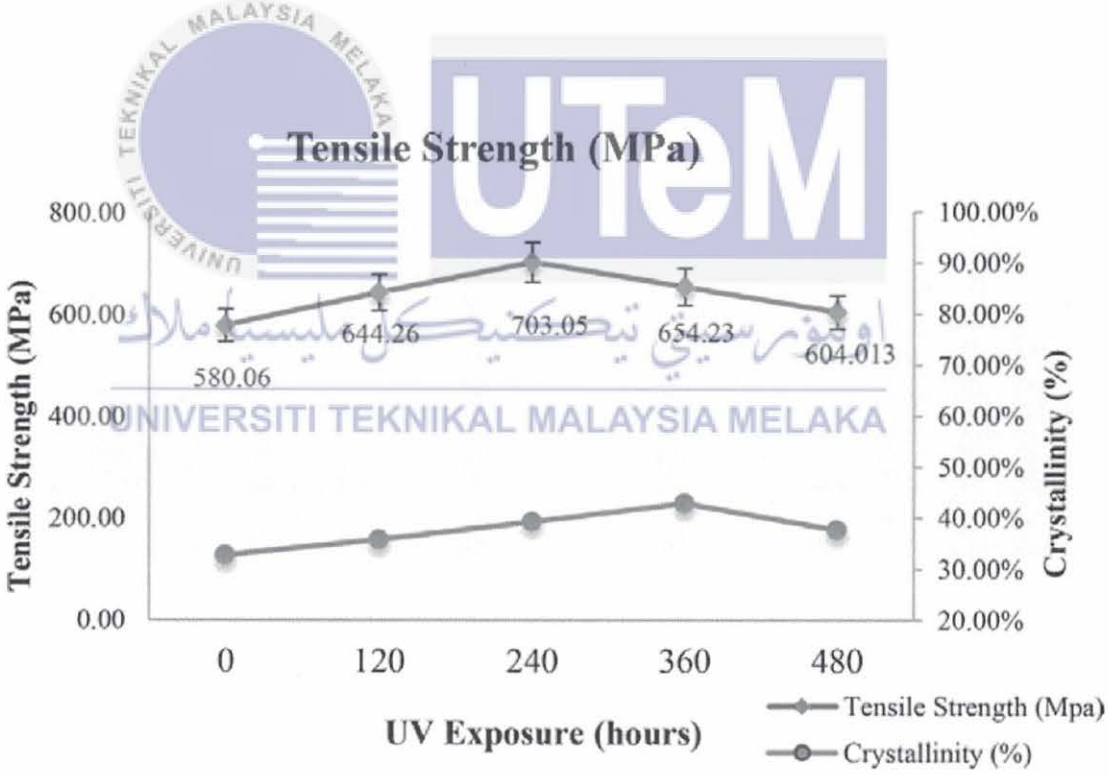


Figure 4.9: The ultimate tensile strength of specimens, crystallinity (%), against UV exposure (Mahat *et al.*, 2016).

### 4.3.2 The Influence of Heat Treatment Process on Mechanical Properties of Surface Treated Volcanic Ash Particles/PPS Composites

Mustafa et. al. (2016) stated that tensile modulus of neat PPS experienced about a 42.85%-fold enhancement with the addition of the VA 25 wt.% according to Figure 4.10 (a). Furthermore, it also indicated that the stress was efficiently transferred from the matrix to the microscale VA fillers. This can be highlighted out that the rapid acceleration of the crystallization rate of PPS due to the nucleating effect of the VA particles promoted the formation of small imperfect crystals that provided high rigidity to the semicrystalline PPS. According to Figure 4.10 (a), the steady increment of flexural modulus values was observed to higher VA concentrations as the same as to tensile modulus results mentioned above. At higher VA concentrations, flexural modulus values were higher than the neat PPS's modulus.

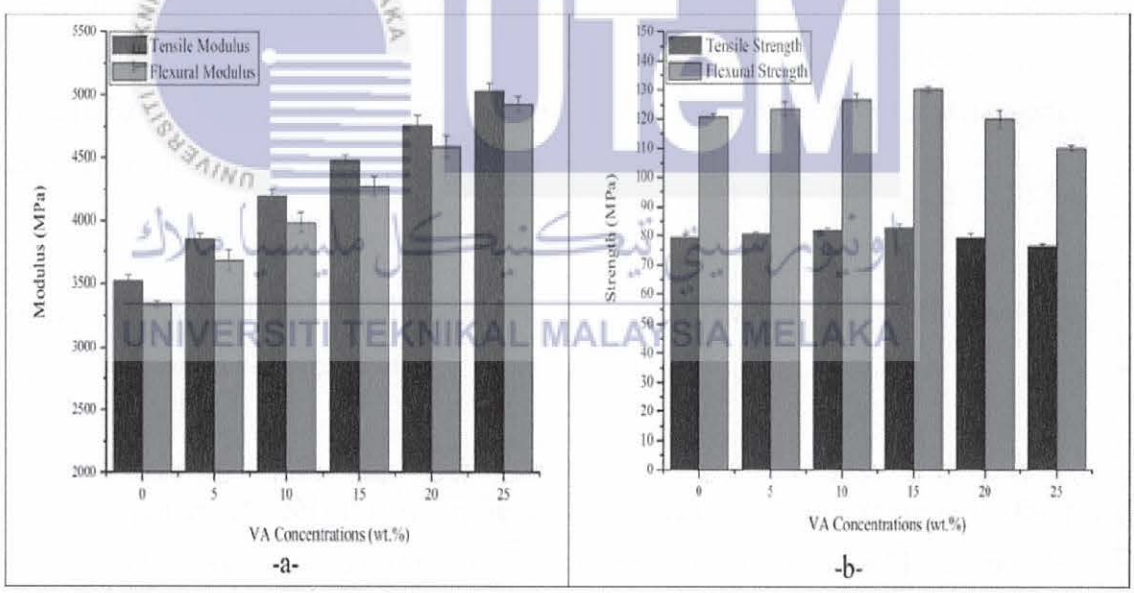


Figure 4.10: PPS composites mechanical properties as a function of various untreated VA concentrations (Mustafa *et al.*, 2016).

VA/PPS composite tensile strength was increased moderately up to the VA content of 15 wt.% and the increased around 4.5 wt.% indicated that inorganic particles contributed more to the enhancement of the stiffness than the strength of the PPS polymer according to Figure 4.10 (b). The increased on tensile strength is because VA particles each behaved as independent units and served to distribute the stress subjected to the sample. However, at higher weight fraction (20 and 25 wt.%), wetting of the VA was poor due to the reason of VA filler phase was more prominent than the PPS matrix phase. Filler-filler interaction was more prominent than polymer-filler interaction at higher weight fractions thus it was responsible for the development of cracks and decreased in tensile strength.

Figure 4.10 (b) showed VA/PPS composites flexural strength values was slightly enhanced by 7.7% in relation to 15 wt.% VA concentration. This is because the matrix encapsulated the inorganic VA particles which had an appropriate pore structure and high specific surface. Unfortunately, VA/PPS composites flexural strength values were decreased significantly at higher concentrations (20 and 25 wt.%) was mainly attributed to the poor compatibility between VA and PPS matrix which formed weak interfacial regions. Thus, it resulted in the reduction in the efficiency of stress transfer from the matrix to the reinforcement component.



### 4.3.3 Possible Use of Volcanic Ash as a Filler in PPS composites for Thermal and Mechanical Properties

Avcu et. al. (2014) used a nitrogen atmosphere for TGA experiments. From Figure 4.11, no significant mass loss (<0.5%) occurred until 450°C for PPS composites with different VA concentration which present a relatively good thermostability. Thermogravimetric curve of neat PPS displayed a single degradation stage that started at 450°C and shows the maximum rate of weight loss at around 540°C. It was observed that at 700°C the residual mass drop to 44% from the initial weight. The mechanism of degradation involved random chain scission followed by depolymerization, cyclization and disproportionation from radical chain ends. Neat PPS onset temperature for thermal degradation ($T_{10}$) was 508°C. There were no significant changes for VA/PPS at $T_{10}$ values occurred up to 20 wt.% filler concentrations. It is safe to say that there was no

earlier degradation of molecules within VA particles. However, from Figure 4.11 it showed that thermal stability of the VA/PPS composites was improved with higher filler concentrations. As an evidence at 10 wt.% filler concentration, VA/PPS composites can be seen that it reached highest thermal stability which can be attributed to the higher thermal conductivity of VA particles than PPS matrix. Similar type of trend of high thermal stability with incorporation of filling material was due to interfacial bonding between polymer matrix and filling particles thus hindered the segmented movement of the polymer matrix. This phenomenon is known as chain mobility restrictions.

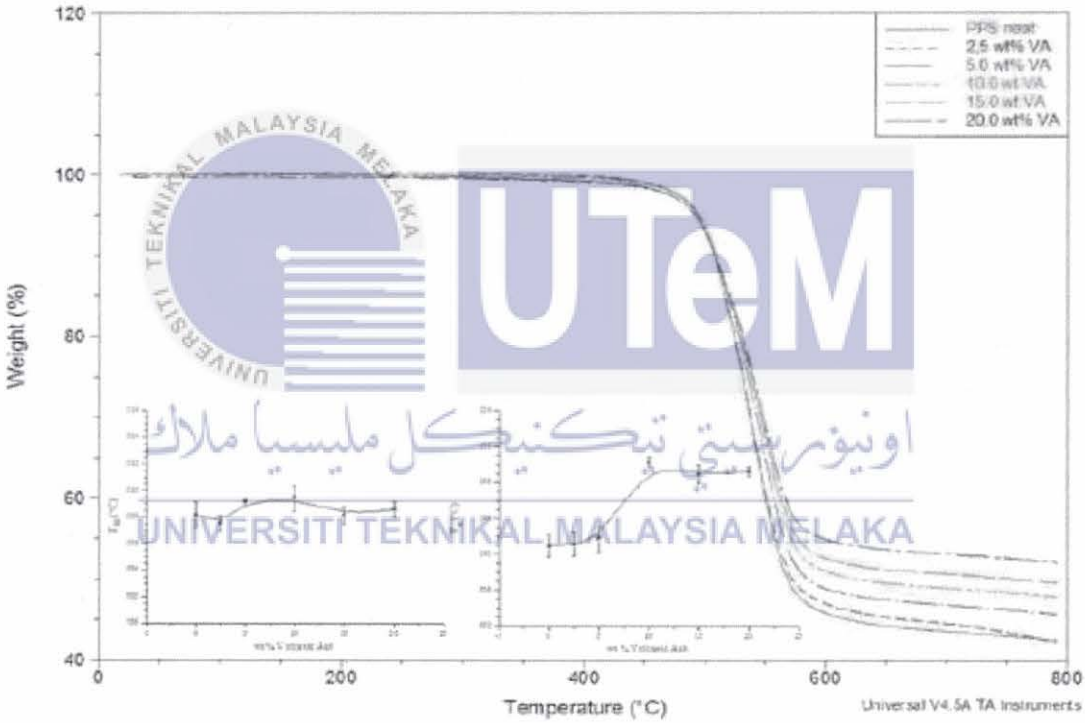


Figure 4.11: Thermal stability properties and thermogravimetric of PPS composites with various VA concentrations (Avcu *et al.*, 2014).

Avcu et. al. (2014) performed a flexural test which clearly seen that flexural modulus displayed a steady increase with increasing VA concentrations according to Figure 4.12 (a). The increasing of VA particle concentrations leads to an increase in the flexural modulus that may possibly exceed the neat PPS resin modulus. Concentration at 20 wt.% was manifested to achieve the highest improvement of 36.6% in flexural modulus compared to neat PPS. Figure 4.12 (b) showed that the flexural strength of uneroded VA/PPS composites which can be seen as flexural strength of VA/PPS composites was slightly enhanced by 11.2% with 10 wt.% VA concentrations. But on the other hand, flexural strength values of polymer composite samples were decreased significantly at higher concentrations of VA (15 wt.% and 20 wt.%). At lower VA concentration (up to 10 wt.%), the matrix encapsulated the inorganic particles which has an appropriate pore structure and high specific surface area thus improving pore structure of VA due to interaction between PPS matrix and VA particles. At higher concentrations there is partially reacted VA particles trapped withing PPS matrix. It was considered that porosity level was increased due to unreacted VA particles. Poor compatibility between VA and PPS matrix which formed weak interfacial regions was the main cause of the reduction of flexural strength values in a highly filled specimens (15 wt.% and 20 wt.%). In addition, the weak interfacial regions resulted the reduction in the efficiency of stress transfer to the reinforcement component from matrix.



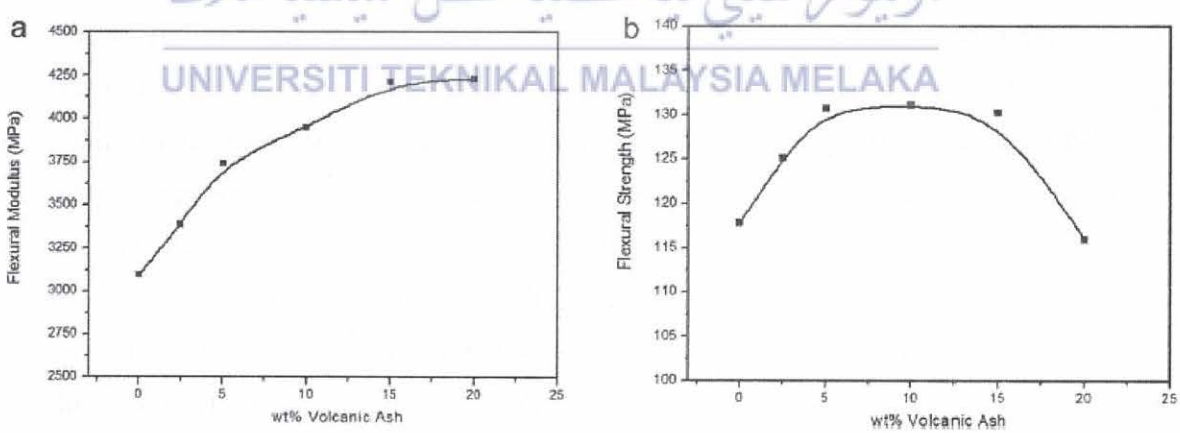


Figure 4.12: Flexural properties of PPS composites as to various VA concentrations: (a) flexural modulus, (b) flexural strength (Avcu *et al.*, 2014).

### 4.3.4 Post Fire Behavior of Carbon Fibers PPS and Epoxy-Based Laminates for Aeronautical Applications

According to Benoit et. al. (2014) based on Figure 4.13 temperature gradually increase at the laminates surface depending on the applied heat flux. The decreased in temperature after 70s in C/Epoxy laminates subjected to 50 $kW/m^2$ was because of the significant fire induced damage. As PPS matrix were exposed to the heat flux, no dripping out of the composite specimens occurred even for the highest heat flux. PPS matrix softens, fiber interface weakens and loses much of their stiffness and strength above $T_g$. The matrix undergoes a series of reaction producing black smoke and incombustible products as well as char when it reached decomposition temperature which was important in retaining the fire structural properties of composites. In addition, the presence of fillers suppressed heat radiation, increased melt viscosity and physical modification of the char. Therefore, CF can reduce melt flow and dripping to prevent the spread of flames in a fire. TGA measurements of CF/PPS provided the remaining mass fraction against temperature curve which revealed two-step decomposition according to Figure 4.14 and three-step decomposition in C/Epoxy except at high heat flux according to Figure 4.15. Chain scission was the main mechanism in first step while oxidation of the carbonaceous char was the second step. The onset for PPS thermal degradation occurred between 350 and 500°C and significant mass loss occurred between 500 and 600°C (first decomposition step) which caused volatilization about 50% of PPS polymer mass. The remaining mass fraction of PPS matrix appeared to be carbonaceous char. For C/Epoxy, its thermal degradation occurred between 350°C to 450°C, and significant mass loss occurred about 20% over the temperature range from 350°C to 450°C (first decomposition step). The temperature range for second decomposition step was between 450°C and 600°C with another 20% decreased in terms of specimen's weight.

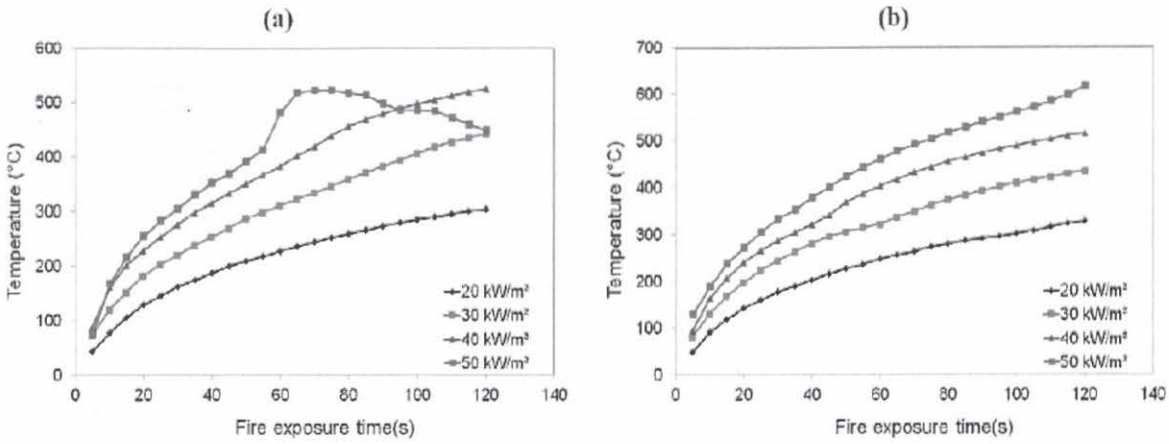


Figure 4.13: Surface temperature for different thermal stress: (a) C/Epoxy, (b) C/PPS (Benoit *et al.*, 2014).

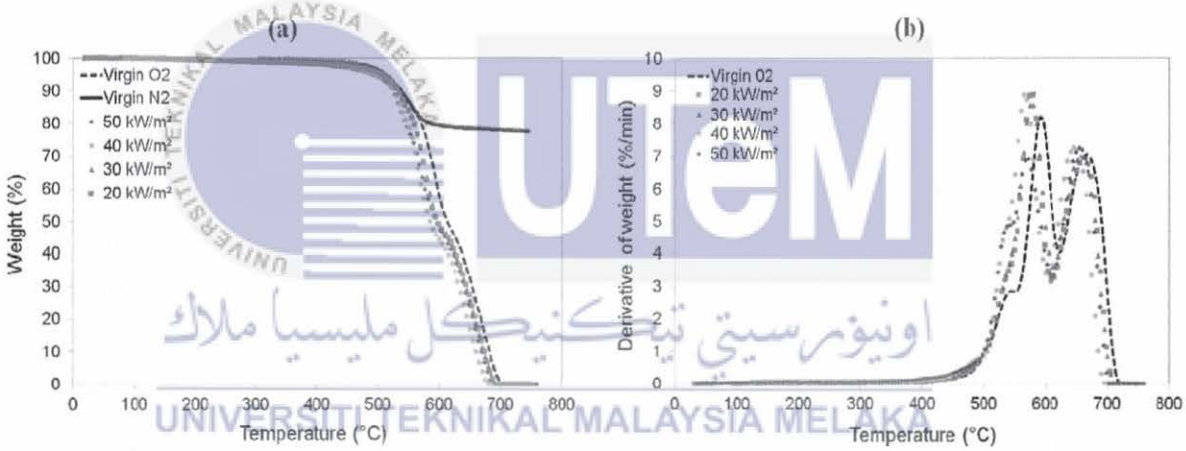




Figure 4.14: Thermal decomposition of CF/PPS under nitrogen and air: (a) Weight vs temperature, (b) Derivative weight vs temperature (Benoit *et al.*, 2014).

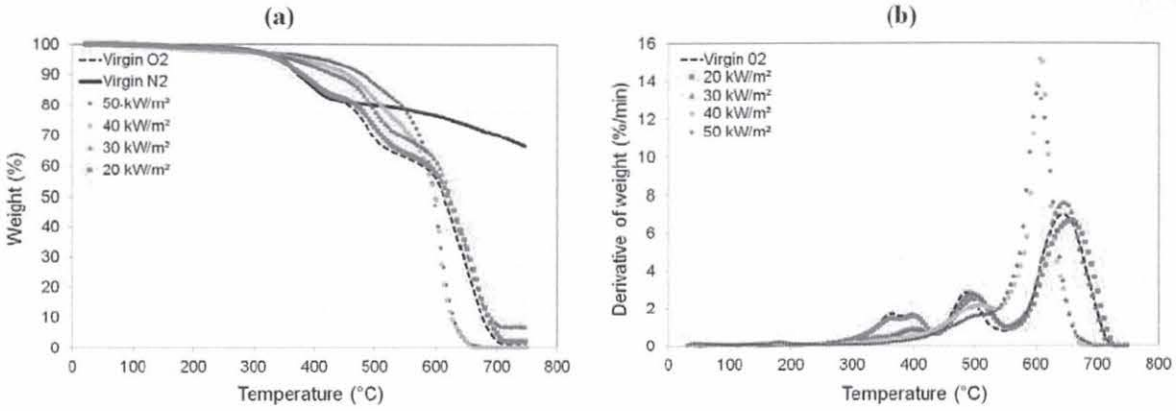


Figure 4.15: Thermal decomposition of C/Epoxy under nitrogen and air: (a) Weight vs temperature, (b) Derivative weight vs temperature (Benoit *et al.*, 2014).

According to Figure 4.16 the tensile response was virtually elastic/brittle for all the fire conditions despite PPS matrix highly ductile behaviour at high temperature. For C/Epoxy laminates it appeared that both exposure time and heat flux significantly reduce both strength and axial stiffness according to Figure 4.17. An increased of heat flux from 20 to 30kW/m$^2$ leads to 50% loss in mechanical properties while a change in the fire exposure time from 2 to 5 min leads to about 40% loss in these properties. At high heat flux, the decreased in both strength and stiffness reached 70%. Surprisingly, PPS fire exposure seems to experience less influenced in terms of tensile properties even though a low heat flux degrades this material with a 20% loss according to Figure 4.17. From the analysis of tensile properties, it appeared that severed fire condition was worse for C/Epoxy than to CF/PPS laminates which showed that strength and axial stiffness of CF/PPS was higher than C/Epoxy after severed exposure.

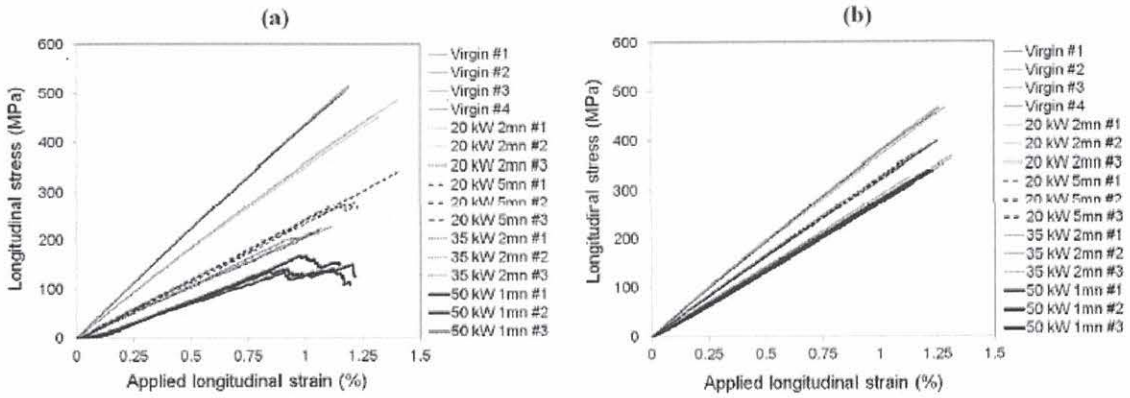


Figure 4.16: Tensile mechanical responses of quasi-isotropic laminates at 120°C: (a) C/Epoxy, (b) C/PPS (Benoit *et al.*, 2014).

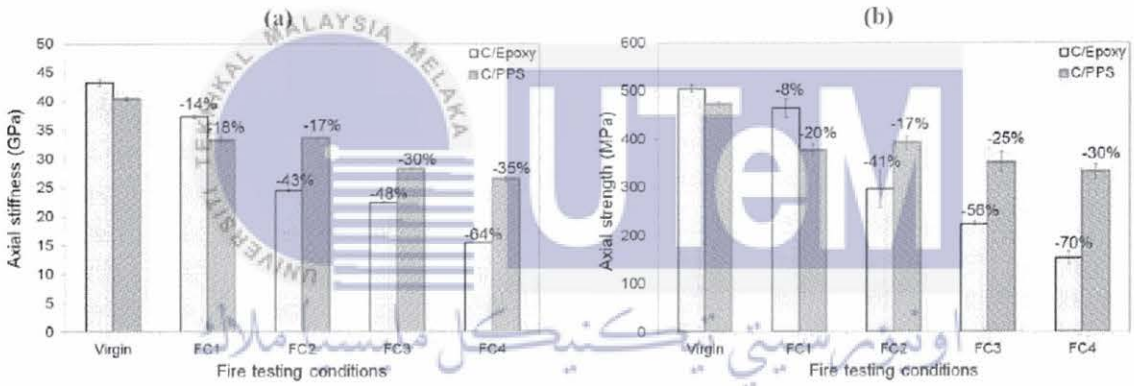




Figure 4.17: Comparative changes in the axial tensile properties of quasi-isotropic C/Epoxy and C/PPS laminates at 120°C: (a) Stiffness, (b) Strength (Benoit *et al.*, 2014).

### 4.3.5 Mechanical and Thermal Behavior of CF/PPS Composites Exposed to Radiant Heat Flux and Constant Compressive Force

Carpier et. al. (2018) stated that maximal, mean, and minimal temperatures measured are represented while the laminates were exposed to 50 kW/m$^2$ based on Figure 4.18. During a transient phase, CF/PPS temperature rises quickly on an average of 400°C/min on the front face and 150°C/min on the back face. The melting temperature of the back surface reached in 350 seconds while it only took 20 seconds for front face. From TGA measurements, the time required to reach decomposition onset temperature which was 490°C on the exposed surface varies from 40 to 80 seconds. Thermal equilibrium was reached at 100 seconds for front face and the temperature levels off at a mean value of 560°C and 280°C at the back of the specimens. From the graph, the matrix pyrolysis begins T ≈500°C which resulting the volatilization of 55% from the PPS mass and the formation of carbonaceous char.

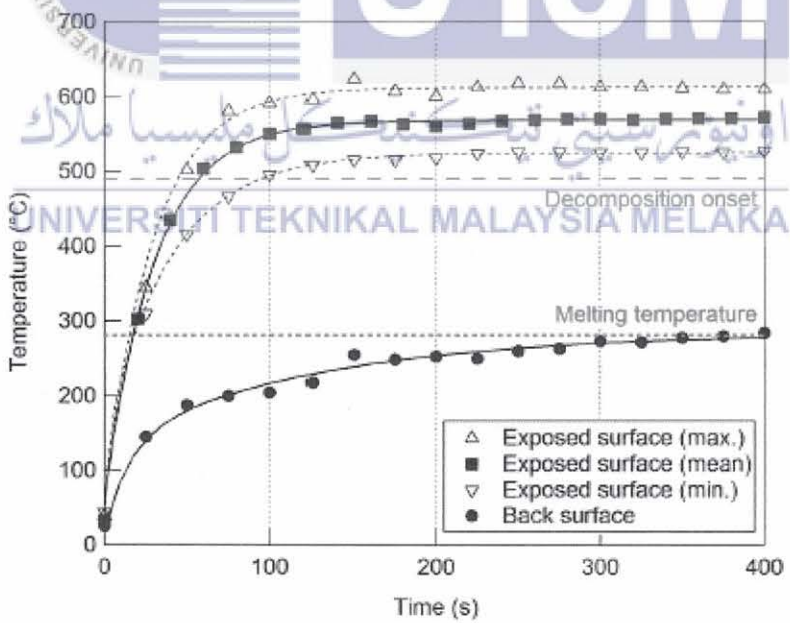


Figure 4.18: Temperature measurements for CF/PPS laminates (Carpier *et al.*, 2018).

Figure 4.19 represents a typical strain-time curve for CF/PPS laminates exposed to simultaneous radiant heat flux and compressive stress. The temperature evolution was added in the diagram to ease the analysis. The first stage was defined as transient stage which was driven by temperature. The total longitudinal strain first evolved towards elongation for 20 seconds due to the matrix thermal expansion although compression was applied. Meanwhile, the matrix experienced a loss of mechanical properties due to the increasing temperature which leads to an increase of compressive strain.

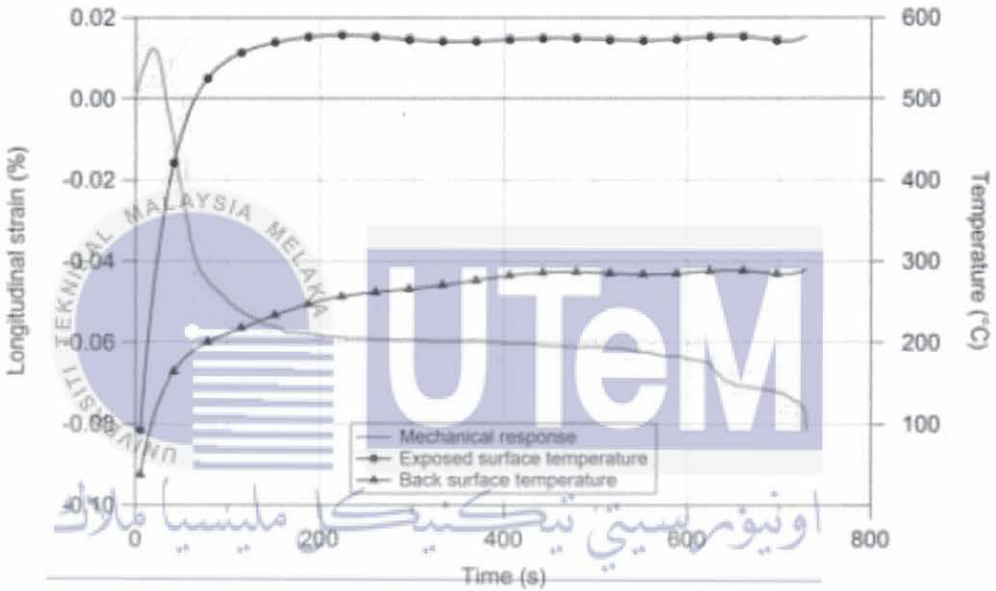




Figure 4.19: Strain-time curve on simultaneous compressive stress (F = 0.50 $F_u$) and heat flux (Carpier *et al.*, 2018).

### 4.3.6 Effect of Isothermal Heat Treatment on Crystallinity, Tensile Strength and Failure Mode of CF/PPS Laminate

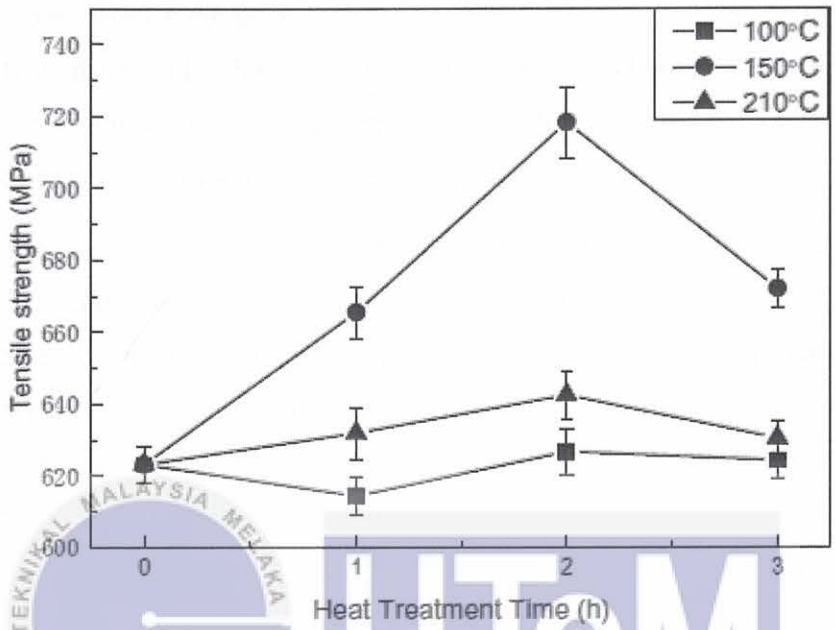


Figure 4.20: Tensile strength of CF/PPS laminate under different duration of isothermal heat treatment time (Liu *et al.*, 2020).



Liu et. al (2020) stated that the tensile strength of the CF/PPS had improved under different heat treatment time compared with the as-received specimen (CF/PPS laminate without heat treatment). At temperature 100°C with the heat treatment from 1 hour to 3 hours, the tensile strength of the sample was 614.3 MPa, 626.6 MPa, and 624.2 MPa, respectively. There was little effect when compared to as-received specimen's tensile strength whose value stands at 623.1 MPa. This can be explained due to the low dynamic energy of the PPS molecular chain which 100°C was merely above its glass transition temperature stands at 90°C. In addition, the molecular chain cannot be effectively arranged in a crystalline state and the effect of improving the crystal integrity of the material is poorer thus the molecular chain remained the same which makes the change in tensile strength was very little.

At 150°C of isothermal heat treatment temperature, the tensile strength of CF/PPS had a significant increase compared to 100°C batch. The values were 665.4 MPa, 718.2 MPa, and 671.9 MPa for 1 hour, 2 hours, and 3 hours, respectively. From the Figure 4.20 a rise of tensile strength of 6.8%, 15.3%, and 7.8% from the previous batch. The objective for the increasing temperature was to allow the molecular chain to move sufficiently. Besides that, it can also eliminate internal pores inside the structure and induced PPS resin to crystallize around CF so that they are better combined thus contributed a positive influence on the mechanical properties of CF/PPS.

When the temperature of the isothermal heat treatment was increased to 210°C, then tensile strength of the samples was decreased to 631.8 MPa, 642.4 MPa, and 630.3 MPa for heat treatment of 1 hour, 2 hours and 3 hours, respectively. The decreased in 5.0%, 10.6%, and 6.2% compared to 150°C heat treatment was because 210°C is closer to melting temperature of PPS material which is 285°C. The thermal oxygen cross-linking reaction of the molecular chain was excessively intensified which hinder the ability of the segment to enter the lattice. Therefore, the reduction of the interface resulting a weaker bond strength. Finally, the effective load that should be transferred by resin to the fibre was also reduced thus weakened the tensile strength of the material.

Table 4.1: Value of tensile strength under different isothermal heat treatment conditions (Liu *et al.*, 2020).



| Specimen number | Tensile Strength/MPa |
|---|---|
| T-as-received | 623.1 ± 5.0 |
| T-100°C-1 h | 614.3 ± 5.2 |
| T-100°C-2h | 626.6 ± 6.3 |
| T-100°C-3h | 624.4 ± 5.3 |
| T-150°C-1h | 665.4 ± 7.1 |
| T-150°C-2h | 718.2 ± 9.8 |
| T-150°C-3h | 671.9 ± 5.1 |
| T-210°C-1h | 631.8 ± 7.2 |
| T-210°C-2h | 642.4 ± 6.5 |
| T-210°C-3h | 630.3 ± 4.6 |

### 4.3.7 The Effect of The Ocean Water Immersion and UV Ageing on the Dynamic Mechanical Properties of the PPS/GF Composites

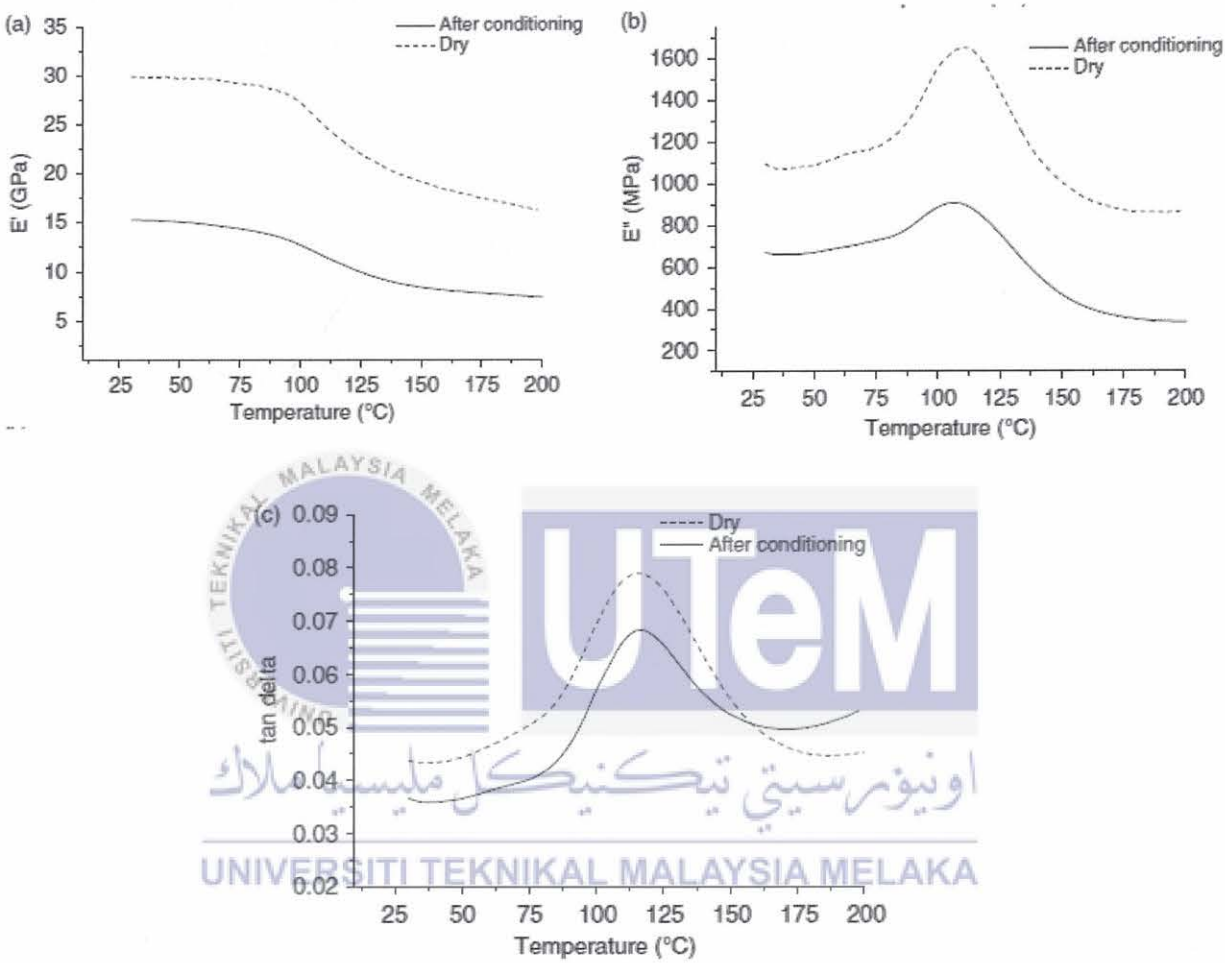




Figure 4.21: DMA curves of PPS/GF laminate dry and after to be submitted to ocean water conditioning: (a) elastic modulus, (b) loss modulus, and (c) tan delta (Faria *et al.*, 2021).

Faria et. al. (2011) showed the DMA curves as function of the temperature for dry and artificial ocean water conditioning specimens. According to Figure 4.21, the beginning of E' and the E'' curves which was around 30°C the values of dry specimen were higher than the wet value for the same specimens. This event can be known as plasticizers agent which confirmed the results obtained from the glass transition temperature according to Table 4.2.

Besides that, the decrease in the values of E' and E'' also indicated that there was a reduction in the interaction between fiber and matrix. The moisture affected the fiber-matrix interface which made it weaker thus explaining the reduction of E' value. There were microcracks and superficial cracks were from the moisture absorption in the composite which damaged the matrix interface. As a result, the strength, glass transition temperature, interlaminar shear strength, stiffness and compressive strength of laminates were reduced.

Table 4.2: Glass transition temperature for PPS/GF into different conditionings (Faria *et al.*, 2021).

| **Conditioning** | **Exposure time (h)** | **$T_g$ (°C)** |
|---|---|---|
| Dry | - | 97.0 ± 0.2 |
| Ocean water | 840 | 92.0 ± 1.5 |
| UV | 650 | 93.0 ± 0.5 |
| UV | 1300 | 91.0 ± 0.7 |
| UV | 1900 | 84.0 ± 0.5 |

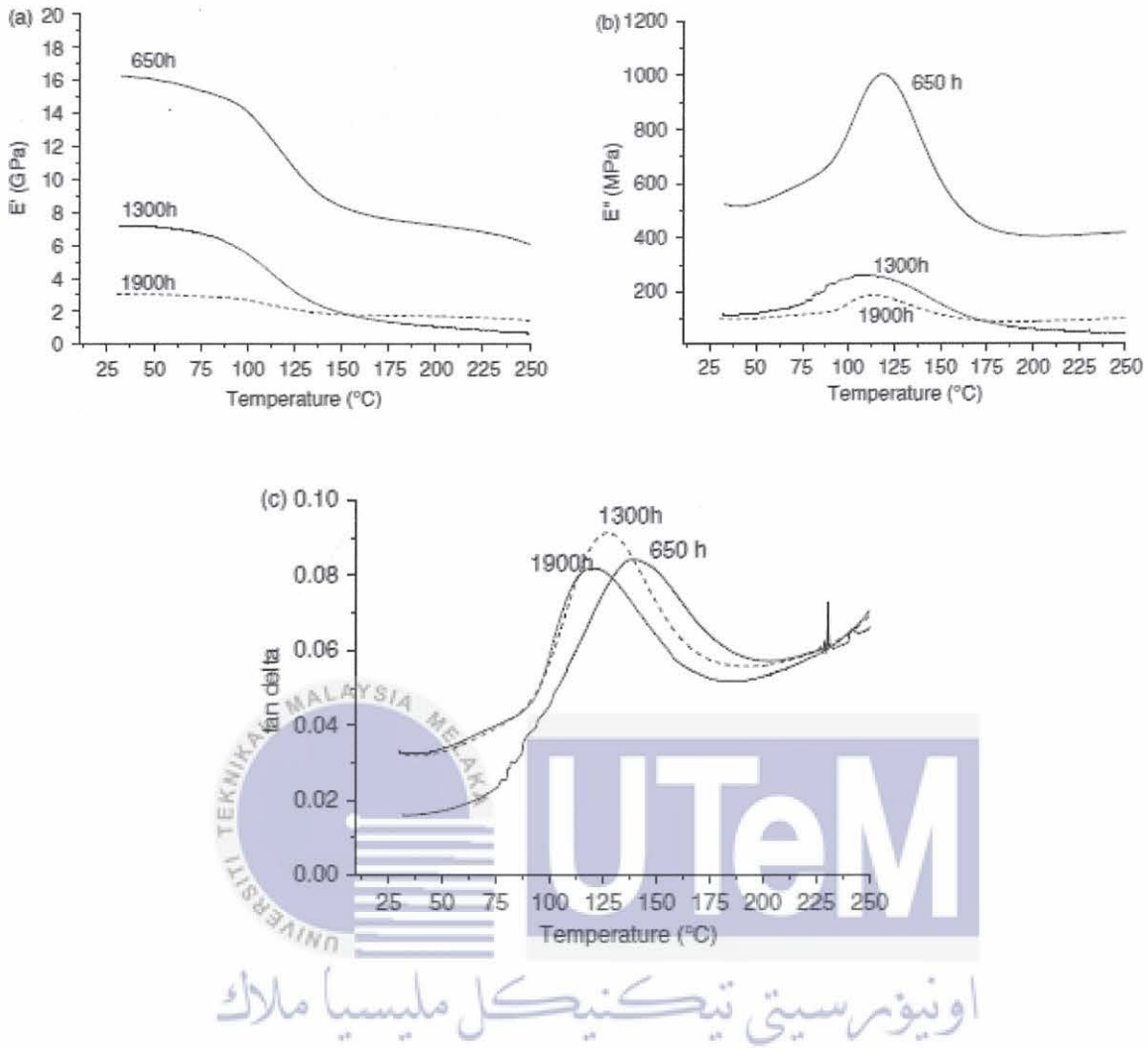


Figure 4.22: DMA curves of PPS/GF laminate after exposure to UV radiation: (a) elastic modulus, (b) loss modulus, and (c) tan delta (Faria *et al.*, 2021).



Figure 4.22 and Table 4.2 showed the DMA results which UV light conditioning during periods of 650 and 1200 h induced almost the same as $T_g$ values decreased. The PPS/GF $T_g$ decreased more significant when the specimens were conditioned at 1900 h. It decreased about 13% when compared to non conditioned specimen. This is due to combination effect of UV light radiation and moisture which leads to degradation of the interface between GF and matrix. It was also possible matrix molecular mass reduction to happen due to chain scission reaction contributed by a photooxidation during the UV light radiation.

From Figure 4.22 (a) at 30°C, the E' values obtained were in rage of 3 – 16 GPa and they were much lower than PPS/GF in Figure 4.21 which the value was 30 GPa. As a result, the UV radiation leads to the reduction of E' values because of the polymer matrix degradation occurred in the sample and provoked by an intensed exposure to UV radiation. Therefore, the small amount of decreasing in $T_g$ values indicated that PPS matrix underwent irreversible plasticization and hyrolysis.

### 4.3.8 Effect of Thermal Treatment on the In-Plane Shear Behavior of Carbon Fiber Reinforced PPS Composite Specimens.

Pantelakis et.al (2007) showed a comparison for the reference material in a stress-strain curves (refer Figure 4.23). The derived in-plane shear strength values for both thermal treated materials and reference were displayed over Figure 4.24 as the decrease in-plane shear strength for TT2 and TT4 after heat treatment procedure of 46 and 24%, respectively. On the other hand, an improvement of 24% in-plane shear strength values of TT1 after thermal treatment.

The values of in-plane shear moduli of thermal treated and reference specimens were shown in Figure 4.25. A decreased in 64% of in-plane shear modulus for TT2 and 8% decreased of in-plane shear modulus for TT4 after thermal treatment was recorded. For TT1, it seems had not affected by the heat treatment as the in-plane shear modulus gave an increase of 1%.



On the contrary, the in-plane shear strength properties decreased when the duration of the heat treatment increased subjected to ply-by-ply. It was expected as it allows the matrix degradation phenomena such as decrease of crystallinity, increase of porosity, and crosslinking to occur. When the whole set of plies was subjected for shorter duration of heater treatment, it was safe to say that the matrix degradation only occurred to the outer plies rather than in plies within the interior of the laminate.

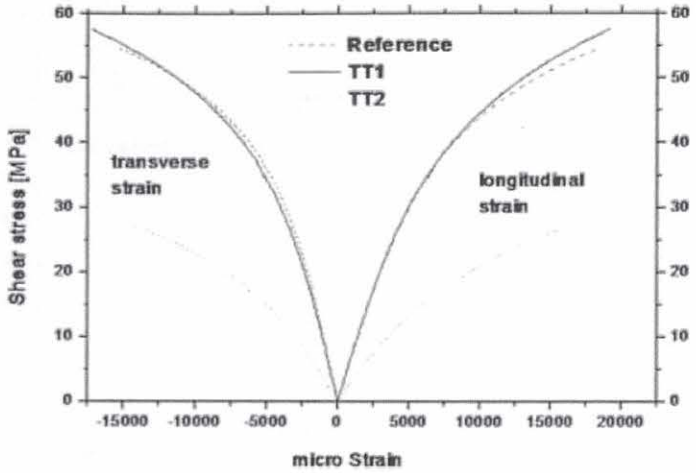


Figure 4.23: In-plane shear stress-strain curves for TT1, TT2 and reference (Pantelakis *et al.*, 2021).

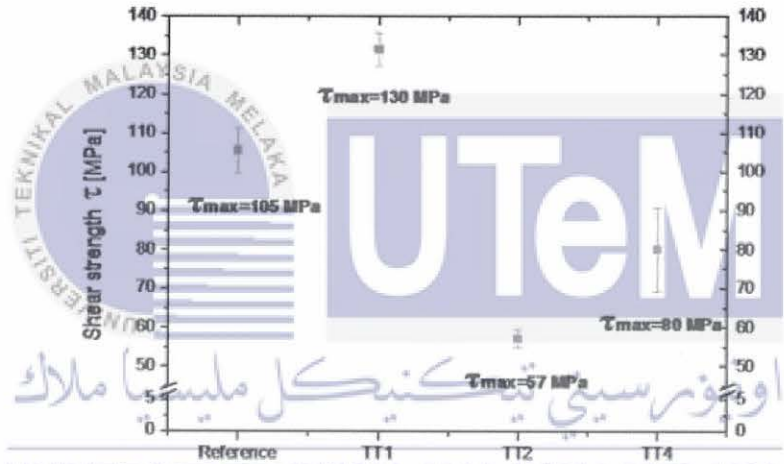




Figure 4.24: In-plane shear strength for TT1, TT2, TT4 and reference (Pantelakis *et al.*, 2021).

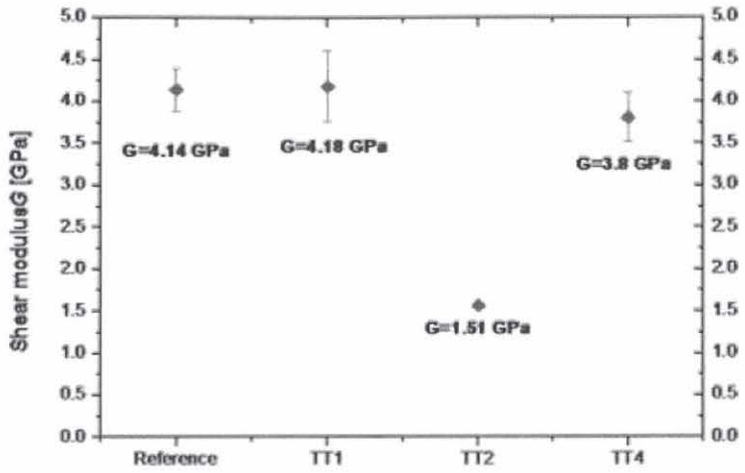


Figure 4.25: In-plane shear modulus of TT1, TT2, TT4 and reference (Pantelakis *et al.*, 2021).

### 4.3.9 About the Influence of Stamping on Thermoplastic Based Composites for Aeronautical Applications

Table 4.3: Influence of stamping on CF/PPS laminates under severe conditions (Zhang *et al.*, 2014).

| | Consolidated | Stamp | Influence of stamping (%) |
|---|---|---|---|
| $E_{xx}$ (GPa) | 54.91 ± 0.43 | 55.66 ± 1.05 | +1.2 |
| $\varepsilon^{u}_{xx}$ (%) | 1.28 ± 0.04 | 1.28 ± 0.02 | - |
| $\sigma^{u}_{xx}$ (MPa) | 649 ± 11 | 655 ± 23 | +0.9 |

Vieille et. al. (2013) did a tensile test on [(0/90)] laminates. The 0° oriented fiber withstand the load and its responded is dominated by the behavior resulting in an elastic/brittle behavior temperature higher than its $T_g$ despite PPS matrix was known as highly ductile behavior according to Figure 4.26. The tensile properties for PPS matrix as shown in Table 4.3 are virtually the same in consolidated and stamped laminates.

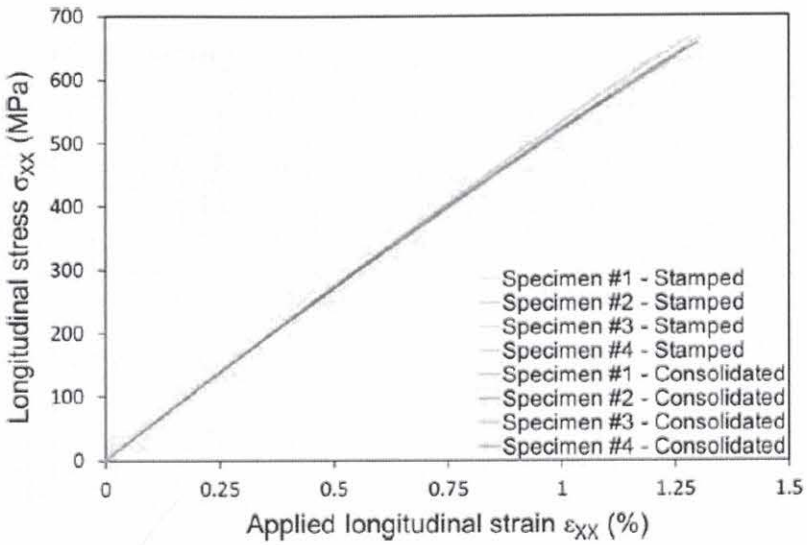


Figure 4.26: Influence of stamping on CF/PPS under severe condition (Zhang *et al.*, 2014).

### 4.3.10 Effect of aminated PPS on the Mechanical Properties of Short Carbon Fiber Reinforced PPS composites



Zhang et. al. (2014) stated that PPS/CF composites with PPS-$NH_2$ had much higher than the pure PPS/CF in terms of tensile strength, flexural strength, and flexural modulus according to Figure 4.27. In addition, PPS-$NH_2$ (0.6) – (1.2) blends showed little variation in mechanical properties compared with pure PPS. It was safe to say that PPS-$NH_2$ had a positive influenced on CF/PPS composites mechanical properties because of the physical effect and physical bonding. Meanwhile, CF/PPS composites with PPS-$NH_2$ obtained the highest flexural strength, tensile strength, and flexural modulus with the addition PPS-$NH_2$ (1.0). On the other hand, there were some strange results obtained in Figure 4.27. The increased of CF/PPS composites in mechanical properties with different aminated PPS was not linear in some way. This event occurred because of different melt viscosity and molecular weight of aminated PPS thus lead the nonlinear increased of CF/PPS mechanical properties.

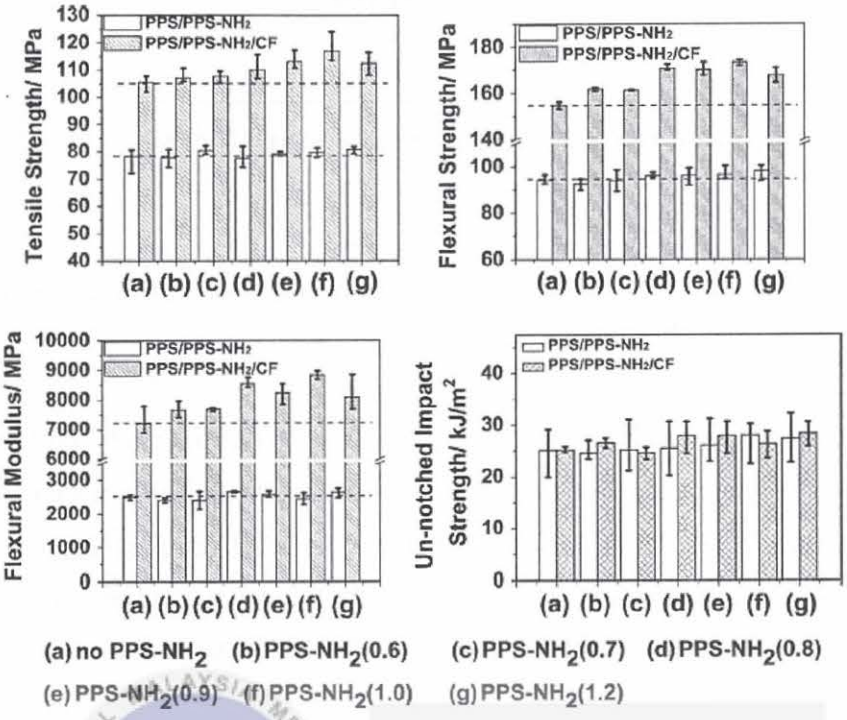


Figure 4.27: The mechanical properties of PPS resin with aminated PPS and CF/PPS and without aminated PPS (Zhang *et al.*, 2014).

# CHAPTER 5

# CONCLUSION AND RECOMMENDATION

## 5.1 Conclusion and Recommendation

In this study, there is effect of heater distance at different heater temperature and effects of heater temperature at different heater distances. Setting up maximum temperature of 400°C could achieved minimum of 320°C for a distance at least 270 mm. However, larger distance up to 500 mm manages to have at least 300°C for the PPS plate temperature. Unfortunately, the PPS plate will not be achieved 320°C within 8 minutes if the heater temperature is set lower than 350°C. Ideally, the temperature of 400°C with IR heater distance of 250 – 300 mm could yield the PPS plate to the temperature in the range of 300°C – 320°C.

In this study, 10 papers have been reviewed to study the mechanical and thermal properties of PPS composite. This study can enlighten future generation of engineers to identify PPS behavior under various parameter; therefore, it can help us to understand more about the influence of those experiments towards PPS. Their findings can provide some preliminary knowledge to engineers and scientists in the field and develop new set of structural composites.

# REFERENCE


Ageorges, C., Ye, L. and Hou, M. (2006) 'Advances in fusion bonding techniques for joining thermoplastic matrix composites : a review', 32(2001).

Ahmed, H. *et al.* (2018) 'Investigation and development of friction stir welding process for unreinforced polyphenylene sulfide and reinforced polyetheretherketone'. doi: 10.1177/0892705718785676.

Alves, F. J. L., Baptista, A. M. and Marques, A. T. (2016) *3 - Metal and ceramic matrix composites in aerospace engineering*, *Advanced Composite Materials for Aerospace Engineering*. Elsevier Ltd. doi: 10.1016/B978-0-08-100037-3.00003-1.

Balakrishnan, P. *et al.* (2016) *12 - Natural fibre and polymer matrix composites and their applications in aerospace engineering*, *Advanced Composite Materials for Aerospace Engineering*. Elsevier Ltd. doi: 10.1016/B978-0-08-100037-3.00012-2.

Bandyopadhyay, S. (2014) 'hardening 2014 Al / Sic and 6061 Al / SIC composites', 185(1995), pp. 125–130.

Carpier, Y. *et al.* (2018) 'Mechanical behavior of carbon fibers polyphenylene sulfide composites exposed to radiant heat flux and constant compressive force', *Composite Structures*, 200, pp. 1–11. doi: 10.1016/j.compstruct.2018.05.086.

Chang, I. Y. and Lees, J. K. (1988) 'Recent Development in Thermoplastic Composites: A Review of Matrix Systems and Processing Methods', *Journal of Thermoplastic Composite Materials*, 1(3), pp. 277–296. doi: 10.1177/089270578800100305.

Ching, Y. C. *et al.* (2017) *Applications of thermoplastic-based blends*, *Recent Developments in Polymer Macro, Micro and Nano Blends: Preparation and Characterisation*. Elsevier Ltd. doi: 10.1016/B978-0-08-100408-1.00005-4.

Das, T. K., Ghosh, P. and Das, N. C. (2019) 'Preparation , development , outcomes , and application versatility of carbon fiber-based polymer composites : a review'.

Eguemann, N. *et al.* (2014) 'Compression moulding of complex parts for the aerospace with discontinuous novel and recycled thermoplastic composite materials To cite this version : HAL Id : hal-00983314 COMPRESSION MOULDING OF COMPLEX PARTS FOR THE

AEROSPACE WITH DISCONTINUOUS NOVEL A'.

Favaloro, M. (2018) 'Properties and Processes of Linear Polyphenylene Sulfide ( PPS ) for Continuous Fiber Composites Aerospace Applications', 4970.

Kumar, D., Agnihotri, G. and Purohit, R. (2015) 'Advanced Aluminium Matrix Composites : The Critical Need of Automotive and Aerospace Engineering Fields', *Materials Today: Proceedings*, 2(4–5), pp. 3032–3041. doi: 10.1016/j.matpr.2015.07.290.

Lindroos, V. K. and Talvitie, M. J. (1995) 'IVo ., ra t . o lCoo . t d . a . tens . elCo', 53, pp. 273–284.

Liu, Y., Zhou, X. and Wang, Z. (2020) 'Effect of isothermal heat treatment on crystallinity, tensile strength and failure mode of CF/PPS laminate', *High Performance Polymers*. doi: 10.1177/0954008320969843.

Mahat, K. B. *et al.* (2016) 'Effects of UV Light on Mechanical Properties of Carbon Fiber Reinforced PPS Thermoplastic Composites', *Macromolecular Symposia*, 365(1), pp. 157–168. doi: 10.1002/masy.201650015.

Ning, H. *et al.* (2007) 'Design , manufacture and analysis of a thermoplastic composite frame structure for mass transit', 80, pp. 105–116. doi: 10.1016/j.compstruct.2006.04.036.

Offringa, A. R. (1996) 'Thermoplastic composites - Rapid processing applications', *Composites Part A: Applied Science and Manufacturing*, 27(4 PART A), pp. 329–336. doi: 10.1016/1359-835X(95)00048-7.

Post, W. *et al.* (2020) 'A Review on the Potential and Limitations of Recyclable Thermosets for Structural Applications', *Polymer Reviews*, 60(2), pp. 359–388. doi: 10.1080/15583724.2019.1673406.

Richard Sharp, Scott Holmes, C. W. (1995) 'from the SAGE Social Science Collections . All Rights', 8(1).

S, M. K., K, R. R. and Govindaraju, H. K. (2018) 'ScienceDirect Development of E-Glass Woven Fabric / Polyester Resin Polymer Matrix Composite and Study of Mechanical Properties', *Materials Today: Proceedings*, 5(5), pp. 13367–13374. doi: 10.1016/j.matpr.2018.02.329.

Steyer, T. E. (2013) 'Shaping the future of ceramics for aerospace applications', *International*

*Journal of Applied Ceramic Technology*, 10(3), pp. 389–394. doi: 10.1111/ijac.12069.

Sudhin, A. U. *et al.* (2020) 'Comparison of Properties of Carbon Fiber Reinforced Thermoplastic and Thermosetting Composites for Aerospace Applications', *Materials Today: Proceedings*, 24, pp. 453–462. doi: 10.1016/j.matpr.2020.04.297.

Vaidya, U. K. and Chawla, K. K. (2008) 'Processing of fibre reinforced thermoplastic composites', *International Materials Reviews*, 53(4), pp. 185–218. doi: 10.1179/174328008X325223.

Wang, Y. *et al.* (2018) 'Compressive behavior of notched and unnotched carbon woven-ply PPS thermoplastic laminates at different temperatures', *Composites Part B: Engineering*, 133, pp. 68–77. doi: 10.1016/j.compositesb.2017.09.027.

Williams, J. C. and Starke, E. A. (2003) 'Progress in structural materials for aerospace systems &', 51, pp. 5775–5799. doi: 10.1016/j.actamat.2003.08.023.

Zhang, K. *et al.* (2014) 'Effect of aminated polyphenylene sulfide on the mechanical properties of short carbon fiber reinforced polyphenylene sulfide composites', *Composites Science and Technology*, 98, pp. 57–63. doi: 10.1016/j.compscitech.2014.04.020.

Zhu, D. (2019) 'Aerospace Ceramic Materials : Thermal , Environmental Barrier Coatings and SiC / SiC Ceramic Matrix Composites For Turbine Engine Applications', (May 2018).

Zhu, D., Sakowski, B. A. and Fisher, C. (2019) 'Film Cooled Recession of SiC / SiC Ceramic Matrix Composites : Test Development , CFD Modeling and Experimental Observations', pp. 1–16.

Zuo, P. *et al.* (2018) 'Multi-scale analysis of the effect of loading conditions on monotonic and fatigue behavior of a glass fiber reinforced polyphenylene sulfide (PPS) composite', *Composites Part B: Engineering*, 145, pp. 173–181. doi: 10.1016/j.compositesb.2018.03.031.

Chris Red. (2014). "Thermoplastic in Aerospace Composite Outlook, 2014-2023" 9th January 2014 retrieved from https://www.compositesworld.com/articles/the-outlook-for-thermoplastics-in-aerospace-composites-2014-2023

J. Kasper Oestergaard. (2019). "Airbus and Boeing Report June 2019 Commercial Aircraft Orders and Deliveries" 16th July 2019 retrieved from https://dsm.forecastinternational.com/wordpress/2019/07/16/airbus-and-boeing-report-june-2019-commercial-aircraft-orders-and-deliveries/

E. Olson. (2019). "Thermoplastic Composite for Aerospace Application" 12th September 2019 retrieved from https://insights.globalspec.com/article/12596/thermoplastic-composites-for-aerospace-applications.

Ageorges, C., Ye, L. and Hou, M. (2006) 'Advances in fusion bonding techniques for joining thermoplastic matrix composites : a review', 32(2001).

Ahmed, H. *et al.* (2018) 'Investigation and development of friction stir welding process for unreinforced polyphenylene sulfide and reinforced polyetheretherketone'. doi: 10.1177/0892705718785676.

Alves, F. J. L., Baptista, A. M. and Marques, A. T. (2016) *3 - Metal and ceramic matrix composites in aerospace engineering*, *Advanced Composite Materials for Aerospace Engineering*. Elsevier Ltd. doi: 10.1016/B978-0-08-100037-3.00003-1.

Balakrishnan, P. *et al.* (2016) *12 - Natural fibre and polymer matrix composites and their applications in aerospace engineering*, *Advanced Composite Materials for Aerospace Engineering*. Elsevier Ltd. doi: 10.1016/B978-0-08-100037-3.00012-2.

Bandyopadhyay, S. (2014) 'hardening 2014 Al / Sic and 6061 Al / SIC composites', 185(1995), pp. 125–130.

Carpier, Y. *et al.* (2018) 'Mechanical behavior of carbon fibers polyphenylene sulfide composites exposed to radiant heat flux and constant compressive force', *Composite Structures*, 200, pp. 1–11. doi: 10.1016/j.compstruct.2018.05.086.

Chang, I. Y. and Lees, J. K. (1988) 'Recent Development in Thermoplastic Composites: A Review of Matrix Systems and Processing Methods', *Journal of Thermoplastic Composite Materials*, 1(3), pp. 277–296. doi: 10.1177/089270578800100305.

Ching, Y. C. *et al.* (2017) *Applications of thermoplastic-based blends*, *Recent Developments in Polymer Macro, Micro and Nano Blends: Preparation and Characterisation*. Elsevier Ltd. doi: 10.1016/B978-0-08-100408-1.00005-4.

Das, T. K., Ghosh, P. and Das, N. C. (2019) 'Preparation , development , outcomes , and application versatility of carbon fiber-based polymer composites : a review'.

Eguemann, N. *et al.* (2014) 'Compression moulding of complex parts for the aerospace with discontinuous novel and recycled thermoplastic composite materials To cite this version : HAL Id : hal-00983314 COMPRESSION MOULDING OF COMPLEX PARTS FOR THE

AEROSPACE WITH DISCONTINUOUS NOVEL A'.

Favaloro, M. (2018) 'Properties and Processes of Linear Polyphenylene Sulfide ( PPS ) for Continuous Fiber Composites Aerospace Applications', 4970.

Kumar, D., Agnihotri, G. and Purohit, R. (2015) 'Advanced Aluminium Matrix Composites : The Critical Need of Automotive and Aerospace Engineering Fields', *Materials Today: Proceedings*, 2(4–5), pp. 3032–3041. doi: 10.1016/j.matpr.2015.07.290.

Lindroos, V. K. and Talvitie, M. J. (1995) 'IVo ., ra t . o lCoo . t d . a . tens . elCo', 53, pp. 273–284.

Liu, Y., Zhou, X. and Wang, Z. (2020) 'Effect of isothermal heat treatment on crystallinity, tensile strength and failure mode of CF/PPS laminate', *High Performance Polymers*. doi: 10.1177/0954008320969843.

Mahat, K. B. *et al.* (2016) 'Effects of UV Light on Mechanical Properties of Carbon Fiber Reinforced PPS Thermoplastic Composites', *Macromolecular Symposia*, 365(1), pp. 157–168. doi: 10.1002/masy.201650015.

Ning, H. *et al.* (2007) 'Design , manufacture and analysis of a thermoplastic composite frame structure for mass transit', 80, pp. 105–116. doi: 10.1016/j.compstruct.2006.04.036.

Offringa, A. R. (1996) 'Thermoplastic composites - Rapid processing applications', *Composites Part A: Applied Science and Manufacturing*, 27(4 PART A), pp. 329–336. doi: 10.1016/1359-835X(95)00048-7.

Post, W. *et al.* (2020) 'A Review on the Potential and Limitations of Recyclable Thermosets for Structural Applications', *Polymer Reviews*, 60(2), pp. 359–388. doi: 10.1080/15583724.2019.1673406.

Richard Sharp, Scott Holmes, C. W. (1995) 'from the SAGE Social Science Collections . All Rights', 8(1).

S, M. K., K, R. R. and Govindaraju, H. K. (2018) 'ScienceDirect Development of E-Glass Woven Fabric / Polyester Resin Polymer Matrix Composite and Study of Mechanical Properties', *Materials Today: Proceedings*, 5(5), pp. 13367–13374. doi: 10.1016/j.matpr.2018.02.329.

Steyer, T. E. (2013) 'Shaping the future of ceramics for aerospace applications', *International*

*Journal of Applied Ceramic Technology*, 10(3), pp. 389–394. doi: 10.1111/ijac.12069.

Sudhin, A. U. *et al.* (2020) 'Comparison of Properties of Carbon Fiber Reinforced Thermoplastic and Thermosetting Composites for Aerospace Applications', *Materials Today: Proceedings*, 24, pp. 453–462. doi: 10.1016/j.matpr.2020.04.297.

Vaidya, U. K. and Chawla, K. K. (2008) 'Processing of fibre reinforced thermoplastic composites', *International Materials Reviews*, 53(4), pp. 185–218. doi: 10.1179/174328008X325223.

Wang, Y. *et al.* (2018) 'Compressive behavior of notched and unnotched carbon woven-ply PPS thermoplastic laminates at different temperatures', *Composites Part B: Engineering*, 133, pp. 68–77. doi: 10.1016/j.compositesb.2017.09.027.

Williams, J. C. and Starke, E. A. (2003) 'Progress in structural materials for aerospace systems &', 51, pp. 5775–5799. doi: 10.1016/j.actamat.2003.08.023.

Zhang, K. *et al.* (2014) 'Effect of aminated polyphenylene sulfide on the mechanical properties of short carbon fiber reinforced polyphenylene sulfide composites', *Composites Science and Technology*, 98, pp. 57–63. doi: 10.1016/j.compscitech.2014.04.020.

Zhu, D. (2019) 'Aerospace Ceramic Materials : Thermal , Environmental Barrier Coatings and SiC / SiC Ceramic Matrix Composites For Turbine Engine Applications', (May 2018).

Zhu, D., Sakowski, B. A. and Fisher, C. (2019) 'Film Cooled Recession of SiC / SiC Ceramic Matrix Composites : Test Development , CFD Modeling and Experimental Observations', pp. 1–16.

Zuo, P. *et al.* (2018) 'Multi-scale analysis of the effect of loading conditions on monotonic and fatigue behavior of a glass fiber reinforced polyphenylene sulfide (PPS) composite', *Composites Part B: Engineering*, 145, pp. 173–181. doi: 10.1016/j.compositesb.2018.03.031.

Ageorges, C., Ye, L. and Hou, M. (2006) 'Advances in fusion bonding techniques for joining thermoplastic matrix composites : a review', 32(2001).

Ahmed, H. *et al.* (2018) 'Investigation and development of friction stir welding process for unreinforced polyphenylene sulfide and reinforced polyetheretherketone'. doi: 10.1177/0892705718785676.

Alves, F. J. L., Baptista, A. M. and Marques, A. T. (2016) *3 - Metal and ceramic matrix*

*composites in aerospace engineering*, *Advanced Composite Materials for Aerospace Engineering*. Elsevier Ltd. doi: 10.1016/B978-0-08-100037-3.00003-1.

Balakrishnan, P. *et al.* (2016) *12 - Natural fibre and polymer matrix composites and their applications in aerospace engineering*, *Advanced Composite Materials for Aerospace Engineering*. Elsevier Ltd. doi: 10.1016/B978-0-08-100037-3.00012-2.

Bandyopadhyay, S. (2014) 'hardening 2014 Al / Sic and 6061 Al / SIC composites', 185(1995), pp. 125–130.

Carpier, Y. *et al.* (2018) 'Mechanical behavior of carbon fibers polyphenylene sulfide composites exposed to radiant heat flux and constant compressive force', *Composite Structures*, 200, pp. 1–11. doi: 10.1016/j.compstruct.2018.05.086.

Chang, I. Y. and Lees, J. K. (1988) 'Recent Development in Thermoplastic Composites: A Review of Matrix Systems and Processing Methods', *Journal of Thermoplastic Composite Materials*, 1(3), pp. 277–296. doi: 10.1177/089270578800100305.

Ching, Y. C. *et al.* (2017) *Applications of thermoplastic-based blends*, *Recent Developments in Polymer Macro, Micro and Nano Blends: Preparation and Characterisation*. Elsevier Ltd. doi: 10.1016/B978-0-08-100408-1.00005-4.

Das, T. K., Ghosh, P. and Das, N. C. (2019) 'Preparation , development , outcomes , and application versatility of carbon fiber-based polymer composites : a review'.

Eguemann, N. *et al.* (2014) 'Compression moulding of complex parts for the aerospace with discontinuous novel and recycled thermoplastic composite materials To cite this version : HAL Id : hal-00983314 COMPRESSION MOULDING OF COMPLEX PARTS FOR THE AEROSPACE WITH DISCONTINUOUS NOVEL A'.

Favaloro, M. (2018) 'Properties and Processes of Linear Polyphenylene Sulfide ( PPS ) for Continuous Fiber Composites Aerospace Applications', 4970.

Kumar, D., Agnihotri, G. and Purohit, R. (2015) 'Advanced Aluminium Matrix Composites : The Critical Need of Automotive and Aerospace Engineering Fields', *Materials Today: Proceedings*, 2(4–5), pp. 3032–3041. doi: 10.1016/j.matpr.2015.07.290.

Lindroos, V. K. and Talvitie, M. J. (1995) 'IVo ., ra t . o lCoo . t d . a . tens . elCo', 53, pp. 273–284.

Liu, Y., Zhou, X. and Wang, Z. (2020) 'Effect of isothermal heat treatment on crystallinity, tensile strength and failure mode of CF/PPS laminate', *High Performance Polymers*. doi: 10.1177/0954008320969843.

Mahat, K. B. *et al.* (2016) 'Effects of UV Light on Mechanical Properties of Carbon Fiber Reinforced PPS Thermoplastic Composites', *Macromolecular Symposia*, 365(1), pp. 157–168. doi: 10.1002/masy.201650015.

Ning, H. *et al.* (2007) 'Design , manufacture and analysis of a thermoplastic composite frame structure for mass transit', 80, pp. 105–116. doi: 10.1016/j.compstruct.2006.04.036.

Offringa, A. R. (1996) 'Thermoplastic composites - Rapid processing applications', *Composites Part A: Applied Science and Manufacturing*, 27(4 PART A), pp. 329–336. doi: 10.1016/1359-835X(95)00048-7.

Post, W. *et al.* (2020) 'A Review on the Potential and Limitations of Recyclable Thermosets for Structural Applications', *Polymer Reviews*, 60(2), pp. 359–388. doi: 10.1080/15583724.2019.1673406.

Richard Sharp, Scott Holmes, C. W. (1995) 'from the SAGE Social Science Collections . All Rights', 8(1).

S, M. K., K, R. R. and Govindaraju, H. K. (2018) 'ScienceDirect Development of E-Glass Woven Fabric / Polyester Resin Polymer Matrix Composite and Study of Mechanical Properties', *Materials Today: Proceedings*, 5(5), pp. 13367–13374. doi: 10.1016/j.matpr.2018.02.329.

Steyer, T. E. (2013) 'Shaping the future of ceramics for aerospace applications', *International Journal of Applied Ceramic Technology*, 10(3), pp. 389–394. doi: 10.1111/ijac.12069.

Sudhin, A. U. *et al.* (2020) 'Comparison of Properties of Carbon Fiber Reinforced Thermoplastic and Thermosetting Composites for Aerospace Applications', *Materials Today: Proceedings*, 24, pp. 453–462. doi: 10.1016/j.matpr.2020.04.297.

Vaidya, U. K. and Chawla, K. K. (2008) 'Processing of fibre reinforced thermoplastic composites', *International Materials Reviews*, 53(4), pp. 185–218. doi: 10.1179/174328008X325223.

Wang, Y. *et al.* (2018) 'Compressive behavior of notched and unnotched carbon woven-ply PPS thermoplastic laminates at different temperatures', *Composites Part B: Engineering*,

133, pp. 68–77. doi: 10.1016/j.compositesb.2017.09.027.

Williams, J. C. and Starke, E. A. (2003) 'Progress in structural materials for aerospace systems ☪', 51, pp. 5775–5799. doi: 10.1016/j.actamat.2003.08.023.

Zhang, K. *et al.* (2014) 'Effect of aminated polyphenylene sulfide on the mechanical properties of short carbon fiber reinforced polyphenylene sulfide composites', *Composites Science and Technology*, 98, pp. 57–63. doi: 10.1016/j.compscitech.2014.04.020.

Zhu, D. (2019) 'Aerospace Ceramic Materials : Thermal , Environmental Barrier Coatings and SiC / SiC Ceramic Matrix Composites For Turbine Engine Applications', (May 2018).

Zhu, D., Sakowski, B. A. and Fisher, C. (2019) 'Film Cooled Recession of SiC / SiC Ceramic Matrix Composites : Test Development , CFD Modeling and Experimental Observations', pp. 1–16.

Zuo, P. *et al.* (2018) 'Multi-scale analysis of the effect of loading conditions on monotonic and fatigue behavior of a glass fiber reinforced polyphenylene sulfide (PPS) composite', *Composites Part B: Engineering*, 145, pp. 173–181. doi: 10.1016/j.compositesb.2018.03.031.